Sperm motility in mice with oligo-astheno-teratozoospermia restored by *in vivo* injection and electroporation of naked mRNA

Charline Vilpreux[1#], Paul Fourquin[1#],Guillaume Martinez[1,4], Magali Court[1], Florence Appaix[6], Jean-Luc Duteyrat[2], Maxime Henry[7], Julien Vollaire[7], Camille Ayad[3], Altan Yavuz[3], Geneviève Chevalier[1], Lisa De Macedo[1], Sofia Andrade Rebelo[1], Edgar Del Llano [1], Célia Tebbakh [1,4] , Zine-Eddine Kherraf [1,4], Emeline Lambert[1], Sekou Ahmed Conte[1], Zeina Wehbe[1,4], Elsa Giordani[1], Véronique Josserand[7], Jacques Brocard[2], Coutton Charles[1,4], Bernard Verrier[3], Pierre F. Ray[1,5], Corinne Loeuillet[1], Christophe Arnoult[1] and Jessica Escoffier[1*].

[1] Université Grenoble Alpes, Inserm U1209, CNRS UMR 5309, Team Genetic, Epigenetic and Therapies of infertility, Institute for Advanced Biosciences 38 000 Grenoble, France

[2] Université Claude Bernard Lyon 1, CNRS UAR3444, Inserm US8, ENS de Lyon, SFR Biosciences, Lyon 69007, France

[3]Université Claude Bernard Lyon 1 - Laboratoire de Biologie Tissulaire et d'Ingénierie Thérapeutique, UMR 5305, Université Lyon 1, CNRS, IBCP, Lyon, France

[4] UM de Génétique Chromosomique, Hôpital Couple-Enfant, CHU Grenoble Alpes, Grenoble, France.

[5] UM GI-DPI, CHU Grenoble Alpes, Grenoble, France.

[6] University Grenoble Alpes, INSERM U1209, CNRS UMR5309, Optical microscopy and cell imaging (MicroCell) facility, Institute for Advanced Biosciences, 38000 Grenoble, France

[7] Université Grenoble Alpes, Inserm U1209, CNRS UMR 5309, plateforme Optimal, Institute for Advanced Biosciences 38 000 Grenoble, France

Shared first authorship.

* To whom correspondence should be addressed: Jessica Escoffier, Team "Genetics, Epigenetics and Therapies of Infertility", Institute for Advanced Biosciences (IAB), INSERM 1209, CNRS UMR 5309 University Grenoble Alpes, Grenoble, FRANCE.
Contact:mail to jessica.escoffier@univ-grenoble-alpes.fr
tel: 33 (0)4 76 63 71 11

Ethics statement

All procedures involving animals were performed in line with the French guidelines for the use of live animals in scientific investigations. The study protocol was approved by the local ethics committee (ComEth Grenoble # 318) and received governmental authorization (ministerial agreement # 38109-2022072716142778).

Abstract

Oligo-astheno-teratozoospermia (OAT), a recurent cause of male infertility, is the most frequent disorder of spermatogenesis with a probable genetic cause. Patients and mice bearing mutations in the *ARMC2* gene have a decreased sperm concentration, and individual sperm show multiple morphological defects and a lack of motility – a canonical OAT phenotype. Intracytoplasmic sperm injection (ICSI) is required to treat such a condition but it is associated with a small increase in birth defects in comparison to pregnancies not involving assisted conception. Consequently, new targeted treatments are needed to restore fertility. Here, a combination of *in vivo* injection and electroporation of capped and poly-A-tailed naked mRNA is tested as a strategy to treat *ARMC2*-related infertility in mouse. mRNAs coding for several reporter genes are tested and the efficiency and the kinetic of expression are assessed using *in vivo* and *in vitro* 2D and 3D imaging experiments. We show that mRNA-coded reporter proteins are detected for up to 3 weeks in germ cells, making the use of mRNA possible to treat infertility. We compare these results with those obtained with a non-integrative plasmid Enhanced Episomal Vector (EEV), which induces low and transient expression in spermatogenic cells. Consequently, injection and electroporation of naked mRNA-*Armc2* into the testes of *Armc2*-deficient males were performed and we show the presence of normal and motile sperm in the epididymis. These motile sperm were able to produce embryos by IVF and ICSI. This study demonstrates, for the first time, that mRNA electroporation can restore sperm motility and partially fertilizing ability, providing a proof-of-concept for mRNA-based strategies to correct monogenic causes of male infertility and opening new avenues for male infertility treatment.

Key words: Sperm cells, infertility, protein therapy, mRNA, EEV, *In Vivo* Microinjection and Electroporation, *in vivo* imaging, Whole Testis Optical clearing, lightsheet microscopy.

63 **Introduction**

64 Worldwide, 10-15 % of couples (or 70 million) face infertility [1]. Infertility is thus a major
65 public health issue presenting significant medical, scientific and economic challenges (a
66 multibillion € annual market)[2]. A significant proportion of infertilities is due to altered
67 gametogenesis, where the sperm and eggs produced are incompatible with fertilization
68 and/or embryonic development [3]. Approximately 40 % of cases of infertilities involve a male
69 factor, either exclusively, or associated with a female deficiency [4].

70 Male gametogenesis, or spermatogenesis, is a highly complex physiological process which can
71 be split into three successive steps: proliferation (mitosis of spermatogonia), reduction of the
72 number of chromosomes (meiosis of spermatocytes), and morphogenesis of spermatozoa
73 (spermiogenesis). Spermatogenesis involves the coordinated expression of a large number of
74 genes, with approximately 2,000 showing testis-enriched expression, about 60% of which are
75 expressed exclusively in the testes [5]. Because of this multiplicity of genes, spermatogenesis
76 is strongly affected by genetic factors [5], with most severe disorders likely to be of genetic
77 origin.

78 Among male infertility disorders, oligo-astheno-teratozoospermia (OAT) is the most frequent
79 (50 % [6]) and it is likely to be of genetic origin. Spermatocytograms of OAT patients show a
80 decrease in sperm concentration, multiple morphological defects and defective motility [7, 8].
81 Because of these combined defects, patients are infertile and can only conceive by
82 intracytoplasmic sperm injection (ICSI).

83 ICSI can efficiently overcome the problems faced. Nevertheless, concerns persist regarding
84 the potential risks associated with this technique, including blastogenesis defect,
85 cardiovascular defect, gastrointestinal defect, musculoskeletal defect, orofacial defect,
86 leukemia, central nervous system tumors, and solid tumors [9-12]. Statistical analyses of birth
87 records have demonstrated an elevated risk of birth defects, with a 30-40 % increased
88 likelihood in cases involving ICSI [9-12], and a prevalence of birth defects between 1 % and 4
89 % [11]. It is important to note, however, that the origin of these risks remains debated. Several
90 large epidemiological and mechanistic studies indicate that both the procedure itself (direct
91 microinjection and *in vitro* manipulation) and the underlying genetic or epigenetic
92 abnormalities often present in men requiring ICSI contribute to the observed outcomes [9, 11]

93 [13, 14]. To overcome these drawbacks, a number of experimental strategies have been
94 proposed to bypass ARTs and restore spermatogenesis and fertility, including gene therapy
95 [15-18].

96 Gene therapy consists of introducing a DNA sequence into the genome to compensate for a
97 defective gene. It can thus rescue production of a missing protein, and is now applied both in
98 research [19] and for the treatment of human diseases [20] .

99 Given the genetic basis of male infertility, the first strategy, tested in mice, was to overcome
100 spermatogenic failure associated with monogenic diseases by delivery of an intact gene to
101 deficient germ cells [15]. Gene therapy is effective in germ cells, as numerous publications
102 have shown that conventional plasmids can be transferred into spermatogonia in several
103 species with success, allowing their transcription in all cells of the germinal lineage [15-18].
104 Most experiments were performed in mouse models, delivering DNA constructs into living
105 mouse germ cells by testis electroporation after microinjection of a DNA-containing solution
106 into the seminiferous tubules. Using this method, it was possible to rescue meiosis and fertility
107 in mouse models of infertility [15, 18]. However, the genetic changes induced are transmitted
108 to any descendants. Consequently, gene therapy cannot be used to treat infertility in humans,
109 both for ethical reasons and to avoid any eugenic deviations, and currently transmissible
110 changes in humans are illegal in 39 countries [21]. Furthermore, the genetic modification of
111 germ cell lines poses biological risks, including the induction of cancer, off-target effects, and
112 cell mosaicism. Errors in editing may have adverse effects on future generations. It is
113 exceedingly challenging to anticipate the consequences of genetic mosaicism, for instance, in
114 a single individual [22, 23]. Gene therapies have thus raised both ethical controversy and long-
115 term safety issues.

116 For these reasons, we decided to test an alternative strategy to DNA transfection based on
117 the use of naked mRNA. Thanks to this change, the risk of genomic insertion is avoided, and
118 thus there is no question of heritable alterations [24].The first part of this study presents a
119 characterization of the protein expression patterns obtained following transfection of naked
120 mRNA coding for reporter genes into the testes of mice. The second part is to apply the
121 protocol to a preclinical mouse model of OAT. Patients and mice carrying mutations in the
122 *ARMC2* gene present a canonical OAT phenotype and are infertile. The preclinical *Armc2*
123 deficient (*Armc2* KO) mouse model is therefore a valuable model to assess whether *in vivo*

124 injection of naked mRNA combined with electroporation can restore spermatogenesis. We
125 chose this model for several reasons: first, *Armc2* KO mice are sterile and all sperm exhibit
126 short, thick or coiled flagella [13]. As a result, 100 % of sperm are immobile, thus it should be
127 easy to determine the efficacy of the technique by measuring sperm motility with a CASA
128 system. Second, the *Armc2* gene codes for an 867-amino acid protein and this large size
129 represents a challenge for expression in the testis following electroporation.

130 To determine the efficacy of naked mRNA transfection as a method to achieve protein
131 expression in the testes, we first assessed the level of transcription of reporter proteins after
132 mRNA injection compared to the injection of a non-integrating plasmid, the Enhanced
133 Episomal Vector (EEV). EEV is a vector derived from Epstein-Barr virus, it includes an origin of
134 replication (EBV Ori) and the EBNA1 protein. Both elements, allows the synchronous initiation
135 of extra-chromosomal EEV replication with host DNA at each S phase of the cell cycle and the
136 segregation of the EEV episome in daughter cells. It is notable that EEV is maintained at a rate
137 of 90-95% per cell division. It does not integrate or modify the host genome [11, 12].

138 In the present *in vivo* work, we injected and electroporated three distinct mRNAs coding for
139 the following reporter proteins: green fluorescent protein (GFP), luciferase (Luc) and mCherry,
140 and an EEV episome vector containing the sequences coding for both GFP and luciferase
141 reporter proteins. The initial step was to characterize and validate the method of injection in
142 adult males. Subsequently, the kinetics and patterns of expression of the electroporated
143 mRNAs and EEV were compared using a variety of methods, including whole testis imaging, *in*
144 *vivo* bioluminescence imaging, and tissue clearing. Subsequently, the mRNA transfection
145 protocol was tested in a preclinical mouse model of OAT with the objective of restoring
146 fertility.

147

148 **Materials and methods**

149 **Animals**

150 All procedures involving animals were performed in line with the French guidelines for the use
151 of live animals in scientific investigations. The study protocol was approved by the local ethics
152 committee (ComEth Grenoble # 318) and received governmental authorization (ministerial
153 agreement # 38109-2022072716142778).

154 The animals used were (a) B6D2 F1 hybrid (♀ C57BL/6JRj crossed with ♂ DBA/2, Janvier
155 laboratories; France) adult male mice aged between 8 and 25 weeks, (b) the *Armc2* KO mouse
156 strain obtained by CRISPR-Cas9 [25] and (c) CD1 female 6 weeks old (Janvier laboratories, Le
157 Genest-Saint-Isle ,France). Experiments were carried out on wild type (WT) or *Armc2* KO adult
158 male mice aged between 8 and 15 weeks.

159 **Chemicals and reagents**

160 Fast Green (FG) (F7258 – 25 g), phosphate buffered saline (PBS, D853 7-500 mL), hematoxylin
161 (GH5316 – 500 mL), eosin (HT110216 – 500 mL), tert-Butanol (471712 – 100 mL), Histodenz
162 (D2158 – 100 g), sorbitol (S1876 – 100 g), urea (U5128 – 500 g), Potassium Phosphate,
163 Monobasic (P0662), Magnesium Sulfate (anhydrous) (M9397), Sodium Bicarbonate Calcium
164 Chloride · 2H2O (22317), EDTA (E9884), Sodium Lactate (60 % syrup - d= 1.32 g L^{-1}) (L7900),
165 Glucose (G8270), Penicillin (P4333), Streptomycin (P4333), HEPES (H0887), PVA 30,000-70,000
166 (P8136), Albumin, Bovine Fraction V (A3803), RPMI-1640 media (R2405), M2 medium
167 (M7167), Hyaluronidase (H3884), mineral oil (M8410), PolyVinylPyrolidone (PVP360-100G),
168 M16 medium (MR-016), Trypsin (T6567) and Collagenase (C8176) were purchased from Sigma
169 Aldrich (Saint-Quentin-Fallavier, France). Sodium Chloride (1112-A) was purchased from
170 Euromedex (Souffelweyersheim, France). Potassium Chloride (26764), L-Glutamine
171 (35050038), Hoechst 33342 (R37165), Sodium Pyruvate (11360039), KSR serum (10828010),
172 NEAA (11140050) and EAA (11130036) were purchased from Life Technologies, (Waltham, MA
173 USA). Schorr staining solution was obtained from Merck (Darmstadt, Germany). Mfel HF
174 (R35895) and RNase-free DNase I (M03035) were obtained from New England Biolabs
175 (Ipswich, MA, USA). Paraformaldehyde (PFA, 15710) was obtained from Electron Microscopy
176 Science (Hatfield, PA, USA). Ketamine and xylazine were obtained from Centravet (Dinan,
177 France). Fluorescent i-particles (NIRFiP-180) were obtained from Adjuvatis (Lyon, France).
178 Script Gurad RNAse CleanCap AG (040N-7113-1), CleanCAp *EGFP*-mRNA (040L-7601-100), T7-
179 FlashScribe kit (C-ASF3507), poly(A) tail (C-PAP5104H) and CleanCap *Luciferase*-mRNA (L-
180 7602-1000) were obtained from Tebubio (Le Perray en Yvelines, France).

181 **Plasmids**

182 All plasmids, EEV *CAGs-GFP-T2A-Luciferase*, (EEV604A-2; System Bioscience, Palo Alto, CA,
183 USA), mCherry plasmid (given by Dr. Conti MD at UCSF, San Francisco, CA, USA) and EEV-

184 *Armc2-GFP* plasmid (CUSTOM-S017188-R2-3, Trilink, San Diego, CA, USA) were amplified by
185 bacterial transformation (E. coli, EC0112; Thermo Fisher, Courtaboeuf, France). After
186 expansion, plasmids were purified with a NucleoBond Xtra Midi kit (740410-50; Macherey-
187 Nagel, Düren, Germany) using manufacturer's protocol. All plasmids DNA pellets were
188 solubilized in (DNAse- and RNAse-free) milliQ water (Sigma Aldrich, Saint-Quentin-Fallavier,
189 France), before being used.

190 The EEV *CAGs-GFP-T2A-Luciferase* episome contains the cDNA sequences of Green
191 Fluorescent Protein (GFP) and luciferase, under the control of a CAGs promoter (Supp Fig 1).
192 After purification, the EEV *CAGs-GFP-T2A-Luciferase* plasmid concentration was adjusted to
193 9 µg μL^{-1}. Prior to injection, 3.3 µL of this plasmid solution was mixed with 1 µL 0.5 % Fast
194 Green and 5.7 µL sterile PBS to obtain a final EEV concentration of 3 µg μL^{-1}. The EEV-*Armc2-*
195 *GFP* plasmid contains the mouse cDNA sequences of *Armc2 (ENSMUST00000095729.11)* and the
196 Green Fluorescent Protein (GFP) genes under the control of a strong CAGs promoter (Supp Fig
197 1). After amplification and purification, the final plasmid concentration was adjusted to 9 µg
198 μL^{-1} in water. Prior to injection, 3.3 µL of this plasmid solution was mixed with 1 µL of 0.5 %
199 Fast Green and 5.7 µL of sterile PBS to obtain a final EEV concentration of 3 µg μL^{-1}. The
200 *mCherry* plasmid contains the cDNA sequence of *mCherry* under the control of CMV and T7
201 promoters (Supp Fig 1). After amplification and purification, the final plasmid concentration
202 was adjusted to 9 µg μL^{-1}.

203 ***Armc2*-mRNA**

204 *Armc2*-mRNA used for *in vivo* testes microinjection and electroporation was obtained from
205 Trilink (San Diego, CA, USA). The commercial *Armc2*-mRNA has an AG CleanCap, a poly (A) tail
206 of 120 adenosines and 3 HA-FLAG. The main challenge with mRNA-based therapy is mRNA
207 stability. To improve mRNA stability *in vivo* and avoid its degradation by ribonucleases,
208 optimization techniques were implemented. Thus, the used mRNA has codon optimization, a
209 poly (A) tail and a CleanCap[26-30]. To verify the efficiency of cell transfection, an *EGFP*-mRNA
210 was injected together with the *Armc2*-mRNA. During the injection, the concentration of *EGFP*-
211 mRNA and *Armc2*-mRNA were 300 ng μL^{-1} each.

212 ***mCherry*-mRNA transcription *in vitro***

213 The circular *mCherry* plasmid was linearized using the restriction enzyme MfeI HF at 37 °C for
214 1 h. The pm-*mCherry* was then extracted and purified with the DNA Clean and Concentrator-
215 25 ™ kit (D4033; Zymo Research, Irvine, CA, USA). The pm-*mCherry* was subsequently
216 transcribed in vitro using the T7-FlashScribe kit (C-ASF3507; Tebubio, Le Perray en Yvelines,
217 France). The mRNA was capped with a clean cap (CleanCap AG; 040N-7113-1, Tebubio, Le
218 Perray en Yvelines, France), and a poly(A) tail (C-PAP5104H; Tebubio, Le Perray en Yvelines,
219 France) was added before purification using the NucleoSpin RNA Clean Up kit (740948-50;
220 Macherey-Nagel, Düren, Germany). Prior to injection, *mCherry*-mRNA was mixed with Fast
221 Green to obtain a final concentration of 300 ng μL^{-1} (0.05 % FG, PBS).

222 **Agarose gel electrophoresis of the Episomal Vector EEV and mRNA-mCherry**

223 Before loading on a pre-stained (Gel Green) 1.5 % agarose gel, the EEV-plasmid and mRNA
224 were mixed with a loading dye (Promega Blue Orange G1904, Promega, Charbonnières
225 France). An aliquot of each sample (500 ng) was loaded into each well and electrophoresis was
226 performed for 30 min at 100 V at room temperature (RT). A DNA size marker (Gene ruler
227 SM1331, Thermo Scientific, Courtaboeuf, France) was used to assess molecular weight. Gel
228 images were acquired using a ChemiDoc XRS+ (BIORAD, Marnes-la-Coquette, France).

229 ***In vivo* microinjection and electroporation of testes**

230 Electroporation was conducted as previously described [17]. Briefly, male mice B6D2, *Armc2*$^{+/+}$
231 or *Armc2*$^{-/-}$, depending on the experimental conditions, were anesthetized with
232 ketamine/xylazine solution (100 mg μL^{-1} and 10 mg μL^{-1} respectively). The testes were pulled
233 out of the abdominal cavity or scrotum. Under a binocular microscope and using
234 microcapillaries pipettes (FemtoTip II ®, Eppendorf, Montesson, France), 10 μL DNA (3 μg μL^{-}
235 ^{1} - 0.05 % FG) or mRNA (300 ng μL^{-1} -0.05 % FG) was injected into the seminiferous tubules
236 through the *rete testis* applying a constant pressure (microinjector, Femto Jet 4i, Eppendorf,
237 Montesson, France). Two series of 8 square electric pulses (25 V for 50 ms) were applied to
238 the testis using tweezer-type electrodes linked to an electroporator (Gemini, BTX, Holliston,
239 MA, USA). The testes were then replaced in the abdominal cavity, and the abdominal wall and
240 skin were sutured. For each animal, the left testis was injected and electroporated with the
241 different nucleic acids (mRNA, EEV), whereas the right testis was injected with a control
242 solution (PBS, 0.5 % FG) as a control. Both testes were electroporated.

243 **Flash Freezing and Fluorescence Analysis of testes**

244 Depending on the experimental condition, 1-, 3- or 7-days post injection, the testes were
245 collected and washed for 5 min in PBS. Then, they were embedded in Peel-A-Way Cryomolds
246 filled with OCT Mounting media (VWR, Rosny-sous-Bois, France). The samples were flash
247 frozen in a 100 % isopentane solution (524391; Carlo ERBA, Val-de-Reuil, France), pre-cooled
248 with liquid nitrogen. Once frozen, they were cut into 20 µm sections using a cryostat. The
249 cryostat sections were then fixed with 4 % PFA-PBS for 10 min at 4 °C and counterstained with
250 1.8 µM DAPI (nuclear stain) before observation using an Axioscan Z1 slide scanner or a
251 confocal microscope LSM710 (NLO – LIVE7 – Confocor 3). The fluorescence of the different
252 reporter proteins was detected using appropriate filters for DAPI, GFP, Texas Red (for
253 mCherry), and Cy7 (for the Fluorescent i-particles NIRFiP-180).

254 **Tissue collection and histological analysis**

255 For histological analysis, treated and control B6D2 testes were fixed by immersion in 4 %
256 paraformaldehyde (PFA) for 14 h. They were then embedded in paraffin before cutting into 5
257 µm sections using a microtome (Leica biosystems, Wetzlar, Germany). After deparaffination,
258 the sections were stained with hematoxylin and eosin. Stained sections were digitized at 20x
259 magnification using an Axioscan Z1-slide scanner (Zeiss, Jna, Germany). Spermatogenesis was
260 assessed by measuring the area of seminiferous tubules and the cross sections of round
261 tubules (μm^2) ($n > 35$ tubules per testis section; n=5 testis sections per condition). Statistical
262 significance of differences was determined using a Student's *t*-test.

263 ***Ex vivo* Fluorescence Analysis**

264 To analyze the expression of the reporter proteins GFP and mCherry in seminiferous tubules,
265 whole testes were examined under an inverted microscope (CKX53, Olympus, Shinjuku, Tokyo,
266 Japan). Exogenous fluorescence was detected using filters for GFP and Texas Red.

267

268 ***Armc2* Genotyping**

269 DNA was obtained by the digestion of an ear punch using the Direct PCR lysis buffer
270 (Euromedex, Souffelweyersheim, FR) and 1 mg/ml proteinase K (Thermo Fisher Scientific,
271 Waltham, Massachusetts, USA) overnight at 55°C, followed by enzyme inactivation 1 hour at

272 85°C. PCR was performed as follow: 2 µl of undiluted DNA was mixed with 0.4 µM primers
273 against *Armc2* gene (Genscript, Piscataway, NJ, USA, sequences are listed in table 1), Coral
274 Load PCR Buffer 1X (Qiagen, Hilden, DE), 0.8 mM dNTP mix (Thermo Fisher Scientific) and
275 0.625 units of Taq DNA Polymerase (Qiagen) in a final volume of 25 µL. The PCR program used
276 was 94°C 15 min (94°C 30 s, 59°C 30 s, 72°C 1 min) x 32 followed by a finale elongation (72°C
277 10 min). PCR products were then visualized by electrophoresis (BioRad, Hercules, California,
278 USA) on a 1% agarose gel with Gelgreen 1,8X (Interchim, Montluçon, FR).

279 **Purification of Seminiferous Tubule Cells**

280 Depending on the experimental condition, testes were collected at 1, 3-, 7-, 14-, or 21-days
281 post-injection of mRNA-GFP (300 ng/µL) and transferred into a sterile 35 mm Petri dish
282 containing 2 mL of 1× Phosphate Buffered Saline (PBS, pH 7.4). The tunica albuginea was
283 carefully removed under sterile conditions. Testicular tissue was then mechanically
284 dissociated by gently aspirating and expelling the tissue 10–12 times using an 18-gauge needle
285 to isolate individual seminiferous tubules. To enrich for GFP-positive tubules, tubules lacking
286 GFP fluorescence were discarded under a fluorescence microscope. This procedure resulted
287 in a sample containing approximately 25% GFP-positive tubules.

288 The isolated tubules were washed three times with PBS to remove residual debris. Enzymatic
289 dissociation was performed in two steps: first, the tubules were incubated in collagenase (1
290 mg/mL in RPMI 1640 medium (Sigma-Aldrich, Saint-Louis, Missouri, USA)) for 30 minutes at
291 37 °C with gentle agitation. This was followed by a second digestion step using trypsin (2
292 mg/mL in RPMI 1640 medium (Sigma-Aldrich, Saint-Louis, Missouri, USA)) for 15 minutes at
293 37°C with gentle agitation to ensure complete dissociation of seminiferous epithelial cells.

294 To stop the enzymatic digestion, cells were immediately resuspended in RPMI 1640 medium
295 (Sigma-Aldrich, Saint-Louis, Missouri, USA) supplemented with 5% KnockOut™ Serum
296 Replacement (KSR; Thermo Fisher Scientific). The resulting single-cell suspension was then
297 used for downstream applications.

298 **Live mRNA-GFP Fluorescence Imaging of Dissociated Seminiferous Tubule Cells**

299 The isolated seminiferous tubule cell suspensions obtained from testes 24 hours post-
300 injection with mRNA-GFP (300 ng/µL) were cultured in RPMI 1640 medium (Sigma-Aldrich,
301 Saint-Louis, Missouri, USA) in chambered coverglass systems (Nunc™ Lab-Tek™ II, Cat. No.

302 155360PK, Thermo Fisher Scientific, Courtaboeuf, France) at 37 °C in a humidified atmosphere
303 containing 5% CO_2.

304 After 12 hours of culture, the cells were counterstained with 1.8 µM Hoechst 33342 (Thermo
305 Fisher Scientific), a membrane-permeable nuclear dye functionally similar to DAPI. Live-cell
306 fluorescence imaging was performed using an Axio Observer 7 inverted fluorescence
307 microscope (Zeiss, Jena, Germany) equipped with a 63× oil immersion objective. GFP and
308 Hoechst fluorescence signals were detected using the appropriate filter sets. Image
309 acquisition and analysis were conducted using ZEN lite software (Zeiss, Jena, Germany).

310 **Cell Culture**

311 HEK cells were cultured in 100 mm tissue culture dishes (Falcon, Corning, New York, USA) in
312 DMEM/F12 medium (Sigma-Aldrich, Saint Louis, Missouri, USA) supplemented with 10% heat-
313 inactivated fetal bovine serum (FBS; Life Technologies), 1% penicillin/streptomycin (Sigma-
314 Aldrich), and 0.01 mg/mL hygromycin B (Thermo Fisher Scientific). Cells were maintained at
315 37°C in a humidified atmosphere containing 5% CO_2 and were passaged twice weekly at a 1:10
316 dilution.

317 Transfection was performed using 2 µg/mL GFP mRNA (TriLink BioTechnologies, San Diego,
318 USA) and the jetMESSENGER® mRNA transfection reagent (Sartorius, Göttingen, Germany),
319 following the manufacturer's instructions. mRNA was extracted from the cells at 12-, 24-, 48-
320 , and 60-hours post-transfection.

321

322 **mRNA Extraction and qPCR Analysis**

323 Total RNA from isolated seminiferous tubule cell suspensions and HEK cells was extracted
324 using the NucleoSpin® RNA Plus kit (Macherey-Nagel, Düren, Germany) according to the
325 manufacturer's protocol. RNA concentration was measured using the Qubit™ RNA Assay Kit
326 (Life Technologies, Carlsbad, California, USA), and samples were stored at –80°C until further
327 use.

328 Up to 800 ng of total RNA per sample was reverse-transcribed into cDNA using the iScript™
329 cDNA Synthesis Kit (Bio-Rad, Hercules, California, USA), following the manufacturer's protocol.
330 Gene expression was analyzed by quantitative PCR (qPCR) using 1 µL of undiluted cDNA in a

331 final reaction volume of 10 µL, with gene-specific primers (see Table 1), and the
332 SsoAdvanced™ Universal SYBR® Green Supermix (Bio-Rad, Hercules, California, USA).

333 The qPCR program for GAPDH expression in HEK cells included an initial denaturation at 95°C
334 for 3 minutes, followed by 39 cycles of 95°C for 10 seconds, 60°C for 30 seconds, and 72°C for
335 30 seconds. Melt curve analysis was performed by increasing the temperature from 58°C to
336 95°C in 0.5°C increments, holding each step for 2–5 seconds.

337 For GFP expression analysis, the same program was used, except that the annealing
338 temperature was set to 62°C instead of 60°C.

339 Relative gene expression was calculated using the 2^–ΔCT method.

		Primer sequences (5'-3')	Final concentration (µM)
Genotyping			
*Armc2*_WT	Forward	GGCCCGAGCACGCTTCTA	0.4
	Reverse	TTCATGTAAGAACTATCCAGGACCA	0.4
*Armc2*_KO	Forward	TGGGACGCAGCCCTGTAA	0.4
	Reverse	AACCCAAAGCTCCAGCATCTC	0.4
Expression			
Gfp	Forward	ACGACTTCTTCAAGTCCGCC	0.08
	Reverse	TCTTGTAGTTGCCGTCGTCC	0.08
Gadph Human	Forward	TCTCTGCTCCTCCTGTTCGA	0.33
	Reverse	TTCCCGTTCTCAGCCTTGAC	0.33
Gadph mice	Forward		
	Reverse		

340 Table 1. Primer sequences used for mouse genotyping and *Gfp* expression analysis in HEK cells
341 and mouse seminiferous tubules.

342 **Harris-Shorr sperm Analysis**

343 Sperm were collected from the caudae epididymides of mice (Control, injected with EEV-*GFP*,
344 *GFP*-mRNA, or *Armc2*-mRNA). They were allowed to swim for 10 min at 37 °C in 1 mL M2

345 media. Sperm were centrifuged at 500 g, washed once with PBS, and fixed 4 %
346 paraformaldehyde in PBS for 1 min at RT. After washing with 1 mL acetate ammonia
347 (100 mM), the sperm suspensions were spotted onto 0.1 % poly L-lysine precoated slides
348 (Thermo Scientific, Courtaboeuf, France) and left to dry. Harris–Schorr staining was then
349 performed according to the WHO protocol [31], and at least 150 sperm were analyzed per
350 animal.

351 **Whole Testis Optical clearing and 3D image reconstructions**

352 Optical clearing (adapted from uDISCO and Fast 3D clear protocols)

353 Adult mice were euthanized by cervical dislocation and then transcardiac perfused with 1X
354 PBS (Sigma Aldrich, Saint-Quentin-Fallavier, France). The testes were extracted and fixed for
355 two days at 4 °C in 4 % PFA (Electron Microscopy Sciences, Hatfield, PA ,USA). Samples were
356 then washed with PBS for at least two days. Mouse testes were subsequently dehydrated in
357 graded series of tert-butanol solutions (Sigma Aldrich, Saint-Quentin-Fallavier, France) at 35 °C
358 as follows: 30 % overnight (O/N), 50 % for 24 h, 70 % for 10 h, 80 % O/N, 90 % for 10 h, 96 %
359 O/N, and 100 % for 10 h. The testes were cleared in clearing solution (96 % Histodenz, 2 %
360 Sorbitol, 20 % Urea) for 2 days. Then, nuclei were stained with 3.6 μM DAPI (20 % DMSO; 2 %
361 Triton, 1 % BSA) for 2 days. Finally, the testes were then conserved in the clearing solution at
362 4°C until observation by microscopy. All these steps were carried out under agitation and
363 protected from light.

364 3D tissue Imaging

365 The optically-cleared mouse testes were imaged on a lightsheet fluorescence microscope
366 (Blaze, Miltenyi Biotec, Germany), using a 4x NA 0.35 MI PLAN objective protected by a dipping
367 cap for organic solvents, with an overall working distance of 15 mm. Acquisitions on the
368 horizontal plane were obtained with a fixed lightsheet thickness of 3.9 µm at both 488 nm and
369 561 nm with no overlap between horizontal planes. Voxel resolution x = 1.21; y = 1.21; z = 2
370 µm. 3D reconstructions were created using Imaris software (Oxford Instruments plc,
371 Abingdon, UK).

372 Cellular image analysis

373 The optically-cleared mouse testes were imaged using a 'ConfoBright' system which is a
374 unique adaptive optics confocal microscope (Nikon A1R MP, Nikon Europe B.V., The
375 Netherlands) equipped with a deformable mirror module (AOS-micro, AlpAO, Montbonnot,
376 France) to correct geometrical aberrations. Indeed, the 3D confocal imaging of cleared sample
377 requires long distance objectives for deep tissue imaging, resulting in optical aberrations due
378 to inhomogeneous refractive index. The 'ConfoBright' microscope corrects these geometric
379 optical aberrations both in excitation and detection light path and restores locally the high
380 diffraction-limited spatial resolution and the best possible photon collection efficiency. The
381 driving metrics based on molecular brightness was used to optimize the adaptive optics in the
382 isoplanatic patch of ca. 100 mm at each imaged depth. Images were acquired using an apo
383 LWD 40x/1.15 water immersion objective (WD 600 µm) and a Plan apo 10x/0.45 objective. FIJI
384 software (open-source software[32]) was used to process and analyze images and Imaris
385 software for the 3D reconstructions.

386 **Bioluminescence imaging**

387 *In vivo* Bioluminescence imaging was performed at several time points after *in vivo Luciferase*
388 -mRNA or EEV-*GFP-luciferase* injection and electroporation (n=5 mice per condition). Ten
389 minutes before imaging, mice received an intraperitoneal injection of 150 µg g^{-1} of D-luciferin
390 (Promega, Charbonnières France), and were then anesthetized (isoflurane 4 % for induction
391 and 1.5 % for maintenance) before placing in the optical imaging system (IVIS Lumina III,
392 PerkinElmer, Courtaboeuf, France). *In vivo* bioluminescence signals were measured in selected
393 regions of interest (injected testes) and were expressed as mean photons per second (mean
394 ± SEM). Background bioluminescence was measured on images from control mice. When the
395 *in vivo* bioluminescence signal was no longer detectable, testes were collected and immersed
396 in a luciferin solution for a few minutes before performing *ex vivo* imaging to confirm the
397 absence of signal.

398 **Sperm motility**

399 The cauda epididymis was dilacerated in 1 mL of M2 medium (Sigma Aldrich, Saint-Quentin-
400 Fallavier, France) and spermatozoa were allowed to swim out for 10 min at 37 °C. After
401 incubation, 30 µl of the sperm suspension was immediately placed onto analysis chamber (2X-
402 CEL Slides, 80 µm depth, Leja Products B.V., The Netherlands) kept to 37°C for microscopic
403 quantitative study of sperm movement. Motility of the spermatozoa was evaluated at 37°C

404 with an Olympus microscope and Computer Aided Sperm Analysis (CASA) (CEROS II apparatus;
405 Hamilton Thorne, Beverley, MA, USA). The settings employed for analysis were: acquisition
406 rate: 60 Hz; number of frames: 30; minimum contrast: 30; minimum cell size: 4; low-size gate:
407 0.13; high-size gate: 2.43; low-intensity gate: 0.10; high-intensity gate: 1.52; minimum
408 elongation gate: 5; maximum elongation gate: 100; magnification factor: 0.81.

409 The motility parameters measured were: straight line velocity (VSL); curvilinear velocity (VCL);
410 averaged path velocity (VAP); amplitude of lateral head displacement (ALH); beat cross
411 frequency (BCF); linearity (LIN); straightness (STR). Hyperactivated sperm were characterized
412 by VCL > 250 µm s^{-1} , VSL > 30 µm s^{-1}, ALH > 10 µm and LIN < 60, Intermediate by VCL >
413 120 µm s^{-1} and ALH > 10 µm, progressive sperm by VAP > 50 µm s^{-1} and STR > 70 % and slow
414 sperm by VAP < 50 µm $s^{-1}$and VSL < 25 µm s^{-1}.

415 **Western blot**

416 Western blotting was performed on HEK-293T cells (ATCC, Manassas, VA, USA) transfected
417 with EEV-*Armc2* or *Armc2*-mRNA. Cells were transfected using JetPrime (101000027; Polyplus
418 Illkirch, France) for DNA and JetMessenger (101000056; Polyplus Illkirch, France) for mRNA
419 vectors, both according to the supplier's recommendations. After 48 h, the cells were washed
420 with PBS and scraped off before centrifuging at 4 °C, 1500 RPM for 5 min. The cell pellet was
421 then resuspended in lysis buffer (87787; Thermo Scientific, Courtaboeuf, France)
422 supplemented with an EDTA-free cocktail of protease inhibitors (11836170001; Roche, Bale,
423 Swiss). The suspension was stirred at 4 °C for 2 h, and then centrifuged at 16,000 g at 4 °C for
424 10 min. The protein content of the supernatant was estimated with QuantiPro™ BCA Assay kit
425 (Sigma Aldrich, Saint-Quentin-Fallavier, France) before adding 5X Laemmli + 5 % β-
426 mercaptoethanol and heating at 95 °C for 10 min. For the Western blot, 30 µg of proteins were
427 deposited on a ready-made Bis-Tris gel 12 % (Thermo Fisher, Courtaboeuf, France). After the
428 transfer, the PVDF membrane was blocked with 5 % milk in Tris-Buffered Saline solution
429 containing 0.1 % Tween 20 (TTBS) before immunodetection. The anti HA antibody
430 (11867423001; Sigma Aldrich, Saint-Quentin-Fallavier, France) was diluted in TTBS at 1/5000.
431 After incubation with secondary antibodies (AP136P; Sigma Aldrich, Saint-Quentin-Fallavier,
432 France) diluted at 1:10,000 in TTBS, binding was revealed with an enhanced
433 chemiluminescence detection kit (1705062; Clarity Max Western ECL Substrate; BIORAD,

434 Marnes-la-Coquette, France). Membranes were imaged on a ChemiDoc™ system (BIORAD,
435 Marnes-la-Coquette, France).

436 **Immunofluorescence**

437 Immunofluorescence analysis of dissociated testicular cells was performed as follows. After
438 collection, the tunica albuginea was removed from the testes. Then the tissue was
439 mechanically separated with 18G needles. Once washed with PBS, the testicular cells were
440 placed in a dissociation medium containing 1 mg collagenase type V /mL RPMI for 20 min at
441 37 °C. After filtration (100 μm filter) and centrifugation (5 min at 200 g) the pellets were
442 resuspended in PBS before centrifugation once again. The pellet was then fixed in 1 mL PFA 4
443 % for 5 min. Then 10 mL of ammonium acetate (0.1 M) was added. Finally, 2 mL of medium
444 was spread on a slide. Testicular cells were permeabilized with 0.1 % PBS-Triton X-100 for
445 20 min at room temperature. Slides were then blocked in 10 % BSA with PBS-Tween 0.1 % for
446 30 min before incubating overnight at 4 °C with primary antibodies anti-rabbit *ARMC2* (1/50)
447 (HPA053696, Sigma Aldrich, Saint-Quentin-Fallavier, France) and anti-guinea pig tubulin
448 (1/100) (AA345, Swiss Institute of Bioinformatics, Lausanne, Swiss) diluted in PBS-Tween 0.1
449 % - 5 % BSA. Slides were washed with PBS before incubating for 1 h with secondary antibodies:
450 anti-guinea pig (1/500) (A-11073, Thermo Fischer, Courtaboeuf, France) and anti-rabbit
451 (1:1000) (A-11036, Thermo Fischer, Courtaboeuf, France). Samples were counterstained with
452 DAPI and mounted with DAKO mounting media (NC2313308; Life Technology, Courtaboeuf,
453 France). Fluorescence images were acquired under a confocal microscope (Zeiss, Jena,
454 Germany) fitted with a 63× oil immersion objective. Images were analyzed with ZEN lite
455 software (Zeiss, Jena, Germany).

456 **Intra-cytoplasmic sperm injection (ICSI)**

457 Collection of gametes for ICSI

458 *Armc2*$^{-/-}$ sperm or *Armc2*$^{-/-}$ rescued sperm were harvested by dilaceration of the cauda
459 epididymis. They were allowed to swim for 10 min at 37°C in 1 ml of CZB.HEPES medium
460 containing (in mM) (HEPES 20, NaCl 81.6, KCl 4.8, $MgSO_4$ 1.2, $CaCl_2$ 1.7, KH_2PO_4 1.2,
461 EDTA.Na_2 0.1, Na-lactate 31, $NaHCO_3$ 5, Na-pyruvate 0.3, polyvinyl alcohol 0.1 mg mL^{-1}, phenol
462 red 10 mg mL^{-1} (0.5 % (w/v) in DPBS), pH 7.4) KCl 125, NaCl 2.6, Na_2HPO_4 7.8, KH_2PO_4 1.4 and

463 EDTA 3 (pH 7.0)).The sperm head was separated from the tail by applying multiple piezo pulses
464 (PiezoXpert®, Eppendorf, Montesson, France)

465 Eggs preparation

466 CD1 female mice, 7 weeks old, were superovulated by IP injection of 7.5 IU pregnant mare's
467 serum gonadotrophin (PMSG; Centravet, Dinan, France) followed by 7.5 IU HCG (Centravet,
468 Dinan, France) 48 h later. Eggs were collected from oviducts about 14 h after HCG injection.
469 Cumulus cells were removed with 0.1 % hyaluronidase in M2 medium for 5–10 min. Eggs were
470 rinsed thoroughly and kept in KSOM medium containing (in g L^{-1}: NaCl 5.55, KCl 0.19,
471 KH_2PO_4 0.05, $MgSO_4$ 0.05, $NaHCO_3$ 2.1, $CaCl_2 \cdot 2H2O$ 0.250, EDTA 0.004, L-Glutamine 0.146,
472 Na-lactate 1.870, Na-pyruvate 0.020, Glucose 0.04, Penicillin 0.05, Streptomycin 0.07, BSA
473 1.000, NEAA 0.5 % and EAA 1 %.), at 15°C for at least 15 min until required for ICSI.

474 ICSI procedures

475 ICSI was performed according to the method described by Yoshida and Perry (2007)[33].For
476 microinjection, *Armc2*$^{-/-}$ sperm or *Armc2*$^{-/-}$ -rescued motile sperm heads were separated from
477 the tail by applying multiple piezo pulses (PiezoXpert®, Eppendorf, Montesson, France). Sperm
478 heads were introduced into the ooplasm using micromanipulators (Micromanipulator
479 InjectMan®, Eppendorf, Montesson, France) mounted on an inverted Nikon TMD microscope
480 (Nikon, Minato-ku, Tokyo, Japan). Eggs that survived the ICSI procedure were incubated in
481 KSOM medium at 37 °C under in an atmosphere of 5 % CO_2. Pronucleus formation was checked
482 at 6 h after ICSI, and outcomes were scored up to the blastocyst stage.

483 ***In vitro fertilization (IVF).***

484 WT B6D2 sperm, *Armc2*$^{-/-}$ sperm or *Armc2*$^{-/-}$ rescued sperm were harvested by dilaceration of
485 the cauda epididymis. They were allowed to swim in *IVF* well in capacitated media (M16 + 2 %
486 BSA) at 37 °C for 10 minutes. Eggs were collected from mature CD1 females (6 weeks old)
487 synchronized with 7.5 units of pregnant mare serum gonadotrophin (PMSG) and 7.5 units of
488 human chorionic gonadotrophin (hCG) prior to collection. Cumulus were incubated for 10
489 minutes in 500 µL M16 (MR-016; Sigma Aldrich, Saint-Quentin-Fallavier, France) / 1mg L^{-1}
490 collagenase (C8176, Sigma Aldrich). Cumulus-free and zona-free eggs were collected, and
491 rinsed twice with 500 µl M16 medium. Eggs were incubated with either WT B6D2 sperm,
492 *Armc2*$^{-/-}$ sperm or *Armc2*$^{-/-}$ rescued sperm in capacitated medium (37 °C, 5 % CO_2) for 4 hours.

493 After incubation, unbound sperm were washed away and eggs were incubated with KSOM at
494 37 °C, 5 % CO_2. Twenty-four hours after fertilization, we scored the different stages
495 (unfertilized oocytes, aborted embryos, and 2-cell embryos as an indication of successful
496 fertilization).

497 **Statistical analyses**

498 Statistical analyses were performed using SigmaPlot (version 10; Systat Software, Inc., San
499 Jose, CA, USA). To account for sample variability between animals, a paired t-test, Mann-
500 whitney rank sum test, on-way Anova and Wilcoxon test were used. Data are displayed as
501 mean ± SEM. P values of * ≤ 0.05, ** ≤ 0.01, or *** ≤ 0.001 were considered to represent
502 statistically significant differences.

503 **Results**

504 **1. *In vivo* microinjection and electroporation of mouse testes**

505 Two routes have been described for microinjection of DNA into the testes: direct injection
506 through the *tunica albuginea,* or injection into the lumen of the seminiferous tubules via the
507 *rete testis*. We chose the *rete testis* route and evaluated the efficacy of the microinjection
508 protocol. In particular, we wished to better characterize the diffusion of the injected solution
509 in the volume of the testis, as we were unable to find any information on this parameter in
510 the literature. The efficacy of microinjection *via rete testis* was assessed using fluorescent i-
511 particles NIRFiP-180, and by measuring their diffusion in testis cross sections examined by
512 microscopy 3 days post-injection (Fig 1). To avoid lesions due to overfilling, the injection was
513 controlled by measuring the expansion of the staining of the peripheral seminiferous tubules
514 during the injection. Injections were stopped when the testes were filled to 2/3 of their
515 capacity (Fig 1A-B). In testis cross sections, the fluorescent i-particles NIRFiP-180 were
516 heterogeneously distributed, and mainly observed in seminiferous tubules located in the
517 peripheral region of the testes, with fewer particles present in the center of the testes (Fig 1C-
518 D). Moreover, no fluorescent i-particles NIRFiP-180 were visible in the peritubular space.
519 These results indicated that microinjection through the *rete testis* did not produce a
520 homogenous distribution of the particles throughout the seminiferous tubules. Nevertheless,
521 the seminiferous tubules remained intact, as no signal was observed in the peritubular space
522 (Fig 1C-D).

523 Next, we assessed the overall safety of the *rete testis* microinjection and electroporation of
524 mRNA and EEV into testes. The safety of the protocol was evaluated by comparing
525 macroscopic and microscopic anatomies of control (injected with control solution, PBS, 0.05
526 % FG), and treated testes (injected either with EEV-*GFP* (PBS, 0.05 % FG) or *GFP*-mRNA (PBS,
527 0.05 % FG)). Three days post-injection, the testes were first observed under a binocular
528 microscope to identify possible macroscopic degeneration of the seminiferous tubules (Fig 2
529 A1 and 2 B1). Degenerations appears as pearly white lesions at the surface of the testis as
530 illustrated in Supp Fig 2 following over electroporation. With the protocol we have developed,
531 no such lesions were observed. Next, the testes were measured and weighed. No statistical
532 differences in length and weight were observed between control and treated testes (Fig 2 A2,
533 A3, B2, B3). Then, microscopic differences were sought by histological analysis of 5 µm
534 sections (Fig 2C). No difference was observed between the control condition and EEV-*GFP* or
535 *GFP*-mRNA on the full cross sections (Fig 2 C1, C2, C3). Next, we observed all the different
536 testicular cells, including all germ cell types and Sertoli cells (Fig 2 D1, D2, D3) for each
537 condition. The layered structure of germ cells was identical in all conditions. Analysis of the
538 histological sections revealed no differences in the tubules area of the testes injected either
539 with EEV-*GFP* or *GFP*-mRNA (Fig 2 E). At last, Harris-Shorr staining of the epididymal sperm
540 cells demonstrated that there were no increases in morphological defects when mRNA and
541 EEV were used in comparison with the control (Fig 2 F4). Taken together, these results suggest
542 that *in vivo* microinjection and electroporation of EEV or mRNA did not perturb
543 spermatogenesis.

544 **2. Analysis of EEV-*GFP* and *GFP*-mRNA testicular expression by whole testis imaging**

545 After validating the injection method, we compared the kinetics of GFP expression and the
546 maintenance of the fluorescent signals for mRNA and EEV. To do so, we injected and
547 electroporated one testis of adult B6D2 mice with EEV-*GFP* (n=129) or with *GFP*-mRNA (n=65).
548 At 0-, 1-, 7-, 15-, 21-, 28-, 35-, 42- and 49-days post-injection, the whole testes were observed
549 under an inverted microscope. The exogenous fluorescence was directly visible at the surface
550 of the testes when illuminated with light at the appropriate wavelength (Fig 3 and Fig 4). No
551 testicular lesions were observed on the testes at any post injection time (Fig 3 A1-H1 and Fig
552 4 A1-F1). In addition, both *GFP*-mRNA and EEV-*GFP* induced GFP expression in the testes (Fig
553 3 A2-H2 and Fig 4 A2-F2). It is worth noting that both vectors induced GFP expression at one

554 day post-injection. However, the duration of fluorescent signals were different. For EEV, GFP
555 fluorescence was still observable on day 42 for 100 % of samples, and 56 % of samples were
556 positive on day 49, indicating that expression lasted around 1.5 months (Fig 4G). In contrast,
557 for mRNA, 100 % of testes were labeled on day 21, but none showed any fluorescence on day
558 28 (Fig 4G). Thus, EEV transfection allowed a considerably longer duration of expression than
559 mRNA. (Fig 3 and 4). It is important to underline that the signal measured is the fluorescence
560 emitted by the GFP. This signal is dependent on both the half-lives of the plasmid/mRNA and
561 the GFP. Therefore, the kinetic of the signal persistence (which is called here expression) is a
562 combination of the persistence of the vector and the synthesized protein. In addition to
563 differences in duration of expression, the GFP expression patterns were clearly different:
564 mRNA produced a large, diffuse pattern, highlighting the shape of the seminiferous tubules;
565 EEV-*GFP* produced a punctiform pattern (Fig 3B and 4B.)

566 These results suggest that *GFP*-mRNA and EEV-*GFP* targeted different seminiferous cell types,
567 such as Sertoli cells and all germline cells, or that there were differences in terms of
568 transfection efficiency. Moreover, the stability of mRNA-GFP was assessed by RT-QPCR in HEK
569 cells and seminiferous tubule cells (Fig. 5). mRNA-GFP was detected for up to 60 hours in HEK
570 cells and for up to two weeks in seminiferous tubule cells (Fig. 5). Together, these results
571 suggest that the long-lasting fluorescence observed in our experiments reflects a combination
572 of transcript stability, local translation within germ cells and the slow protein turnover that is
573 typical of the spermatogenic lineage.

574 ***3.* Kinetics of EEV and mRNA expression assessed by *in vivo* imaging.**

575 To further assess and compare the kinetics of the expression of the two vectors, we expressed
576 exogenous luciferase in the testis using EEV or mRNA and observed the level of luciferase by
577 *in vivo* bioluminescence imaging. For EEV, we took advantage of the fact that the EEV plasmid
578 contains the DNA sequence of the luciferase protein (*CAGs-GFP-T2A-Luciferase*) in addition to
579 the DNA sequence of the GFP fluorescent protein (Supp Fig 1). For mRNA, we injected
580 commercial naked *luciferase*-mRNA into the *rete testis* according to the same protocol as used
581 for *GFP*-mRNA. For this set of experiments, we injected the EEV-*GFP-Luc* and *luciferase*-mRNA
582 into the testes of 6 adult mice on day 0. We injected a similar number of copies of mRNA and
583 EEV. The testes were imaged *in vivo* to detect bioluminescence expression, on day 1 and
584 weekly until disappearance of the signal, no more than 120 days post-injection (Fig 6). For

585 EEV-*GFP-Luciferase*, the bioluminescence induced by transfection was detected from day 1.
586 After a rapid decrease in signal intensity over the first 3 weeks, a weak but constant signal
587 remained detectable for 3 months, then faded away (Fig 6 A1-A2). For *Luciferase*-mRNA,
588 expression was also detected from day 1. The bioluminescence decreased gradually over 3
589 weeks, becoming undetectable thereafter (Fig 6B1-B2). These results are consistent with our
590 previous results (Fig 3) and confirm that EEV allows a longer expression of exogenous protein
591 within the testis. Fig 6C compare the kinetics of expression observed with EEV and mRNA.
592 Overall, our results indicated a stronger expression for mRNA than for EEV, but with
593 expression decreasing rapidly over-time, and almost no remaining signal after 3 weeks. In
594 contrast, residual expression was detectable for several months with EEV.

595 **4. Assessing testicular and cellular *GFP*-mRNA expression using whole testicle optical**
596 **clearing, lightsheet microscopy, and 3D reconstructions**

597 To better characterize the spatial distribution of *GFP*-mRNA expression in the testis, we
598 performed whole testicular optical clearing. On day 0, we injected and electroporated testes
599 with *GFP*-mRNA (n=6). On day 1, we harvested the testes and cleared them with a modified
600 optical clearing protocol, as described in the MM section. After complete clearing (Fig 7 A), we
601 imaged the whole testes using a lightsheet microscope and performed 3D reconstruction from
602 the images stack obtained (videos 1, 2 and Fig 7 B). From this 3D reconstruction, we
603 determined the volume of the testis stained with GFP by measuring the GFP-positive area in
604 each image and multiplying it by the thickness of the z-step (10 µm). Due to optical issues,
605 only half part of the whole testis was acquired, then the sample was turned by 180 ° to acquire
606 the other half part. A total GFP-stained volume of 0.51 mm^3 and 0.23 mm^3 was determined
607 from the face A and the face B, respectively. The corresponding total volume of half part of
608 the testis was measured as 60 mm^3, therefore 0.81 % and 0.24 % of the testis was transfected
609 for the face A and the face B, respectively (Fig 7 B).

610 **5. Assessing GFP cellular expression using whole testicle optical clearing and adaptive**
611 **optics confocal microscopy**

612 Because the GFP fluorescence patterns were different for the two nucleic vectors when
613 observed under the inverted microscope (Fig 3), we wondered whether the same cell types
614 were targeted in both cases. To address this question, the whole optical cleared testes from

615 EEV-*GFP* and *GFP*-mRNA-transfected mice were imaged using a confocal microscope. The
616 different cell types were identified based on their positions within the seminiferous tubule,
617 their cellular shape and their nuclear morphology - revealed by nuclear staining. For instance,
618 Sertoli cells have an oval to elongated nucleus and the cytoplasm presents a complex shape
619 ("tombstone" pattern) along the basement membrane, with long projections that extend
620 toward the lumen. [34]. Round spermatids have small, round and compact nuclei with a
621 nucleolus and are localized between the spermatocytes and elongated spermatids [35].
622 Depending on the stage of the seminiferous epithelium, round spermatids (steps 1–8) and
623 elongated spermatids (steps 9–16) can be observed in adjacent regions of the same tubule,
624 reflecting the continuous and overlapping progression of spermatid differentiation rather
625 than their constant coexistence within the same stage. For EEV-*GFP*, on day 1 post injection
626 and electroporation, a strong punctiform green fluorescence was visible inside the
627 seminiferous tubules (Fig 8 A). Based on the different morphological criteria, this fluorescent
628 signal was detected in spermatocytes, round spermatids and Sertoli cells (Fig 8 BC). On day 7,
629 the GFP signal induced by EEV-*GFP* was reduced and only isolated signals in a few seminiferous
630 tubules (1 per 11 tubules) were observed (Fig 8 D). These signals were associated only with
631 Sertoli cells only (Fig 8 E).

632 Germ cells are non-adherent in culture, which allowed us to distinguish them from potential
633 somatic cells that may not have been completely lysed during the dissociation step. Moreover,
634 germ cells have specific sizes and nuclear morphologies. For example, round spermatids are
635 small and possess small, round, compact nuclei with a nucleolus. Nuclear staining with
636 Hoechst allows us to examine the nuclear morphology of cells expressing GFP and, by
637 combining this observation with cell size measurements, to determine the cell type.

638 Thus, 24 hours post-injection and electroporation, we were able to observe that GFP was
639 expressed in spermatocytes, round spermatids, and elongated spermatids

640

641 For the mRNA vector, on day 1 and day 7 post-injection and electroporation, an intense
642 fluorescence was observed in all the germ cells and in Sertoli cells in the seminiferous tubules
643 (Fig 9A). At the cellular level, this fluorescent signal was associated with spermatogonia,
644 spermatocytes, round spermatids, elongated spermatids, and mature spermatids cells to

645 similar extents for both post-injection times (Fig 9 B, D). In contrast to what was observed with
646 EEV on day 7, no reduction in the number of fluorescent seminiferous tubules was noted when
647 using *GFP*-mRNA, with 8 out of 10 tubules stained (Fig 9 CD).

648 **6. Assessing GFP-mRNA expression in dissociated germ cells following *in vivo* testicular**
649 **electroporation.**

650 To assess the efficiency of *in vivo* mRNA delivery into testicular germ cells, GFP-mRNA was
651 injected and electroporated into the testes on day 0. On day 1, testes were collected,
652 enzymatically dissociated, (Fig supp 10) and the resulting seminiferous tubule cell suspensions
653 were cultured for 12 hours. Live cells were then analyzed by fluorescence microscopy (Fig 10).
654 We observed GFP expression in various germ cell types, including pachytene spermatocytes
655 (53,4 %) (Fig 10 A-), round spermatids (25 %) (Fig 10B-E) and in elongated spermatids (11,4%)
656 (Fig 10 C-E). Fluorescence imaging revealed strong cytoplasmic GFP signals in each of these
657 populations, confirming efficient transfection and translation of the delivered mRNA. These
658 results demonstrate that the *in vivo* injection and electroporation protocol enables effective
659 mRNA transfection across multiple stages of spermatogenesis.

660 **7. Expression of naked *mCherry*-mRNA in testis following electroporation**

661 Heterologous expression is well known to depend on the protein studied, we therefore tested
662 the same reporter proteins to compare the mRNA and EEV vectors in the experiments
663 presented above. Apart from the bioluminescence experiments with luciferase, we compared
664 only GFP protein expression. To validate and confirm the capacity of naked mRNA to express
665 proteins in the testes after injection and electroporation, we further challenged the method
666 with mCherry, another reporter protein (Supp Fig 1BD). We injected homemade naked mRNA
667 coding for mCherry into the testes. As previously with *GFP*-mRNA, no testicular lesions were
668 observed (Supp Fig 3 A1, B1, C1, D1, E1, F1).

669 The assessment of the temporal persistence of testicular mCherry fluorescent protein
670 expression revealed a robust red fluorescence from day 1 post-injection, which remained
671 detectable for at least 15 days (Supp Fig 3 B2, C2, and D2). At the cellular level, the fluorescent
672 signal was detected in germ cells, including spermatogonia, spermatocytes, round spermatids,
673 mature spermatids, and Sertoli cells on days 1 and 7 post-injection (Supp Fig 4).

674 Finally, we compared the kinetics and levels of expression of the three different mRNA
675 molecules, coding for mCherry, GFP and luciferase. By comparing the number of mice
676 expressing *mCherry*-mRNA, *GFP*-mRNA and *luciferase*-mRNA fluorescence/luminescence over
677 21 days, we observed first that expression was detectable for all mRNAs on day 1, and second
678 that the duration of expression was slightly different for the individual mRNAs. For instance,
679 on day 15, 100 %, 80 % and 60 % of mice injected with *GFP*-mRNA, *mCherry*-mRNA, and mRNA-
680 *luciferase*, respectively presented fluorescence/bioluminescence and on day 21, 100 % of mice
681 expressed GFP, whereas no signal was observed for mCherry or Luciferase (Supp Fig 5).

682 **8. Endogenous expression of ARMC2 in germ cells**

683 Before attempting to rescue expression, we felt it was important to better characterize *Armc2*
684 expression in healthy germ cells, and in particular to study the timing of expression.

685 IF was used to determine when ARMC2 protein was detectable during spermatogenesis. For
686 these experiments, dissociated cells from testes were observed to detect the presence of
687 ARMC2 on different spermatogenic cells. ARMC2 was present only in the flagella of the
688 elongated spermatids (Fig 11A and Supp Fig 6A). The specificity of the signal was validated
689 using testicular cells from Armc2 KO mice, where no signal was observed on all spermatogenic
690 cells (Fig. 11B). In transversal sections of WT seminiferous tubules, ARMC2 signal was not
691 present in spermatogonia and spermatocytes (Supp Fig 6B), but detected in spermatid layers.

692 By analyzing the RNA-seq database produced by Gan's team [36], we show that the mRNA
693 encoding ARMC2 starts to be expressed at the pachytene spermatocyte stage, then shows a
694 gradual increase at the round spermatid stage, and finally becomes predominantly expressed
695 at the elongated spermatid stage (Supp Fig 6C), a result in agreement with a post-meiotic
696 function of the protein. Finally, we also consistently observed a staining at the base of the
697 manchette of elongating spermatids but we have no explanation for that (Fig 11A3).

698 In conclusion, the results presented here demonstrate that the ARMC2 protein is expressed
699 and translated at the late stages of spermatogenesis.

700 **9. Co-injection of *Armc2*-mRNA and *eGFP*-mRNA followed by electroporation is safe**
701 **and induces green fluorescence in the seminiferous tubules.**

702 We next tested whether the injection and electroporation of *Armc2*-mRNA molecules had any
703 deleterious effects on testis anatomy and seminiferous tubule structure. We first verified the
704 quality of *Armc2*-mRNA synthesis by transfecting HEK cells and performing Western blot (Supp
705 Fig 7). After this validation, we co-injected *Armc2*-mRNA and *eGFP*-mRNA into the left testes
706 of mice, using the right testes as untreated controls. *eGFP*-mRNA was co-injected to verify and
707 monitor transfection efficiency. The testes were observed under a binocular microscope at
708 different times (3-, 6-, 10-, 15-, 21-, 28- and 35-days) after electroporation to identify possible
709 macroscopic degeneration of the seminiferous tubules. No morphological defects were
710 observed in the testes co-injected with *Armc2*-mRNA and *eGFP*-mRNA. An example of control
711 and injected testes from day 15 is presented in Fig 12 A1, B1. The testes were also weighed at
712 different times post-injection, and the weight ratios of injected testes to non-injected control
713 testes were determined. For all-time points, this ratio was close to 1 (Fig 12 C), confirming that
714 the method and the mRNAs did not cause any injury at the organ level. Next, under blue light,
715 the efficiency of the transfection was assessed by observing the GFP fluorescence at the
716 surface of the testes. GFP fluorescence was observed on testes injected with *Armc2*-mRNA
717 and *eGFP*-mRNA 2 weeks after injection (Fig 12 B2), indicating that the naked mRNA was
718 successfully transfected into testicular cells.

719 **10. Motile sperm cells detected in *Armc2* KO mice following *Armc2*-mRNA injection and**
720 **electroporation into testes**

721 We then assessed whether the injection of *Armc2*-mRNA into the testes in *Armc2* KO mice
722 restored sperm motility. We examined motility of sperm cells present in the caudal part of the
723 epididymis at different times post-injection (3- to 35-days post-injection). For each condition,
724 between 3 and 16 KO mice were used.

725 The *Armc2* KO model used is known to produce sperm cells with short and irregular flagella
726 that are therefore immotile on day 0. No motile sperm were observed on days 3, 6, 10, 15 or
727 28 after surgery (Fig 13 A). However, motile sperm cells were found in the epididymis of some
728 *Armc2* KO mice at 21- and 35-days post-treatment (Fig 13 A). Indeed, 1 in 3 mice had motile
729 sperm at 21 days post-surgery, rising to 3 in 4 mice at 35 days post-injection. Nevertheless,
730 the number of motile sperm observed remained low: 5.5 % after 21-days and 7.15 % after 35-
731 days post-injection (Fig 13 A1). Although the number of motile sperm remained low: 5.5% at
732 21 days and 7.15% at 35 days post-injection (Fig. 13 A1), this recovery represents a substantial

733 improvement considering the small fraction of germ cells reached by the current
734 electroporation method (Fig 6 B). The sperm motility parameters of *Armc2*$^{-/-}$-rescued motile
735 sperm were characterized in comparison to those of *Armc2*$^{+/+}$ sperm using the computer-
736 assisted semen analysis (CASA) system (Fig 13 A2). These parameters included VAP, VSL, VCL,
737 ALH, BCF, and STR. We have observed significant differences between WT and rescued sperm.
738 In particular, the VSL and LIN parameters are lower for rescued sperm. Next sperm were
739 sorted as progressive, intermediate, hyperactivated, or slow according to motility parameters
740 of motile sperm and recorded from their track (Figure 13 A3). The percentage of
741 hyperactivated sperm and the proportion of intermediates in the *Armc2*$^{-/-}$-rescued motile
742 sperm population were found to be increased in comparison to the control. Videos showing
743 sperm motility in different conditions are available in the online material associated with this
744 article (Videos 3 to 6).

745 After verifying motility, we looked at the morphology of the spermatozoa present in the cauda
746 epididymis. Six days after injection of *Armc2*-mRNA, the cells detected were mostly round cells
747 and abnormal spermatozoa with a short or coiled flagellum measuring between 7 and 20 µm.
748 The same cell types were observed at 3-, 10-, 15- and 28-days post-surgery. In contrast, the
749 motile sperm detected on days 21 and 35, had a normal morphology with a long flagellum
750 (greater than 100 µm) and a hook-shaped head (Fig 13 B and Supp Fig 8).

751 **11. Motile sperm cells detected in *Armc2* KO mice following *Armc2*-mRNA injection and**
752 **electroporation into testes are fertile**

753 We subsequently evaluated the efficacy of *Armc2*-mRNA injection into the testes of *Armc2* KO
754 mice in restoring sperm fertility. The fertility outcome was assessed through *in vitro*
755 *fertilization* (IVF) and intracytoplasmic sperm injection (ICSI) experiments. The sperm rescued
756 from *Armc2*$^{-/-}$ mice were capable of successfully fertilizing eggs and producing embryos at the
757 two-cell stage by IVF (Fig 14 A-B-C). The 2-cell embryo formation observed after IVF serves as
758 a strong indication of partial functional recovery. Notably, 62.7% of two-cell embryos were
759 obtained with the *Armc2*$^{-/-}$-rescued sperm by IVF, compared to only 2.67% with the *Armc2*$^{-/-}$
760 sperm. Three % of eggs became 2-cell embryos when fertilized with sperm from *Armc2*$^{-/-}$, a
761 rate not significantly different to that observed for eggs incubated 24 h without sperm, and
762 likely corresponding to parthenogenesis activation (Fig 14 A1-A2-A3-A4-B).

763 To gain further insight, a comparative analysis of the developmental outcomes of mouse
764 embryos generated by ICSI with spermatozoa from wild-type (WT), *Armc2*$^{-/-}$ and *Armc2*$^{-/-}$
765 treated mice was performed. It should be noted that in case of *Armc2*$^{-/-}$ treated mice, the ICSI
766 procedure was performed only with the motile *Armc2*$^{-/-}$-rescue spermatozoa. The percentage
767 of live injected oocytes that reached the blastocyst embryos was 46% for WT spermatozoa,
768 25% for *Armc2*$^{-/-}$-rescued spermatozoa and 13% for *Armc2*$^{-/-}$ spermatozoa (Supp Fig.9). The
769 findings indicate that the developmental potential of the embryos was enhanced when *Armc2*$^{-}$
770 $^{/-}$-rescued sperm were utilized as opposed to *Armc2*$^{-/-}$ sperm.

771 Overall, these results demonstrate that the *Armc2*$^{-/-}$-rescue motile spermatozoa can
772 successfully fertilize eggs.

773 **Discussion**

774 The challenge of treating male infertility remains to be addressed. Current assisted
775 reproduction techniques (ARTs) are unable to treat all patients, and alternative strategies
776 need to be developed to meet the legitimate desire to be a father. The aim of this study was
777 to evaluate the potential of naked mRNA as a means to induce an expression of exogenous
778 proteins in male germ cells in a preclinical adult mouse model. Based on previous studies using
779 electroporation, we investigated whether the combination of the injection of naked mRNA
780 and in *vivo* electroporation could lead to an efficient protein expression in spermatogenic
781 cells. We chose to first study the efficiency of capped and poly(A)-tailed mRNA coding for
782 reporter proteins and compared the results to those obtained with a non-integrative
783 enhanced episomal vector plasmid. No EEV plasmid has ever been tested in the context of
784 infertility treatment before this study.

785 Using an adult mouse model, we optimized the micro-injection and electroporation method
786 described by Michaelis et al [17]. We show that the microinjection through the *rete testis* did
787 not provide a homogenous distribution of the particles throughout the seminiferous tubules.
788 Nevertheless, the seminiferous tubules remained intact, with no signal detected in the
789 peritubular space. The peripheral expression observed was due to the close vicinity of cells to
790 the electrodes, and to a peripheral dispersal of the injected solution, as shown by the
791 distribution of the fluorescent i-particles NIRFiP-180. Our results also showed that the
792 combination of injection and electroporation did not perturb spermatogenesis when electric

793 pulses are carefully controlled. Using such a protocol, we were able to induce the expression
794 of 3 reporter proteins, GFP, mCherry and luciferase in the testis by mRNA
795 injection/electroporation.

796 Using whole testicular optical clearing, the reporter proteins were synthesized from the
797 injected mRNA in different types of cells including Sertoli cells, spermatogonia, spermatocytes,
798 round spermatids, and mature spermatids from day 1, and were still detectable after 1 week.
799 These results deserve two comments: first, the expression is very fast and synthesized protein
800 is detectable 24 h injection, second all cell types have the ability to translate mRNAs.
801 Furthermore, the fact that we observed motile sperm at 21 days after injection confirms that
802 spermatids are transfected and that the translation of the protein of interest is possible at this
803 stage. For EEV, we have a similar result at day 1. However, the yields of seminiferous tubules
804 and cellular transfection are lower. In particular, a lower level of transfection of germ cells was
805 observed than with the mRNA. It is worth noting that after one week, the reporter proteins
806 synthesized from injected EEV, were only discernible in the Sertoli cells.

807 Based on whole testes fluorescence and, for the first time, *in vivo* bioluminescence imaging of
808 testes, we characterized the kinetics of mRNA expression. The signal measured is the
809 fluorescence or the bioluminescence emitted by the GFP or luciferase. This signal is dependent
810 on both the half-lives of the plasmid/mRNA and the proteins. Therefore, the kinetic of the
811 signal persistence is a combination of the persistence of the vector and the synthesized
812 protein. Although naked mRNAs are generally short-lived in somatic cells, several factors likely
813 explain the prolonged detection of reporting proteins. RT-qPCR analysis showed that mRNA-
814 GFP persisted for up to 60 hours in HEK cells and two weeks in seminiferous tubule cells (Fig.
815 5), indicating enhanced stability in the testicular environment. Codon optimization and
816 chemical modifications (capping, polyadenylation) are known to improve mRNA stability and
817 translation efficiency [37-40] .

818 The persistence of the reporter proteins is in line with the fact that proteins involved in
819 spermatogenesis exhibit a markedly low turnover rate [41]. This is due to the fact that these
820 proteins are stored within sperm organelles, such as the acrosome, manchette, centrioles or
821 fibrous sheath. These organelles, made during spermiogenesis, remain stable for weeks until
822 the fertilization process occurs because there is no protein synthesis in mature sperm. For

823 example, the $Ca_v3.2$ calcium channel is expressed during meiosis at the pachytene stage and
824 contributes to calcium signaling during acrosome reaction [42-45].

825 When using the EEV vector, expression persisted for longer – up to 119 days – due to the
826 intrinsic property of the EEV plasmid which allows its replication in synchronous manner with
827 the host genome.

828 These results suggest that although EEV expression lasted longer, mRNAs, by targeting more
829 efficiently male germ cells and allowing higher transfection yields of seminiferous tubules,
830 could be a more effective and potent tool to express exogenous proteins in germ cells. By
831 expressing a missing protein in the case of male infertility due to monogenic causes, it could
832 be possible to restore failed spermatogenesis and thus to treat infertility.

833 **ARMC2 is expressed in late spermatogenesis stages**

834 We show that ARMC2 was localized in the flagellum of spermatids obtained by enzymatic
835 dissociation. No *Armc2* expression was detected in earlier germ cell type lineages like
836 spermatogonia or spermatocytes. These results suggest that the ARMC2 protein is expressed
837 late during spermatogenesis, which explains why motile sperm were found in the cauda
838 epididymis from 3-weeks after injection in our treated mice. Indeed, full spermiogenesis (from
839 round cells to sperm) takes around 15 days [46], and the journey across the epididymis lasts
840 around 8 days, making a total of 3-weeks. Our results also confirm those recently published
841 by Lechtreck et al. [47] from their study of the role of ARMC2 in the Intra-Flagellar Transport
842 (IFT) of radial spokes in *Chlamydomonas.* They suggested that the transport of the radial
843 spokes along the flagellum involves ARMC2, acting as an IFT adapter [47]. The presence of
844 ARMC2 in the flagella of elongating spermatid supports this hypothesis.

845

846 **Exogenous *Armc2*-mRNA expression rescued the motility of oligo-astheno-**
847 **teratozoospermic sperm**

848 This is the first demonstration that proteins can be expressed in the testis following
849 electroporation with optimized, capped and poly(A)-tailed mRNA.

850 Our objective was to develop a new targeted therapeutic approach for infertility associated
851 with monogenic defects. The objective of this preclinical study was to ascertain the efficacy of
852 messenger RNA (mRNA) in expressing a missing protein, ARMC2, in a mouse model exhibiting
853 oligo-astheno-teratozospermia due to the absence of *Armc2*, with the aim of restoring

854 flagellar motility and fertility. Our results strongly suggest that the strategy did not alter
855 spermatogenesis, as injection and electroporation of *Armc2*-mRNA or EEV-*Armc2* had no
856 effect on testicular morphology or weight. More importantly, the technique was effective,
857 with motile sperm cells found in cauda epididymis 3 and 5 weeks after *Armc2*-mRNA injection
858 into testes from *Armc2* KO males. Nevertheless, it should be noted that not all injected mice
859 were efficiently treated. For example, only 87.5% of the treated mice (14 of the 16) exhibited
860 motile sperm after 5 weeks. The absence of motile sperm at 5 weeks may be attributed to the
861 specific types of spermatogenic cells that were transfected during the electroporation phase.
862 It is possible that the transfected cells may differ between individuals, potentially influenced
863 by the injection and the position of the electrodes during electroporation. If the mRNA
864 transfection occurs in a spermatogonia, it may take more than six weeks (including the time
865 required to cross the epididymis) before motile epididymal sperm cells emerge. This potential
866 timeline could explain the absence of motile sperm in some mice at 5 weeks.

867 Due to the quantity of motile sperm obtained, it was not possible to produce offspring through
868 natural mating. Nevertheless, the rescued *Armc2*$^{-/-}$ sperm displayed normal morphology and
869 motility and were competent for *in vitro* fertilization (IVF) and intracytoplasmic sperm
870 injection (ICSI). The rescued sperm successfully fertilized oocytes and produced embryos that
871 developed to the two-cell stage following IVF, and to the blastocyst stage after ICSI. these
872 findings support a partial functional recovery of the sperm population. Taken together, these
873 results demonstrate that mRNA electroporation can partially restore sperm function by
874 rescuing motility and enabling early embryonic development. This proof-of-concept supports
875 the feasibility of mRNA-based protein supplementation in spermatogenic cells, paving the way
876 for future therapeutic development.

877

878 It worth to note that the significant modifications of the CASA parameters observed for
879 rescued sperm did not impact their fertilizing potential. Naked mRNA
880 injection/electroporation is therefore a promising method to treat infertility. In contrast, no
881 motile spermatozoa were found after injection/electroporation of EEV-*Armc2*, confirming our
882 previous results suggesting that this nucleic tool does not efficiently enter or transfect germ
883 cells.

884 Despite this success, the transfection rate deserves to be improved to obtain a larger number
885 of sperm cells to produced offspring through natural mating. To increase the testicular
886 transfection rate, encapsulation of mRNA into lipids nanoparticles could be used, as used for
887 Covid vaccination [48]. During the writing of this manuscript, Dong team [49], used a self-
888 amplifying RNA (saRNA) encapsulated in cholesterol-amino-phosphate derived lipid
889 nanoparticle to restore spermatogenesis in infertile mice. They successfully restore the
890 expression of the DNA Meiotic Recombinase 1 (DMC1) [50-52] in *Dmc1* KO infertile mice by
891 injecting a self-amplifying RNA-*Dmc1* in the testes. saRNA are genetically engineered replicons
892 derived from self-replicating single-stranded RNA viruses [53]. The saRNA contains the
893 alphavirus replicase genes and encodes an RNA-dependent RNA polymerase (RdRP) complex
894 which amplifies synthetic transcripts in situ and the target RNA sequence. The target RNA is
895 expressed at high levels as a separate entity. As a result of their self-replicative activity, saRNAs
896 can be delivered at lower concentrations than conventional mRNA to achieve comparable
897 expression levels [54]. Moreover, saRNA constructs need to be condensed by a cationic carrier
898 into a nanoparticle measuring ~100 nm to enable their uptake into target cells and protect the
899 saRNA from degradation [55]. Finally, saRNA will amplify the RNA without cellular regulation.
900 For all these reasons, if such a strategy is to be pursued, a potential toxicity effect due to
901 saRNA over expression must be investigated in the testes and progeny. Another difficulty with
902 saRNA relates to the size of the molecular construct. saRNA sequences are large and complex.
903 The length of the sequence RdRP is around 7 kilobases, which often makes the full length of
904 saRNA more than 9 kilobases once the sequence for the protein of interest has been
905 integrated [55]. Dong et al. [49] successfully used their saRNA construct to rescue
906 spermatogenesis failure induced by the absence of the small protein Dmc1 (37 KDa), but it
907 may be more challenging with larger proteins such as the structural proteins involved in OAT,
908 including the 98-kDa ARMC2 [25].
909 Our next step will be to assess whether encapsulating *Armc2*-mRNA in LNP-CAP could allow a
910 larger number of germ cells to be transfected.

911 **Naked mRNA, a new therapeutic strategy to treat severe infertility**

912 Non-obstructive Azoospermia (NOA) and severe oligozoospermia (SO) are the most severe
913 disorders of spermatogenesis and are the most likely to be of genetic origin. NOA is defined
914 by the complete absence of spermatozoa in the ejaculate. Approximately 10–15 % of infertile

915 men have azoospermia, and a further 15 % have SO [56]. For patients with NOA, few clinical
916 solutions are currently available. Generally, testicular sperm extraction is attempted to collect
917 some spermatozoa from the seminiferous tubules, which can then be used for ICSI [57]. When
918 no sperm are retrieved, intra-conjugal conception is impossible. The results of this study
919 strongly suggest that transient mRNA expression of a missing protein in NOA testes by
920 electroporation could be sufficient to produce normal sperm for IVF and obtain embryos.

921 In conclusion, this work provides the first demonstration that *in vivo* testicular injection and
922 electroporation of capped and poly(A)-tailed mRNA can efficiently transfect male germ cells
923 and produce proteins with sufficient stability to support spermatogenic progression. Our
924 comprehensive analysis revealed that mRNA electroporation is more efficient than episomal
925 vector delivery, despite shorter persistence of expression. Importantly, *Armc2*-mRNA
926 electroporation was able to partially rescue sperm motility and fertilizing ability in *Armc2*$^{-/-}$
927 mice, representing a crucial first step toward developing mRNA-based strategies to correct
928 monogenic causes of male infertility.

929

930 **Legends**

931 **Figure 1: Distribution of I-particles NIRFIP-180 in testis injected *via* the rete testis route.**

932 (A) A solution containing 0.05 % Fast Green and 1 % fluorescent i-particles NIRFiP-180 was
933 prepared, 10 µL was injected into the seminiferous tubules of adult males, through the *rete*
934 *testes* and its efferent channels. Injection was performed at constant pressure under a
935 binocular microscope. The progression of filling of the seminiferous tubules was monitored
936 thanks to the Fast Green. (B) The testes were only filled to 2/3 capacity in order to prevent
937 damage to the tissue. (C) Representative distribution of fluorescent i-particles NIRFiP-180 in a
938 whole cross-section of an injected testis. Nuclei were counterstained with DAPI (blue
939 emission) to reveal tubules. (D) Enlargement of a seminiferous tubule showing particles
940 localized inside the lumens of the tubules. Scales bars: 1 mm and 500 µm.

941 **Figure 2: *In vivo* injection and electroporation do not alter the morphological structure of**
942 **the testes, seminiferous tubules, or sperm cells.**

943 (A, B) Testicular morphology was not affected by *in vivo* injection and electroporation of EEV-
944 *GFP* (A) or *GFP*-mRNA (B). Controls correspond to contralateral testes injected/electroporated
945 with control solution (PBS, 0.05 % FG). (A1, B1) comparison of the testicular morphology of
946 adult testes injected with nucleic acid vectors or control solutions. (A2, B2) Comparison of
947 testicular weight and (A3, B3) testicular length on day 7 after injection/electroporation. Data
948 are represented as a box plot median (n=4 for each condition). A Wilcoxon matched pairs test
949 was used to assess the significance of any differences in testis weights and lengths, and p
950 values of ≤ 0.05 were considered statistically significant. (C) Intact testicular structure after *in*
951 *vivo* injection and electroporation with EEV-*GFP* and *GFP*-mRNA. Comparison of testicular
952 cross section structures. Testes paraffin sections were stained with eosin/hematoxylin and
953 observed by light microscopy (20x magnification). (C1) Control, (C2) EEV-*GFP* injected and (C3)
954 *GFP*-mRNA injected. Scales bars: 1000 µm.

955 (D) Seminiferous tubule structures are not affected by *in vivo* injection and electroporation
956 with EEV-*GFP* and *GFP*-mRNA. Enlargement of cross sections showing the fine structure of a
957 seminiferous tubule for control (D1), EEV-*GFP* (D2) and *GFP*-mRNA (D3). In each tubule the
958 different layers of spermatogenic cells are indicated, Sertoli cells (S), Spermatogonia (Sg),

959 Spermatocytes (Scytes), rounds Spermatids (Stids) mature spermatids cells (m-Sptids), Leydig
960 cells (L). Scales bars: 20 µm.

961 (E) The area of seminiferous tubules is not affected by *in vivo* injection and electroporation
962 with EEV-*GFP* and *GFP*-mRNA. Comparison of the seminiferous tubule diameter after injection
963 of nucleic acid vectors or control solutions. Data are represented as a box plot median. The
964 areas of seminiferous tubules (μm^2) were measured for round cross sections of $n > 35$ tubules
965 per testis section (n= 5 testis sections per condition). Statistical significance was verified using
966 a student's *t*-test.

967 (F) Injection/electroporation do not impact epidydimal sperm cells. Representative sperm
968 observed by light microscopy on day 7 after injection/electroporation with Control solution
969 (F1), EEV-*GFP* (F2), or *GFP*-mRNA (F3). Scale bars: 10 µm. (F4) Percentage of normal
970 epidydimal sperm cells in each condition. The number of males were n=5 for EEV-*GFP*; n=6 for
971 *GFP*-mRNA and n=9 for WT. More than 150 sperm by males were analyzed. Statistical
972 significance was verified using a one-way ANOVA test.

973 **Figure 3: Kinetics of EEV-*GFP* expression following *in vivo* injection/electroporation: whole**
974 **testicular expression**

975 (A1-H1) Whole-mount testes on days 0, 1, 7, 14, 21, 28, 35 and 42 after *in vivo*
976 injection/electroporation with EEV-*GFP*. (A2-H2) Under fluorescence observation, GFP
977 expression was detectable in transfected testes from 12-week-old B6D2 mice. (C3-H3) Insets
978 show the absence of autofluorescence in non-transfected control testes, observed under 4X
979 magnification. The GFP expression presented a punctiform pattern in seminiferous tubules
980 and was detected from 1 day to 42 days. Scales bars: 1 mm and 100 µm.

981 **Figure 4: Kinetics of *GFP*-mRNA expression following *in vivo* injection/electroporation:**
982 **whole testicular expression**

983 (A1-F1) Whole-mount testes on days 0, 1, 7, 15, 21 and 28 after *in vivo* injection/
984 electroporation with *GFP*-mRNA. (A2-F2) Under fluorescence observation, GFP expression was
985 detectable in transfected testes from 12-week-old B6D2 mice. (A3-F3) Insets show the
986 absence of autofluorescence in non-transfected control testes, observed under 4X
987 magnification. The GFP expression presented a continuous pattern in seminiferous tubules
988 and was detected from day 1 to day 15. Scale bars: 1 mm and 100 µm.

989 (G) Comparison of the percentage of injected mice exhibiting reporter gene expression. Mice
990 injected with *GFP*-mRNA exhibited GFP expression from day 1 to day 21. Mice injected with
991 EEV-GFP exhibited GFP expression from day 1 to day 49. (for EEV-*GFP* n=11 on day 1; n=13 on
992 day 2; n=10 on day 3; n=14 on day 7; n= 5 on day 10; n= 12 on day 15; n=11 on day 21; n= 12
993 on day 28; n=15 on day 35; n=17 on day 42 and n=9 on day 49) ; (for *GFP*-mRNA n=3 on day
994 1; n=4 on day 3; n=15 on day 7; n= 21 on day 15; n=15 on day 21 and n= 5 on day 28).

995 **Figure 5. Stability of mRNA-GFP in HEK cells and seminiferous tubule cells.**
996 **(A–C) Analysis of mRNA-GFP stability in HEK cells.** (A) Quantification of relative GFP mRNA
997 levels (2^-ΔCT) at 24-, 48-, and 60-hours post-transfection. (B) RT-qPCR amplification curves
998 of GFP and (C) GAPDH transcripts at the indicated time points, showing a progressive decrease
999 in GFP signal over time while GAPDH expression remained constant.
1000 (D–F) Analysis of mRNA-GFP stability in mouse seminiferous tubule cells after *in vivo* injection
1001 and electroporation. (D) Quantification of relative GFP mRNA levels (2^-ΔCT) at 0-1-, 7-, and
1002 14-days post-transfection. (E) RT-qPCR amplification curves of GFP and (F) ACTB transcripts at
1003 corresponding time points. mRNA-GFP remained detectable for up to two weeks in
1004 seminiferous tubules, indicating enhanced transcript stability in the testicular environment.

1005 **Figure 6: Kinetics of EEV and mRNA expression by *in vivo* bioluminescence imaging.**

1006 (A) *In vivo* bioluminescence imaging quantification of luciferase expression over time following
1007 injection/electroporation of EEV-*GFP-luc*. (A1) EEV-*GFP-Luc* was injected into the testes and
1008 electroporated on day 0. Bioluminescence signal was quantified at several time points. Results
1009 are expressed as a percentage of the maximal signal (mean ± SEM; n=5 mice up to D2; n=4
1010 from D3 to D28; n=3 from D35 to D98 and n=3 from D105 to D119). (A2) *In vivo*
1011 bioluminescence images of a representative mouse at several time points after administering
1012 EEV-*GFP-LUC* or PBS, and ex vivo bioluminescence images of testes after 119 days.

1013 (B) *In vivo* bioluminescence imaging quantification of luciferase expression over time induced
1014 by injection/electroporation of *LUC*-mRNA**.** (B1) *LUC*-mRNA was injected into the testes and
1015 electroporated on day 0. Bioluminescence signal was quantified in the whole testis at several
1016 time points. Results are expressed as a percentage of the maximal signal (mean ± SEM; n = 5
1017 mice). (B2) *In vivo* bioluminescence images of a representative mouse at several time points

1018 after administering *LUC*-mRNA or PBS, and *ex vivo* bioluminescence images of caput, testes,
1019 and cauda after 28 days.

1020 (C) Decay over time of the number of mice expressing reporter genes. Mice were injected on
1021 day 0 with *LUC*-mRNA or EEV-*GFP*-*LUC* and the number of mice showing bioluminescence in
1022 the testis was counted at different time points, from day 1 to day 119. For EEV-*GFP*: n=13 at
1023 D1; n=13 at D2; n=4 from D3 to D28; n=3 from D35 to D98 and n=3 from D105 to D119. For
1024 *LUC*-mRNA: n = 5 mice for all-time points.

1025 **Figure 7: Testicular and cellular *GFP*-mRNA expression measured on optically cleared testis**
1026 **after 3D image reconstructions from lightsheet microscopy imaging.** Testes were
1027 injected/electroporated with *GFP*-mRNA on day 0. On day 1, whole testes were fixed and
1028 subjected to optical clearing. (A) Testes were observed before and after optical clearing on a
1029 binocular microscope. The right image shows the transparency of the testis after complete
1030 clearing, revealing the blue mesh throughout the organ. (B) The 3D internal structure of a
1031 cleared testis was reconstructed from the lightsheet microscopy images. The reconstruction
1032 was possible only for a half testis due to optical issues. Two opposing faces of the same testis
1033 are presented, allowing the distribution of GFP fluorescence throughout the seminiferous
1034 tubules to be measured. Pink fluorescence corresponds to the autofluorescence of interstitial
1035 cells located around the seminiferous tubules. Scale bars A: 1 mm and B: 500 µm.
1036

1037 **Figure 8: Cellular expression of EEV-*GFP* following *in vivo* injection/ electroporation**. Testes
1038 were injected/electroporated with EEV-*GFP* on day 0. On day 1 and on day 7, whole testes
1039 were fixed and subjected to optical clearing. Cleared tested were observed by fluorescence
1040 microscopy. (A1-A3) On day 1, transfected seminiferous tubules showed dotted green
1041 fluorescence at low magnification (10x/0.45). Nuclei were counterstained with DAPI (blue
1042 staining) to reveal the structure of the seminiferous tubules. At the cellular level, fluorescence
1043 was detectable (B1-B3) in germ cells including Spermatogonia (Sg), Spermatocytes (Scytes)
1044 and round Spermatids (RStids), as well as (C1-C3) in Sertoli cells (SC). (D1-D3) On day 7, the
1045 GFP signal was lower at low magnification (10x/0.45) and detectable (E1-E3) only in Sertoli
1046 cells (40x/1.15 WI) (n=3) (PTc =Peri-tubular myoid cell). E4 is an enlargement of the red square
1047 in E3, allowing the cell type to be identified. Scale bars: 100 µm, 15 µm and 3 µm.

1048 **Figure 9: Cellular expression of *GFP*-mRNA following *in vivo* injection/electroporation**.
1049 Testes were injected/electroporated with *GFP*-mRNA on day 0. On day 1 and day 7, whole
1050 testes were fixed and subjected to optical clearing. Cleared testes were observed by
1051 fluorescence microscopy. (A1-A3) On day 1, transfected seminiferous tubules showed strong
1052 broad-ranging green fluorescence at low magnification (10x0/0.45). Nuclei were
1053 counterstained with DAPI (blue staining) to reveal the structure of the seminiferous tubule. At
1054 the cellular level, fluorescence was detectable in germ cells (B1-B3) including Spermatogonia
1055 (Sg), Spermatocytes (Scytes) and round Spermatids (RStids), mature spermatids cells (m-
1056 Sptids) and Sertoli cells (SC). B4 is an enlargement of the red square in B3, allowing the cell
1057 types to be identified. (D1-D3) On day 7, the GFP signal remained strong at low magnification
1058 (10x/0.45) and was still detectable in (E1-E3) all germ cell types and Sertoli cells (40x/1.15 WI)
1059 (n=3). E4 is an enlargement of the red square in E3, showing that testicular sperm were also
1060 stained. Scale bars: 100 µm, 15 µm and 3 µm.

1061 **Figure 10: GFP-mRNA expression in germ cells following *in vivo* injection and**
1062 **electroporation.**
1063 Testes were injected and electroporated with GFP-mRNA on day 0. On day 1, the testes were
1064 dissociated, and the resulting seminiferous tubule cell suspension was cultured for 12 hours.
1065 Live seminiferous cells were then observed by fluorescence microscopy (LD plan-Neofluar
1066 40x/0.6 Korr M27). (A) Representative images of GFP expression in elongated sperm. Panels
1067 show brightfield, DAPI staining (nuclei in blue), GFP fluorescence (green), merged channels,
1068 and overlay with brightfield. Magnified views of selected cells are shown below each row,
1069 highlighting strong cytoplasmic GFP signals in elongated sperm. (B) Representative images of
1070 GFP expression in pachytene spermatocytes. Same panel layout as in (A). Enlarged views show
1071 paired pachytene spermatocytes displaying robust cytoplasmic GFP fluorescence. (C)
1072 Representative images of GFP expression in round spermatids. Same panel layout as above,
1073 showing isolated round spermatids with clear GFP fluorescence in the cytoplasm. Higher
1074 magnification confirms successful mRNA transfection and translation. Scale bars: 50 and 5 µm.
1075 (D) Percentage of GFP-positive and GFP-negative cells in the analyzed population. (E)
1076 Distribution of GFP-positive cells across different germ cell types, showing higher uptake in
1077 spermatocytes compared with round and elongated spermatids. (F) Average diameters of

1078 spermatocytes and round spermatids, indicating cell size differences in the population
1079 analyzed.

1080 **Figure 11: ARMC2 localization in dissociated testicular cells observed by**
1081 **immunofluorescence.** Cells from WT and *Armc2* KO mice were counterstained with Hoechst
1082 (A1-B1) and stained with antibodies against tubulin (A2-B2, green signal) and ARMC2 (A3-B3,
1083 red signal). (A4-B4) overlay of the different staining. In WT mice, ARMC2 is located in the
1084 flagellum of spermatids. In KO mice, no ARMC2 signal (red fluorescence) was observed in any
1085 cells.

1086 **Figure 12: *In vivo* co-injection of *Armc2*-mRNA and *eGFP*-mRNA followed by electroporation**
1087 **do not affect testes morphology and weight.** Adult WT mouse testes were injected with a
1088 solution containing *Armc2*-mRNA and *eGFP*-mRNA. After injection, the testes were
1089 electroporated and mice were euthanized two weeks later. (A): Whole testis under white and
1090 blue lights on a fluorescence microscope (A1): control testes not injected/electroporated (A2):
1091 testes injected with *Armc2*-mRNA and *eGFP*-mRNA. *eGFP*-mRNA was co-injected to follow the
1092 transfection efficiency. (B): Ratio of injected/electroporated testis weights to control testis
1093 weights at several time points post-injection (3-, 6-, 10-, 15-, 21-, 28- and 35-days post-
1094 surgery). n= 1 mouse per time.

1095 **Figure 13: Sperm motility is restored in *Armc2* KO mice at 21 and 35 days after injection and**
1096 **electroporation of *Armc2*-mRNA**. (A) Adult *Armc2* KO mouse testes were injected with a
1097 solution containing *Armc2*-mRNA. After injection, the testes were electroporated. At different
1098 times (3-, 6-, 10-, 15-, 21-, 28-, and 35-days *post*-injection), sperm were extracted from the
1099 cauda epididymis of the injected testis, and the sample was then examined with a CASA
1100 system to identify the percentage of motile spermatozoa (A1). n= 2 for day 15, n= 3 for days
1101 3, 6 and 21, n= 4 for day 10, and n= 5 for days 28 and 35. (A2) Sperm motility parameters of
1102 *Armc2*$^{-/-}$ -rescued sperm in comparison to *Armc2*$^{+/+}$ sperm. The motility parameters measured
1103 were: averaged path velocity (VAP); straight line velocity (VSL); curvilinear velocity (VCL);
1104 amplitude of lateral head displacement (ALH); beat cross frequency (BCF); straightness (STR);
1105 linearity (LIN). Black dots: sperm cells from *Armc2* null mice, green dots: sperm cells from
1106 *Armc2* null mice 35 days after injection with *Armc2*-mRNA. Results are expressed as
1107 mean ± SD. (A3) Sperm motility population of *Armc2*$^{-/-}$ -rescued sperm in comparison to
1108 *Armc2*$^{-/-}$ sperm. Black column: sperm cells from *Armc2* null mice, green column: sperm cells

1109 from *Armc2* null mice 35 days after injection with *ARmc2*-mRNA. Statistical significance was
1110 verified using a Mann-Whitney sum test. Data are displayed as mean ± SEM. P values of * ≤
1111 0.05, ** ≤ 0.01, or *** ≤ 0.001 were considered to represent statistically significant
1112 differences.

1113 (B) Morphology of sperm cells in *Armc2* KO mice injected or not with *Armc2*-mRNA. (B1-B2):
1114 microscopic observation of epididymal sperm cells from a mature WT mouse. (B3-B4):
1115 epididymal sperm cells from a mature *Armc2* KO mouse 35 days after
1116 injection/electroporation with *Armc2*-mRNA. (B5-B6): epididymal sperm cells from a control
1117 *Armc2* KO male. Normal sperm cells were observed in the injected condition with *Armc2*-
1118 mRNA. (White arrows), Scale bars: 10 µm.

1119 **Fig 14: *Armc2* $^{-/-}$-rescued sperm can fertilize eggs and produce embryos by IVF.**

1120 (A) Illustrations showing eggs/embryos obtained 24 h after egg collection in the following
1121 conditions. (A1) W/O sperm (A2) IVF with *Armc2*$^{-/-}$ sperm from *Armc2*$^{-/-}$ males (#444), (A3) IVF
1122 with *Armc2*$^{-/-}$ rescued sperm from *Armc2*$^{-/-}$ males treated with mRNA-*Armc2* (males #399,
1123 #389, and #406) and (A4) IVF with WT B6D2 sperm. Green and red asterisks show 2-cell
1124 embryos, red asterisks showing 2-cell embryos obtained by parthenogenesis. White asterisks
1125 show unfertilized oocytes or degenerated. (B) Histograms showing the mean percentage ± SD
1126 of alive eggs reaching the 2-cell embryo stage at 24 hours after IVF without sperm (n=4), with
1127 *Armc2*$^{-/-}$ sperm (n=4), with *Armc2*$^{-/-}$ rescued sperm (n=5), and with WT B6D2 sperm (n=5).
1128 Statistical significance was verified using a one-way ANOVA test. (C) The table presents the
1129 data pertaining to the number of two-cell embryos obtained by IVF with *Armc2*$^{-/-}$ rescued
1130 sperm from five different *Armc2*$^{-/-}$ males treated with mRNA-*Armc2* (males #399, #406, #389,
1131 #388, and #395). The data is presented in terms of the percentage of two-cell embryos
1132 obtained in relation to the total number of eggs collected.

1133 **Supp Fig 1: EEV and mRNA maps**

1134 (A) EEV-plasmid map. The EEV-plasmid contains GFP, EVB ori, GFP, Luciferase, and EBNA
1135 sequences under the control of the GAGs promotor. (B) The mCherry plasmid contains the
1136 mCherry gene under the control of a T7 promotor. (C) The EEV-*Armc2* plasmid contains GFP,
1137 oriP, EBNA and *Armc2* sequences under the control of the CMV and T7 promotors. (D)
1138 *mCherry*-mRNA was synthesized as described in Material and Methods. It was validated by

1139 agarose gel electrophoresis: Lane 1: DNA size marker ladder (100 bp), lane 2: capped *mCherry*-
1140 mRNA (IVT product), lane 3: *mCherry*-mRNA after DNAse treatment. Capped and poly A tailed
1141 *mCherry*-mRNA migrated to the expected size of 876 bp.

1142 **Supp Fig 2: Damaged tubules observed by optical microscopy following overstimulation**

1143 Adult mouse testes were *in vivo* injected and over electroporated using 10 square electric
1144 pulses to induce damage. (A) Control testis (no injection/electroporation). (B1-B2) Over
1145 electroporated testes showing damaged tubules as pearly white striations. Scale bars: 1 mm.

1146 **Supp Fig 3: Testicular expression of *mCherry*-mRNA following in vivo electroporation**

1147 (A1, B1, C1, D1, E1 and F1) Whole-mount testes on days 0, 1, 7, 14, 21, 28 after *in vivo*
1148 injection/ electroporation. (A2, B2, C2, D2, E2 and, F2) Using fluorescence microscopy,
1149 transfected testes from 12-week-old B6D2 mice express red mCherry fluorescence. mCherry
1150 was detected in a diffuse pattern throughout the seminiferous tubules from day 1 to day 15.
1151 (A3, B3, C3, D3, E3 and F3) images showing the absence of autofluorescence in non-
1152 transfected control testes observed at 4x magnification. Scales bars: 1 mm and 100 µm.

1153 **Supp Fig 4: Cellular expression of *mCherry*-mRNA following in vivo injection/**
1154 **electroporation.**
1155 Cross sections (20 µm) of mouse testes on day 1 (AB) and day 7 (CD) after in vivo injection and
1156 electroporation with *mCherry*-mRNA, observed under fluorescence microscopy. Red signals
1157 correspond to successfully transfected testicular tubular cells; nuclei were counterstained
1158 with DAPI (blue). At the cellular level, mCherry fluorescence was detectable in Sertoli cells
1159 (SC); Spermatogonia (SG); Spermatocytes (Scytes); round Spermatids (RStids), and mature
1160 spermatids (m-Sptids); Scale bars: 10 µm and 5 µm.
1161 **Supp Fig 5: Decay over time of the number of mice exhibiting reporter gene expression**
1162 **following injection/electroporation of the three different mRNAs.**

1163 Mice were injected on day 0 with *LUC*-mRNA, *GFP*-mRNA or *mCherry*-mRNA and the number
1164 of mice showing bioluminescence or fluorescence in the testis was counted at different time
1165 points. For *LUC*-mRNA n= 5 mice at each time point. For *mCherry*-mRNA n=3 on day 1; n=4 on
1166 day3; n=15 on day 7; n= 21 on day 15; n=15 on day 21; n= 5 on day 28; n=5 on day 35; and for
1167 *GFP*-mRNA n=3 on day 12; n=7 on day 2; n=7 on day 3; n=12 on day 7; n= 13 on day 15; n=10
1168 on day 21 ; n= 9 on day 28; n=17 on day 35 and n=5 on day 42.

1169 **Supp Fig 6: *Armc2* expression and localization in mice testis**

1170 (A) IF experiment on dissociated spermatogenic cell from WT male. (A1) Nuclei were
1171 counterstained with DAPI (blue staining), (A2) tubulin (green signal) and (A3) ARMC2 (red
1172 signal). (A4) overlay. ARMC2 is located in the flagellum of spermatids Scale bars: 5 µm. (B)
1173 Cross-sections of seminiferous tubules (B1) Nuclei were counterstained with DAPI (blue
1174 staining), (B2) and (B2) ARMC2 (red signal). (B3) overlay. B4 is an enlargement of the red
1175 square in B3, showing that only elongating/mature spermatids were stained. (C) Expression of
1176 *Armc2* in mouse spermatogenic cells based on the RNA-sequencing study from Gan et al. 2013.
1177 Primitive type A spermatogonia (priSG-A) were isolated from 6 dpp mice; Type A
1178 spermatogonia (SG-A) and type B spermatogonia (SG-B) were from 8 dpp mice; preleptotene
1179 spermatocytes (plpSC) and pachytene spermatocytes (pacSC) were from 17 dpp mice; and
1180 round spermatids (rST), elongating spermatids (eST) and spermatozoa (SZ) were from 60 dpp
1181 mice. Artificial units (AU). Dpp: day post-partum

1182 **Supp Fig 7: Validation of *Armc2*-mRNA in HEK cells.**

1183 HEK cells were transfected with *Armc2*-mRNA or EEV-*Armc2.* ARMC2 protein was detected by
1184 Western blot with an anti-HA primary antibody. The expected size of the ARMC2 protein is
1185 98 kDa**.**

1186 **Supp Fig 8: Morphology of sperm cells from WT, *Armc2* KO and *Armc2*-rescued males.**

1187 Microscopic observation of epididymal sperm cells from WT, *Armc2* KO and *Armc2* KO-*Armc2*-
1188 mRNA injected males at 20x (left column), 40x (middle column) and 100x (right column)
1189 magnifications. In the rescue condition, rescued sperm cells were labeled with a white
1190 asterisk. Scale bars: 100, 50 and 10 µm.

1191 **Supp Fig 9: *Armc2* $^{-/-}$-rescued sperm can fertilize eggs and produce embryos by ICSI.**

1192 Comparative analysis of the percentage of blastocysts produced by ICSI with spermatozoa
1193 from wild-type (WT), *Armc2*$^{-/-}$ and *Armc2*$^{-/-}$-rescued individuals. For *Armc2*$^{-/-}$-rescued
1194 individuals, only motile sperm were injected.

1195 **Supplementary Figure 10. Expression of GFP following mRNA injection in seminiferous**
1196 **tubules.**

1197 Representative images of seminiferous tubule fluorescence, used to produce seminiferous

1198 tubule cell suspensions for qRT-PCR and fluorescence imaging assays. Tubules were collected
1199 one day after *in vivo* injection and electroporation of GFP mRNA. Strong GFP fluorescence is
1200 visible along the tubular segments, indicating efficient uptake and translation of mRNA in
1201 germ cells. Images were acquired using a fluorescence stereomicroscope. Scale bars: 200 µm

1202 **Videos 1 and 2: 3D-microscopic reconstructions of faces 1 and 2 of a testis injected with *GFP*-**
1203 **mRNA.**

1204 **Video 3: CASA recording of WT epidydimal sperm cells**

1205 **Video 4: CASA recording of *Armc2* KO epidydimal sperm cells**

1206 **Videos 5 and 6: CASA recordings of epidydimal sperm cells from *Armc2* KO mice on day 21**
1207 **and day 35, respectively, after injection/electroporation with *Armc2*-mRNA.**

1208

1209 **Acknowledgments**

1210 This work was supported by CNRS, INSERM and ANR-20-CE18-0007 grant to JE. This work was
1211 supported by the Fondation pour la Recherche Médicale, grant number « ECO202006011669
1212 » to CV.

1213 We acknowledge the MicroCell facility (GIS IBiSA, ISdV, IAB), member of the national
1214 infrastructure France-BioImaging supported by the French National Research Agency (ANR-
1215 10-INBS-04)) for optical microscopy.

1216 **Authors'roles**

1217 C.V., P.F., and J.E. performed research. C.V., P.F., F.A., J.L.D., and J.B. conducted light sheet
1218 experiments. C.V., P.F., M.H., J.V., and V.J. performed in vivo imaging experiments. C.A., A.Y.,
1219 and B.V. produced fluorescent i-particles. C.V., P.F., F.A and M.C. performed
1220 immunofluorescence analysis. C.V., P.F., L.D.M., and S.A.C. carried out histological analysis.
1221 C.V., P.F., Z.W., and G.M. conducted Harris-Shorr sperm analysis. C.V., P.F., and G.C.
1222 performed genotyping analysis. P.F., C.T, Z.K and C.L. carried out RT-qPCR analysis. C.V., P.F.,
1223 and J.E. analyzed sperm motility. P.F., J.E., and S.A.R. performed fluorescence germ cell
1224 analysis. P.F., J.E., E.D.L., and E.L. conducted IVF and ICSI experiments. J.E. coordinated the
1225 study. C.C., C.L, P.F.R., C.A., and J.E. contributed to the discussion, study design, and data
1226 interpretation. J.E. wrote the manuscript.

1227 **Bibliography**

1228 1. Boivin, J., et al., *International estimates of infertility prevalence and treatment-seeking:*
1229 *potential need and demand for infertility medical care.* Hum Reprod, 2007. **22**(6): p. 1506-12.
1230 2. Thonneau, P. and A. Spira, *Prevalence of infertility: international data and problems of*
1231 *measurement.* Eur J Obstet Gynecol Reprod Biol, 1991. **38**(1): p. 43-52.
1232 3. Kekalainen, J., *Genetic incompatibility of the reproductive partners: an evolutionary*
1233 *perspective on infertility.* Hum Reprod, 2021. **36**(12): p. 3028-3035.
1234 4. Kumar, N. and A.K. Singh, *Trends of male factor infertility, an important cause of infertility: A*
1235 *review of literature.* J Hum Reprod Sci, 2015. **8**(4): p. 191-6.
1236 5. Uhlen, M., et al., *Transcriptomics resources of human tissues and organs.* Mol Syst Biol, 2016.
1237 **12**(4): p. 862.
1238 6. Thonneau, P., et al., *Incidence and main causes of infertility in a resident population (1,850,000)*
1239 *of three French regions (1988-1989).* Hum Reprod, 1991. **6**(6): p. 811-6.
1240 7. Cavallini, G., *Male idiopathic oligoasthenoteratozoospermia.* Asian J Androl, 2006. **8**(2): p. 143-
1241 57.
1242 8. Colpi, G.M., et al., *European Academy of Andrology guideline Management of oligo-asthenO-*
1243 *teratozoospermia.* Andrology, 2018. **6**(4): p. 513-524.
1244 9. Hansen, M., et al., *Assisted reproductive technologies and the risk of birth defects--a systematic*
1245 *review.* Hum Reprod, 2005. **20**(2): p. 328-38.
1246 10. Halliday, J.L., et al., *Increased risk of blastogenesis birth defects, arising in the first 4 weeks of*
1247 *pregnancy, after assisted reproductive technologies.* Hum Reprod, 2010. **25**(1): p. 59-65.
1248 11. Davies, M.J., et al., *Reproductive technologies and the risk of birth defects.* N Engl J Med, 2012.
1249 **366**(19): p. 1803-13.
1250 12. Kurinczuk, J.J., M. Hansen, and C. Bower, *The risk of birth defects in children born after assisted*
1251 *reproductive technologies.* Curr Opin Obstet Gynecol, 2004. **16**(3): p. 201-9.
1252 13. Graham, M.E., et al., *Assisted reproductive technology: Short- and long-term outcomes.* Dev
1253 Med Child Neurol, 2023. **65**(1): p. 38-49.
1254 14. Palermo, G.D., et al., *Intracytoplasmic sperm injection: state of the art in humans.*
1255 Reproduction, 2017. **154**(6): p. F93-f110.
1256 15. Usmani, A., et al., *A non-surgical approach for male germ cell mediated gene transmission*
1257 *through transgenesis.* Sci Rep, 2013. **3**: p. 3430.
1258 16. Raina, A., et al., *Testis mediated gene transfer: in vitro transfection in goat testis by*
1259 *electroporation.* Gene, 2015. **554**(1): p. 96-100.
1260 17. Michaelis, M., A. Sobczak, and J.M. Weitzel, *In vivo microinjection and electroporation of*
1261 *mouse testis.* J Vis Exp, 2014(90).
1262 18. Wang, L., et al., *Testis electroporation coupled with autophagy inhibitor to treat non-*
1263 *obstructive azoospermia.* Mol Ther Nucleic Acids, 2022. **30**: p. 451-464.
1264 19. Duan, D., *Full-length dystrophin gene therapy for Duchenne muscular dystrophy.* Mol Ther,
1265 2024. **32**(9): p. 2817-2818.
1266 20. Jacobson, S.G., et al., *Safety and improved efficacy signals following gene therapy in childhood*
1267 *blindness caused by GUCY2D mutations.* iScience, 2021. **24**(5): p. 102409.
1268 21. Liu, S., *Legal reflections on the case of genome-edited babies.* Glob Health Res Policy, 2020. **5**:
1269 p. 24.
1270 22. Sadelain, M., E.P. Papapetrou, and F.D. Bushman, *Safe harbours for the integration of new DNA*
1271 *in the human genome.* Nat Rev Cancer, 2011. **12**(1): p. 51-8.
1272 23. Ishii, T., *Germ line genome editing in clinics: the approaches, objectives and global society.* Brief
1273 Funct Genomics, 2017. **16**(1): p. 46-56.
1274 24. Parhiz, H., E.N. Atochina-Vasserman, and D. Weissman, *mRNA-based therapeutics: looking*
1275 *beyond COVID-19 vaccines.* Lancet, 2024. **403**(10432): p. 1192-1204.

25. Coutton, C., et al., *Bi-allelic Mutations in ARMC2 Lead to Severe Astheno-Teratozoospermia Due to Sperm Flagellum Malformations in Humans and Mice.* Am J Hum Genet, 2019. **104**(2): p. 331-340.
26. Wu, Q., et al., *Translation affects mRNA stability in a codon-dependent manner in human cells.* eLife, 2019. **8**: p. e45396.
27. Gallie, D.R., *The cap and poly(A) tail function synergistically to regulate mRNA translational efficiency.* Genes & Development, 1991. **5**(11): p. 2108-2116.
28. Henderson, J.M., et al., *Cap 1 messenger RNA synthesis with co-transcriptional CleanCap® analog improves protein expression in mammalian cells.* Nucleic Acids Research, 2021. **49**(8): p. e42.
29. Stepinski, J., et al., *Synthesis and properties of mRNAs containing novel "anti-reverse" cap analogs.* RNA, 2001. **7**(10): p. 1486-1495.
30. Sachs, A.B., P. Sarnow, and M.W. Hentze, *Starting at the beginning, middle, and end: translation initiation in eukaryotes.* Cell, 1997. **89**(6): p. 831-838.
31. in *Transforming and Scaling Up Health Professionals' Education and Training: World Health Organization Guidelines 2013*. 2013: Geneva.
32. Schindelin, J., et al., *Fiji: an open-source platform for biological-image analysis.* Nat Methods, 2012. **9**(7): p. 676-82.
33. Yoshida, N. and A.C. Perry, *Piezo-actuated mouse intracytoplasmic sperm injection (ICSI).* Nat.Protoc., 2007. **2**(2): p. 296-304.
34. Ruthig, V.A. and D.J. Lamb, *Updates in Sertoli Cell-Mediated Signaling During Spermatogenesis and Advances in Restoring Sertoli Cell Function.* Front Endocrinol (Lausanne), 2022. **13**: p. 897196.
35. de Boer, P., M. de Vries, and L. Ramos, *A mutation study of sperm head shape and motility in the mouse: lessons for the clinic.* Andrology, 2015. **3**(2): p. 174-202.
36. Gan, H., et al., *Dynamics of 5-hydroxymethylcytosine during mouse spermatogenesis.* Nat Commun, 2013. **4**: p. 1995.
37. Liu, A. and X. Wang, *The Pivotal Role of Chemical Modifications in mRNA Therapeutics.* Front Cell Dev Biol, 2022. **10**: p. 901510.
38. Presnyak, V., et al., *Codon optimality is a major determinant of mRNA stability.* Cell, 2015. **160**(6): p. 1111-24.
39. Karikó, K., et al., *Incorporation of pseudouridine into mRNA yields superior nonimmunogenic vector with increased translational capacity and biological stability.* Mol Ther, 2008. **16**(11): p. 1833-40.
40. Pardi, N., et al., *mRNA vaccines — a new era in vaccinology.* Nature Reviews Drug Discovery, 2018. **17**(4): p. 261-279.
41. Hermann, B.P., et al., *The Mammalian Spermatogenesis Single-Cell Transcriptome, from Spermatogonial Stem Cells to Spermatids.* Cell Rep, 2018. **25**(6): p. 1650-1667 e8.
42. Arnoult, C., et al., *Control of the low voltage-activated calcium channel of mouse sperm by egg ZP3 and by membrane hyperpolarization during capacitation.* Proc Natl Acad Sci U S A, 1999. **96**(12): p. 6757-62.
43. Escoffier, J., et al., *Expression, localization and functions in acrosome reaction and sperm motility of Ca(V)3.1 and Ca(V)3.2 channels in sperm cells: an evaluation from Ca(V)3.1 and Ca(V)3.2 deficient mice.* J Cell Physiol, 2007. **212**(3): p. 753-63.
44. Saunders, C.M., et al., *PLC zeta: a sperm-specific trigger of Ca(2+) oscillations in eggs and embryo development.* Development, 2002. **129**(15): p. 3533-44.
45. Saunders, C.M., K. Swann, and F.A. Lai, *PLCzeta, a sperm-specific PLC and its potential role in fertilization.* Biochem Soc Symp, 2007(74): p. 23-36.
46. Ibtisham, F., et al., *Progress and future prospect of in vitro spermatogenesis.* Oncotarget, 2017. **8**(39): p. 66709-66727.
47. Lechtreck, K.F., et al., *Chlamydomonas ARMC2/PF27 is an obligate cargo adapter for intraflagellar transport of radial spokes.* Elife, 2022. **11**.

48. Schoenmaker, L., et al., *mRNA-lipid nanoparticle COVID-19 vaccines: Structure and stability.* Int J Pharm, 2021. **601**: p. 120586.
49. Du, S., et al., *Cholesterol-Amino-Phosphate (CAP) Derived Lipid Nanoparticles for Delivery of Self-Amplifying RNA and Restoration of Spermatogenesis in Infertile Mice.* Adv Sci (Weinh), 2023. **10**(11): p. e2300188.
50. Takemoto, K., et al., *Meiosis-Specific C19orf57/4930432K21Rik/BRME1 Modulates Localization of RAD51 and DMC1 to DSBs in Mouse Meiotic Recombination.* Cell Rep, 2020. **31**(8): p. 107686.
51. Habu, T., et al., *The mouse and human homologs of DMC1, the yeast meiosis-specific homologous recombination gene, have a common unique form of exon-skipped transcript in meiosis.* Nucleic Acids Res, 1996. **24**(3): p. 470-7.
52. Shinohara, A., et al., *Saccharomyces cerevisiae recA homologues RAD51 and DMC1 have both distinct and overlapping roles in meiotic recombination.* Genes Cells, 1997. **2**(10): p. 615-29.
53. Tews, B.A. and G. Meyers, *Self-Replicating RNA.* Methods Mol Biol, 2017. **1499**: p. 15-35.
54. Bloom, K., F. van den Berg, and P. Arbuthnot, *Self-amplifying RNA vaccines for infectious diseases.* Gene Ther, 2021. **28**(3-4): p. 117-129.
55. Kim, J., et al., *Self-assembled mRNA vaccines.* Adv Drug Deliv Rev, 2021. **170**: p. 83-112.
56. Cocuzza, M., C. Alvarenga, and R. Pagani, *The epidemiology and etiology of azoospermia.* Clinics (Sao Paulo), 2013. **68 Suppl 1**: p. 15-26.
57. Ma, Y., et al., *A risk prediction model of sperm retrieval failure with fine needle aspiration in males with non-obstructive azoospermia.* Hum Reprod, 2019. **34**(2): p. 200-208.

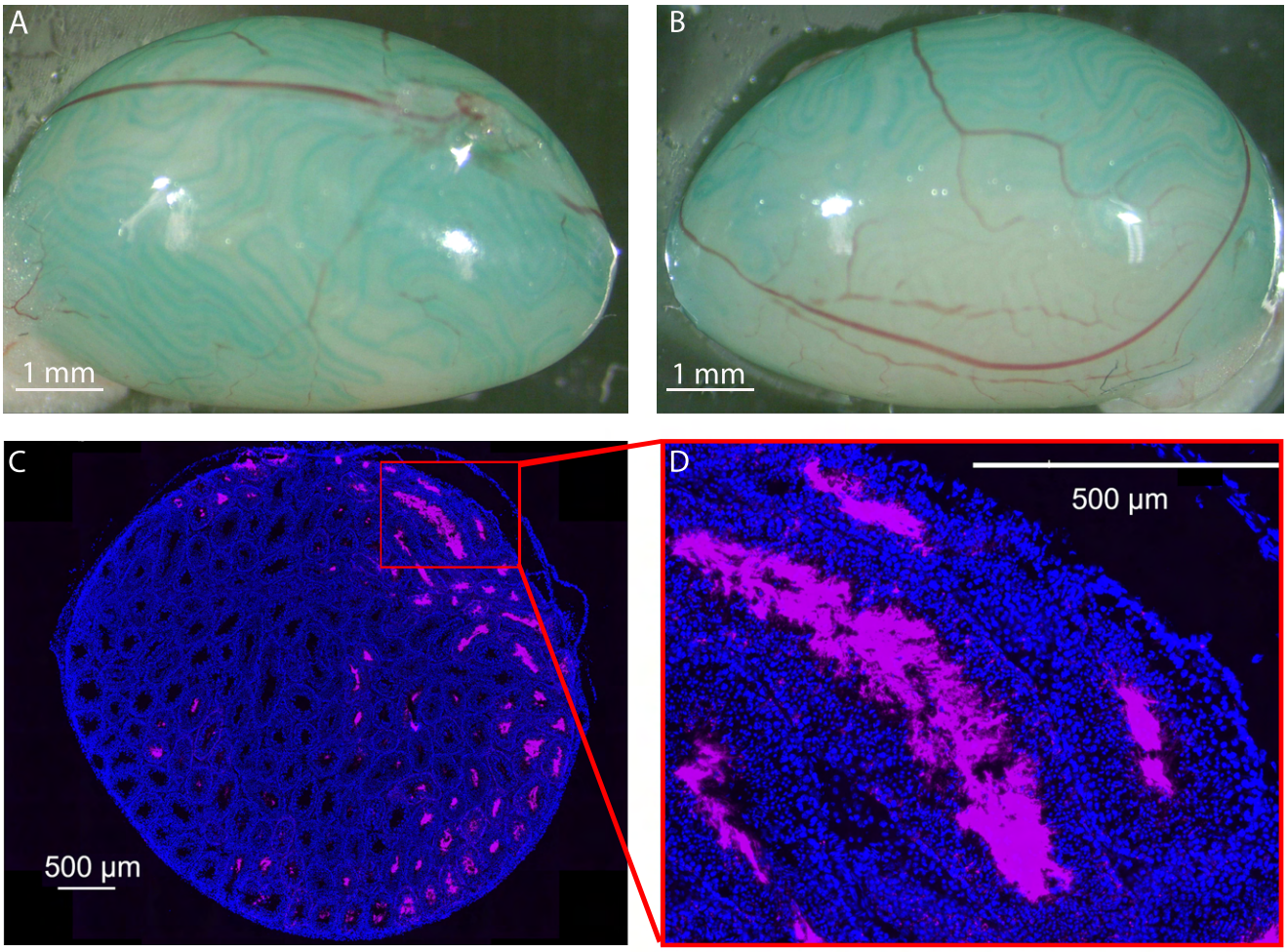

Figure 1, Vilpreux et al 2025

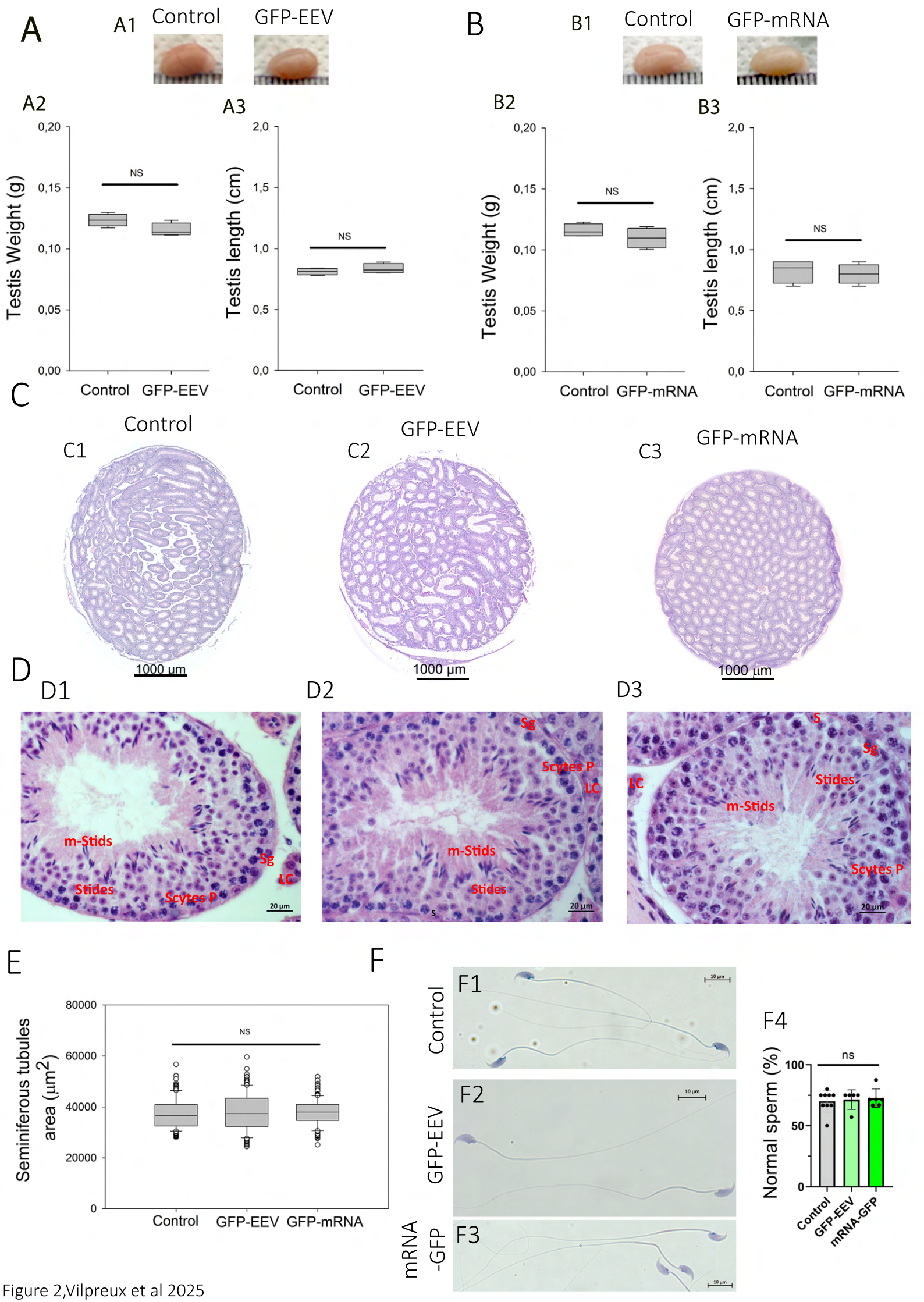

Figure 2,Vilpreux et al 2025

GFP-EEV

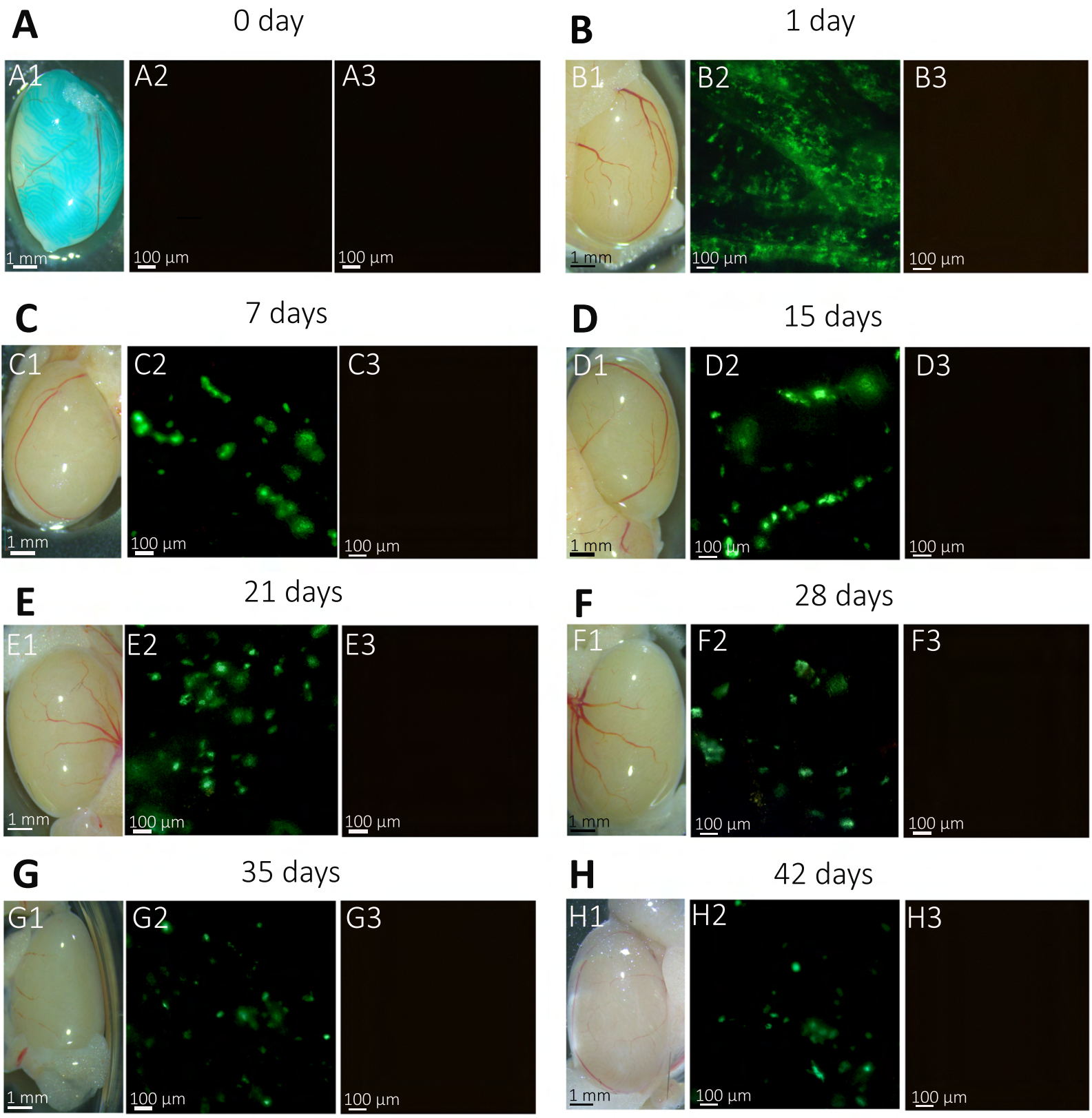

Figure 3,Vilpreux et al 2025

GFP-mRNA

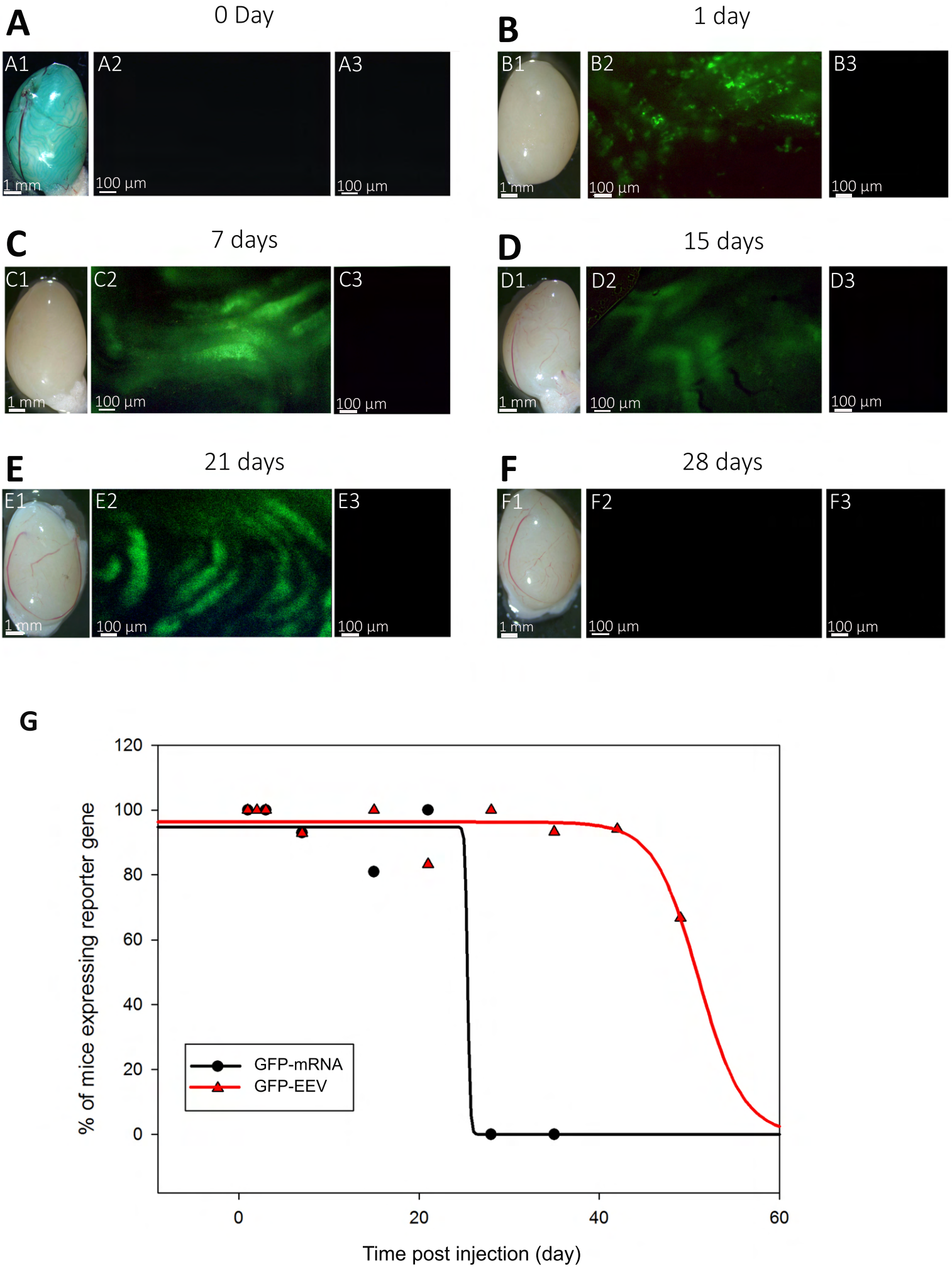

Figure 4, Vilpreux et al 2025

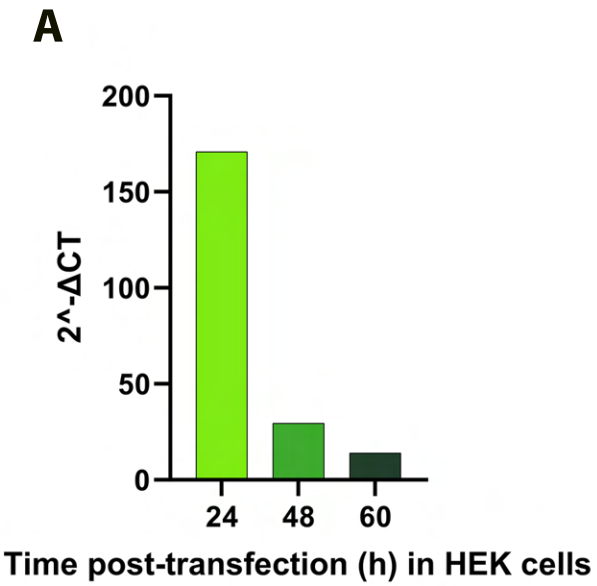

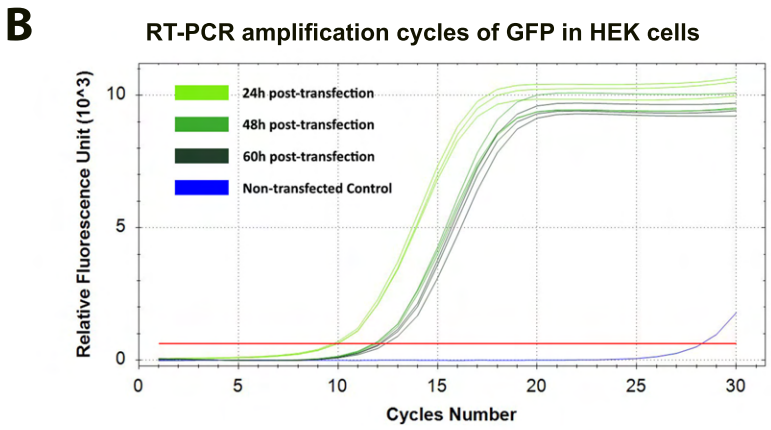

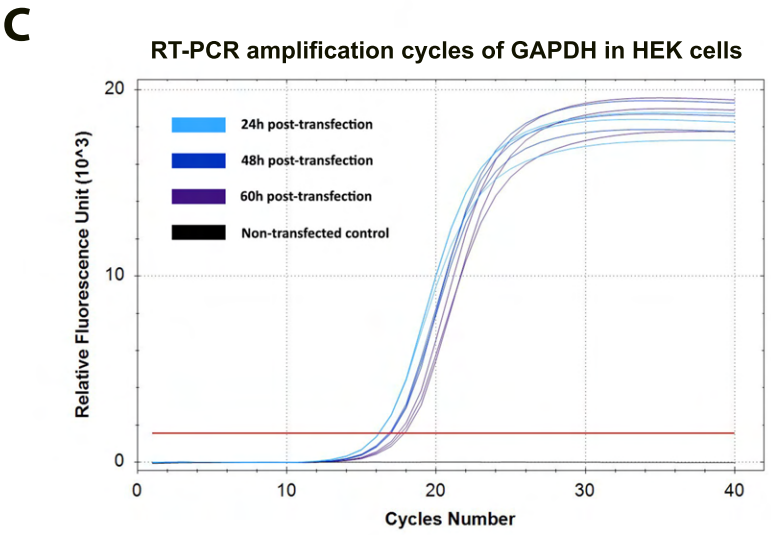

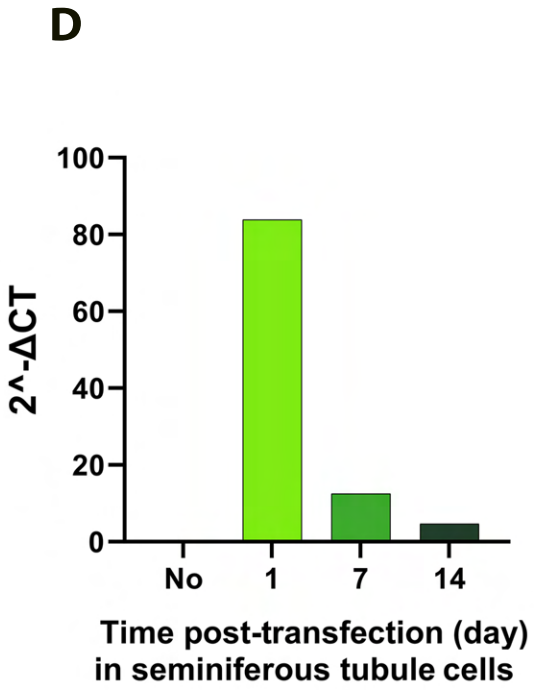

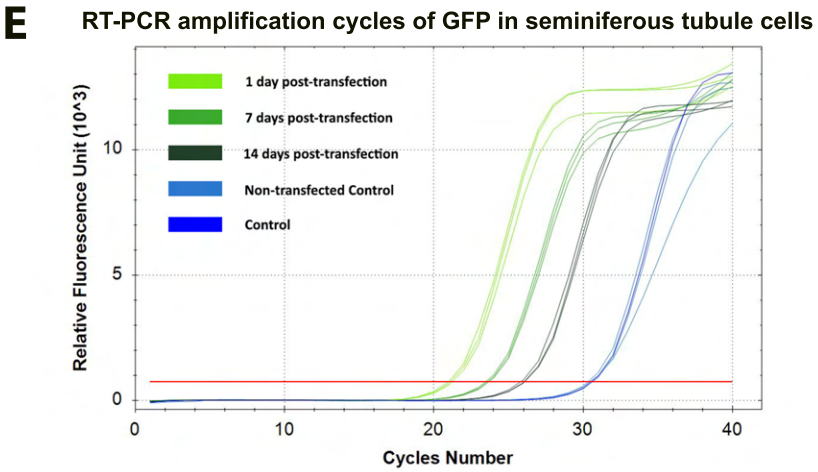

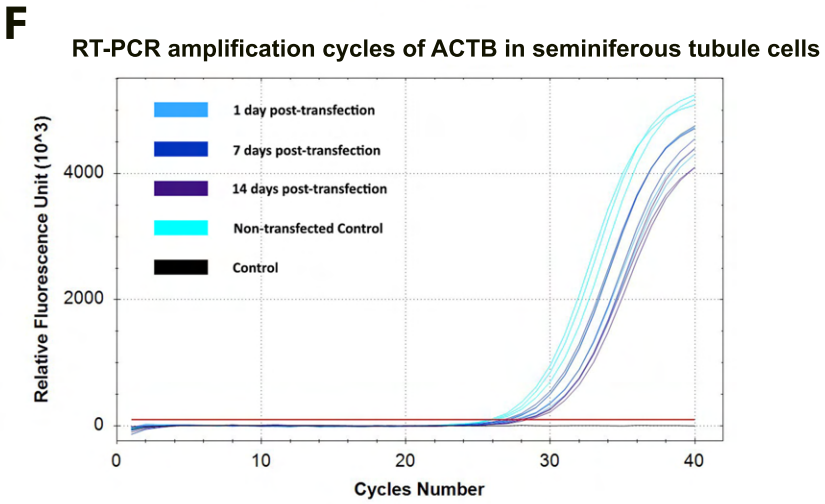

Figure 5, vilpreux et al 2025

A

LUC-EEV expression

A1

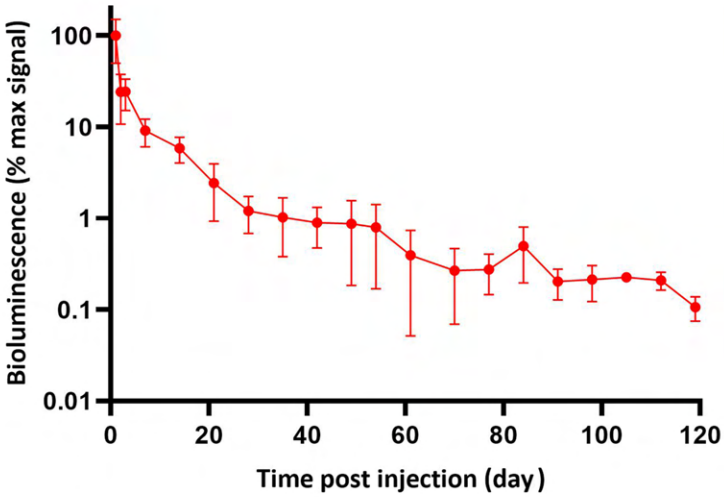

A2

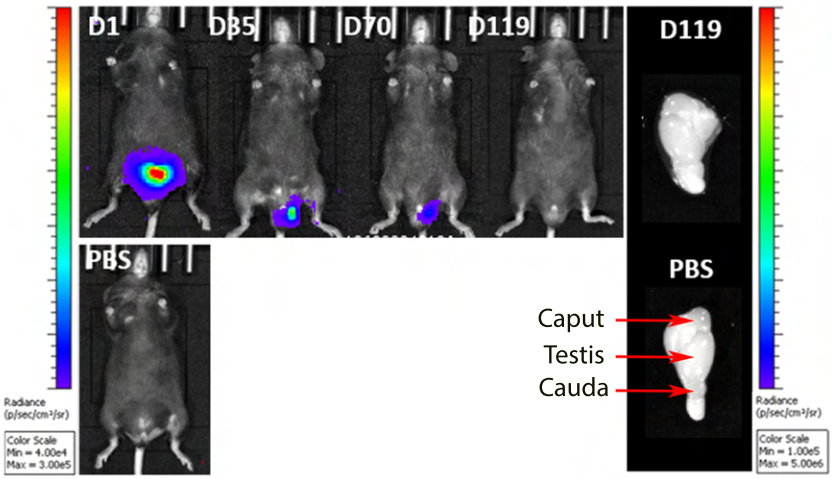

B

LUC-mRNA expression

B1

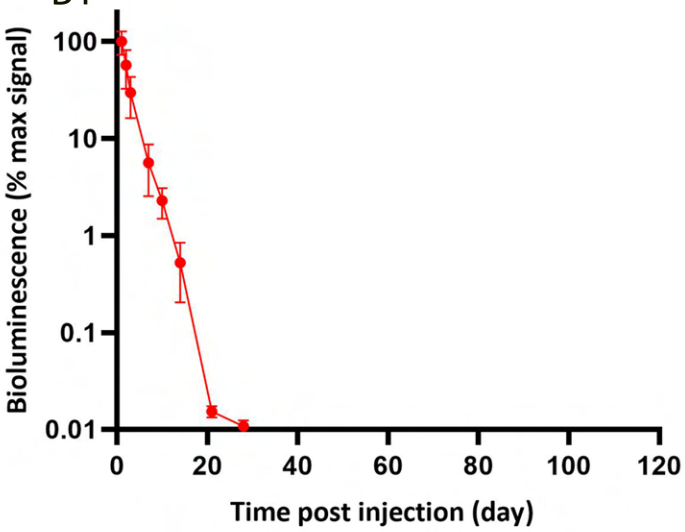

B2

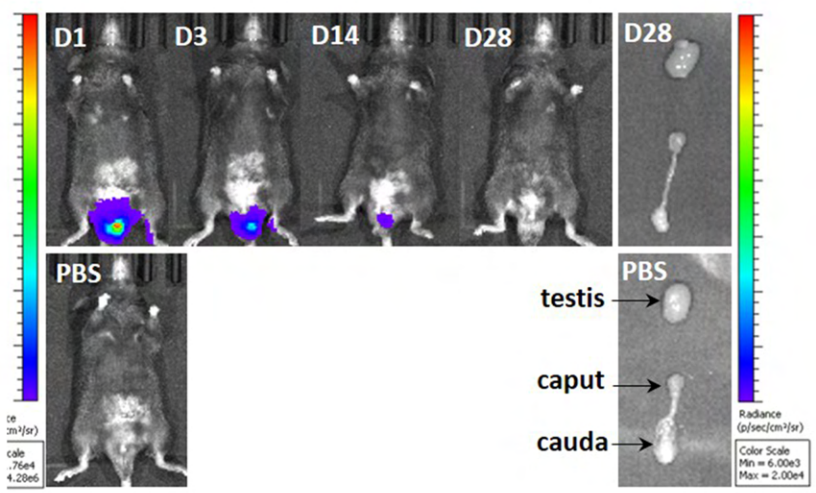

C

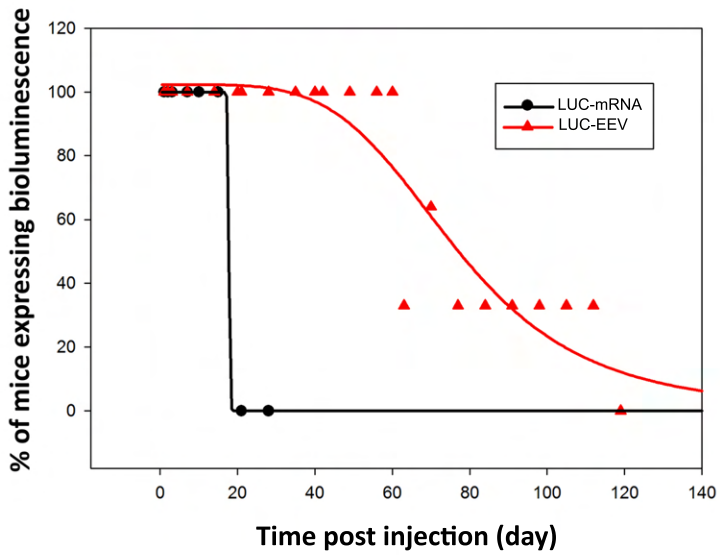

Figure 6, Vilpreux et al 2025

GFP-mRNA 1 day post injection

A

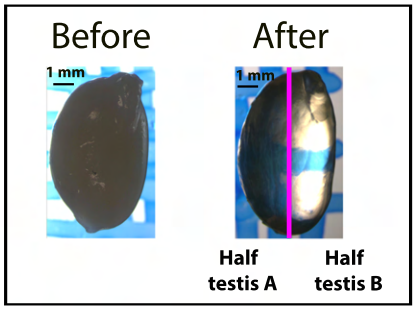

B

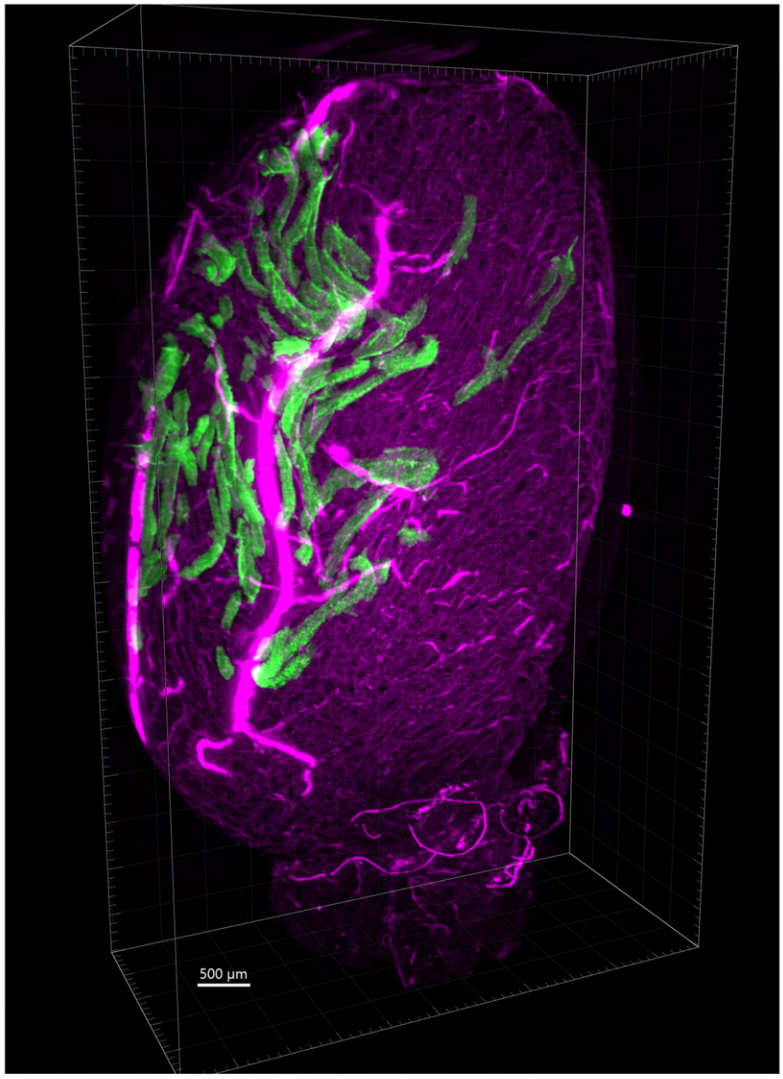

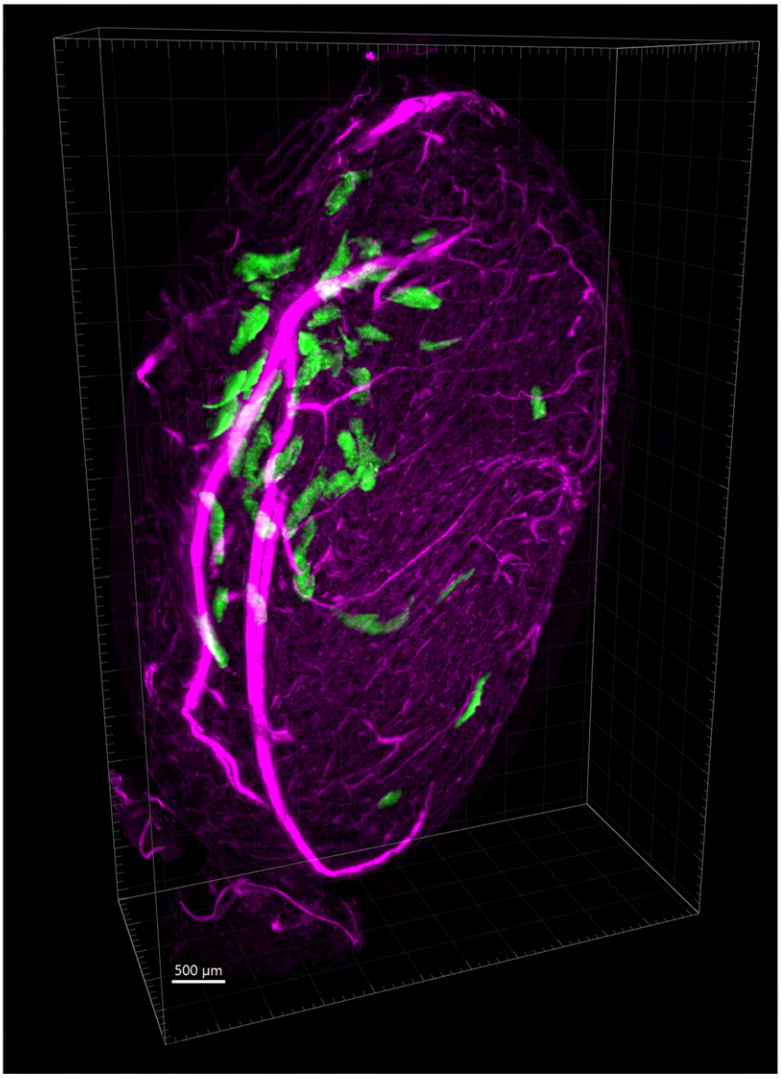

Half testis A **Half testis B**

Figure 7, Vilpreux et al 2025

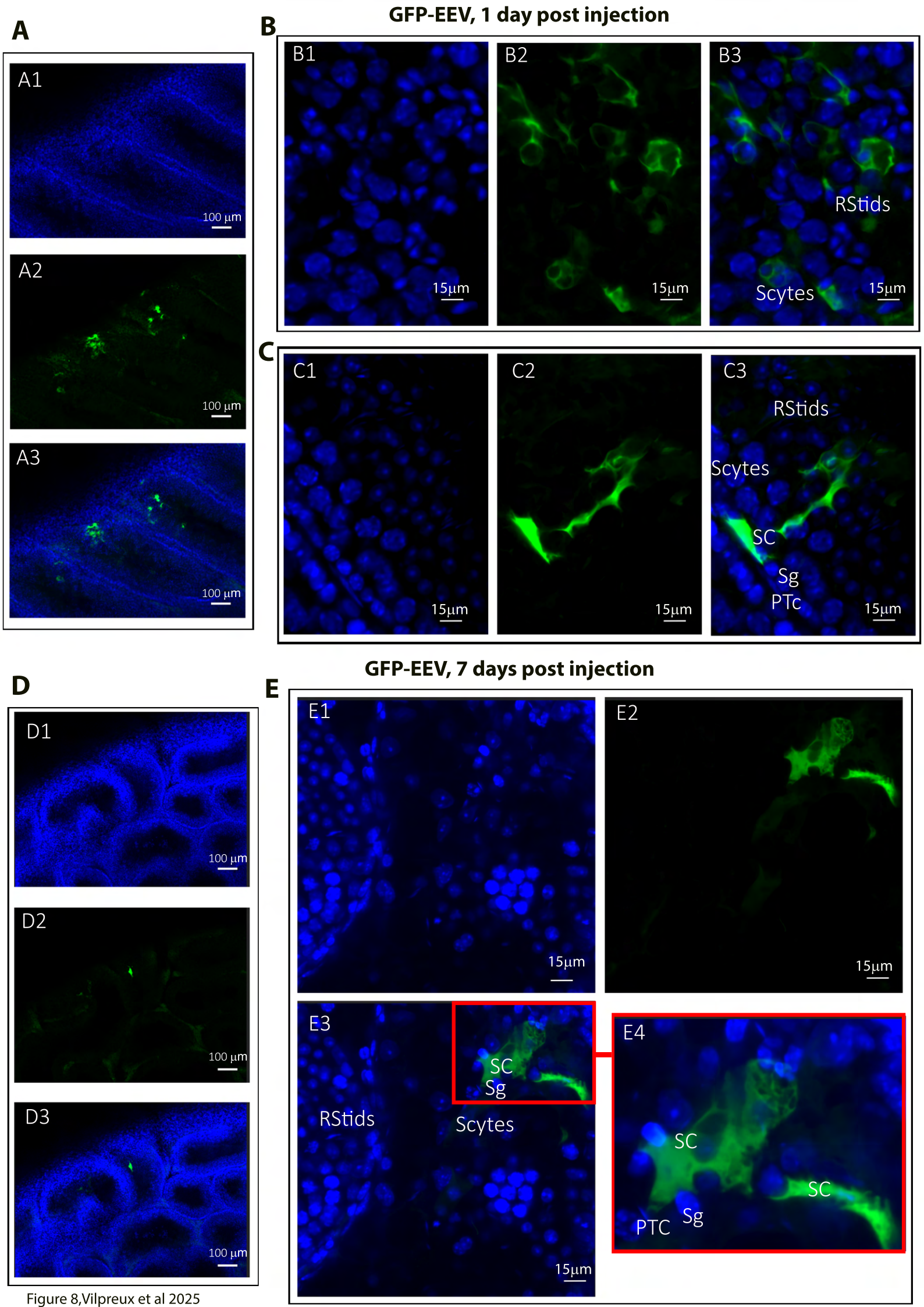

Figure 8,Vilpreux et al 2025

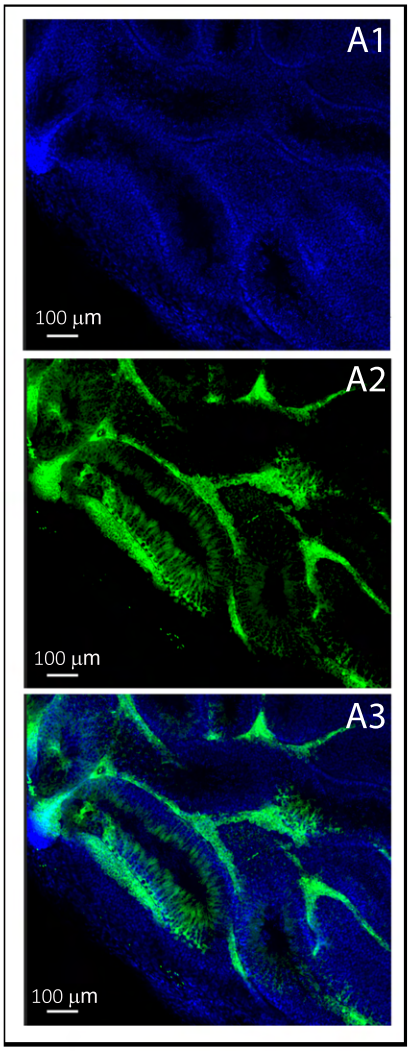

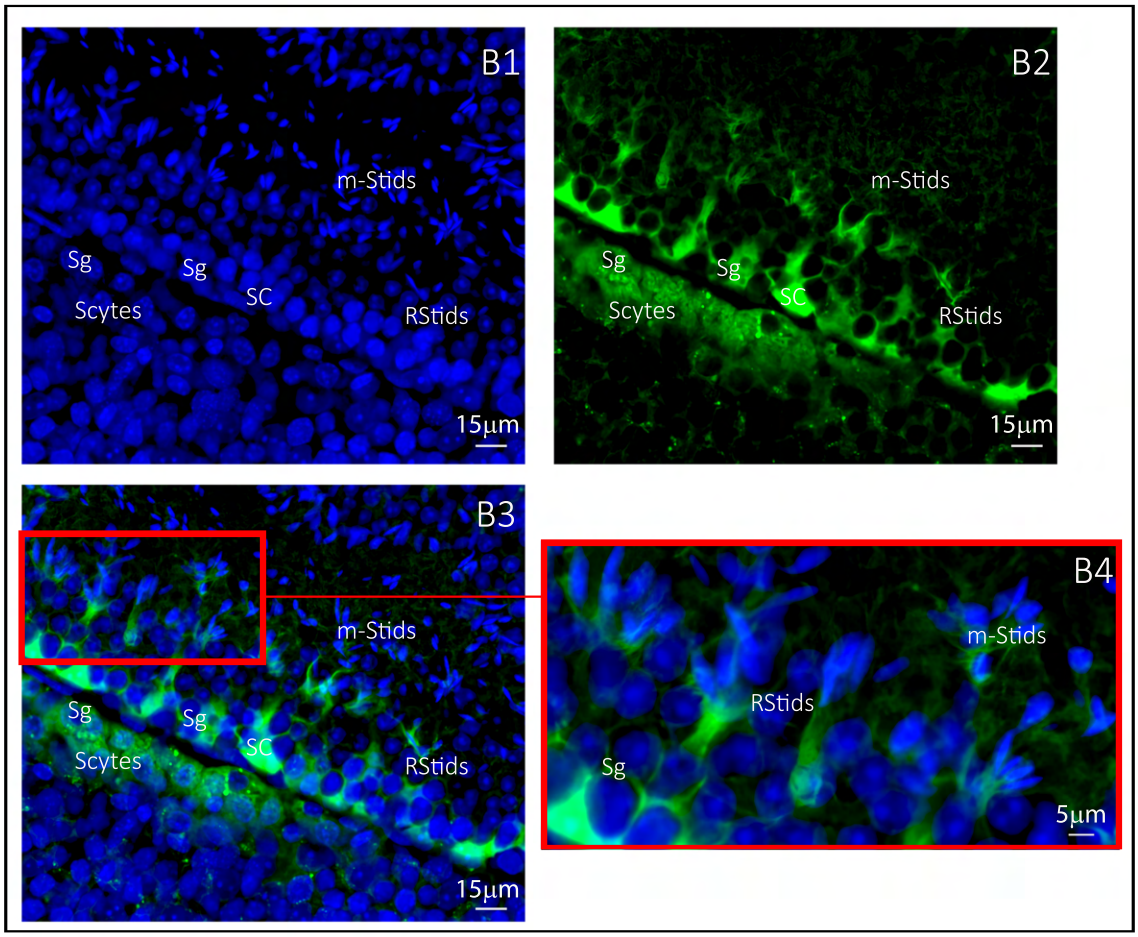

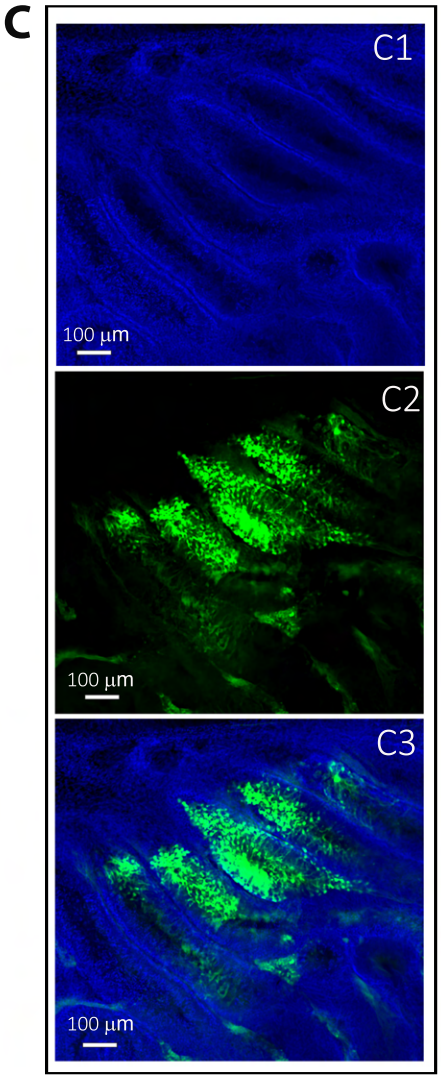

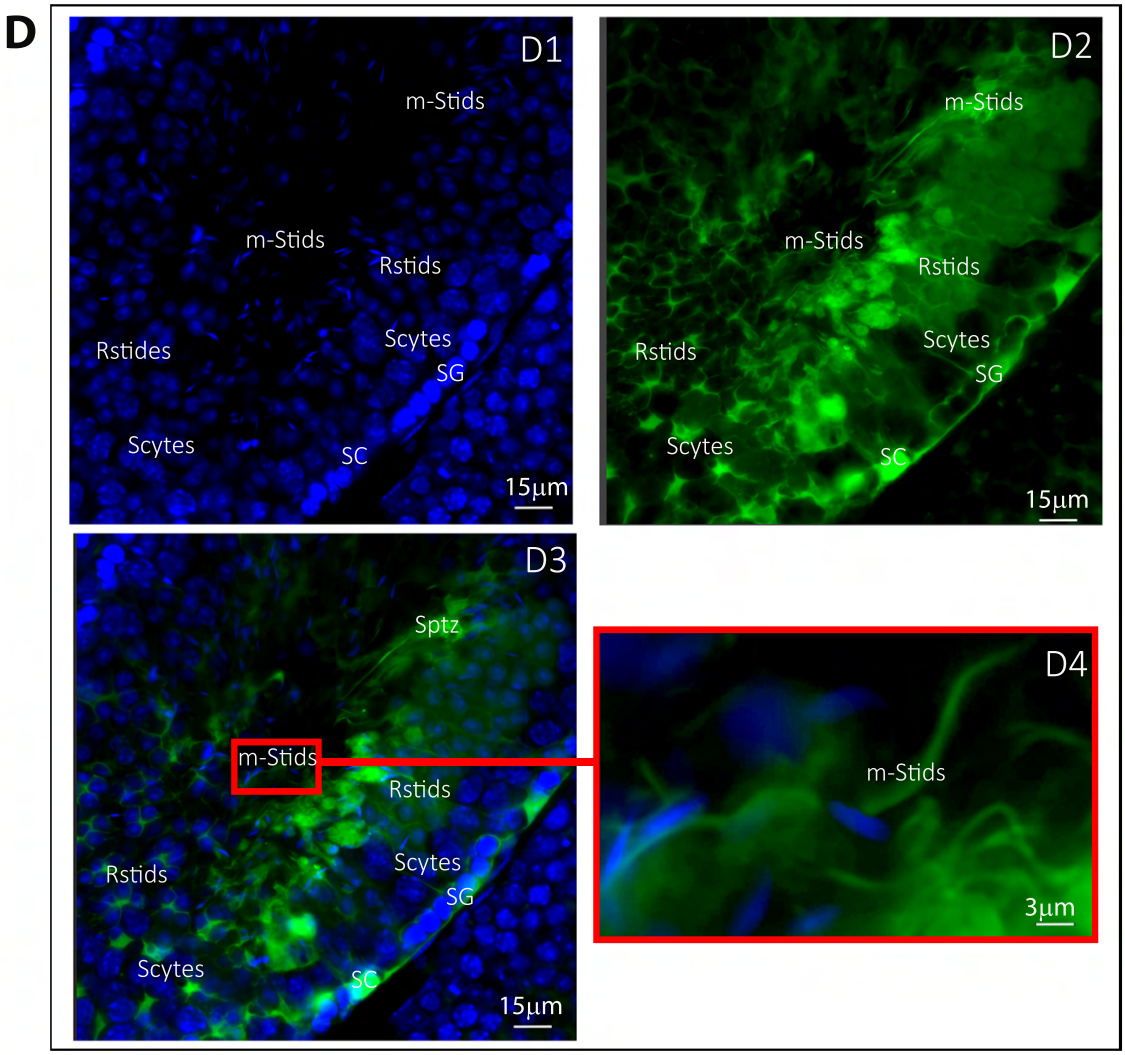

Figure 9, Vilpreux et al 2025

GFP-mRNA , 1 day post injection

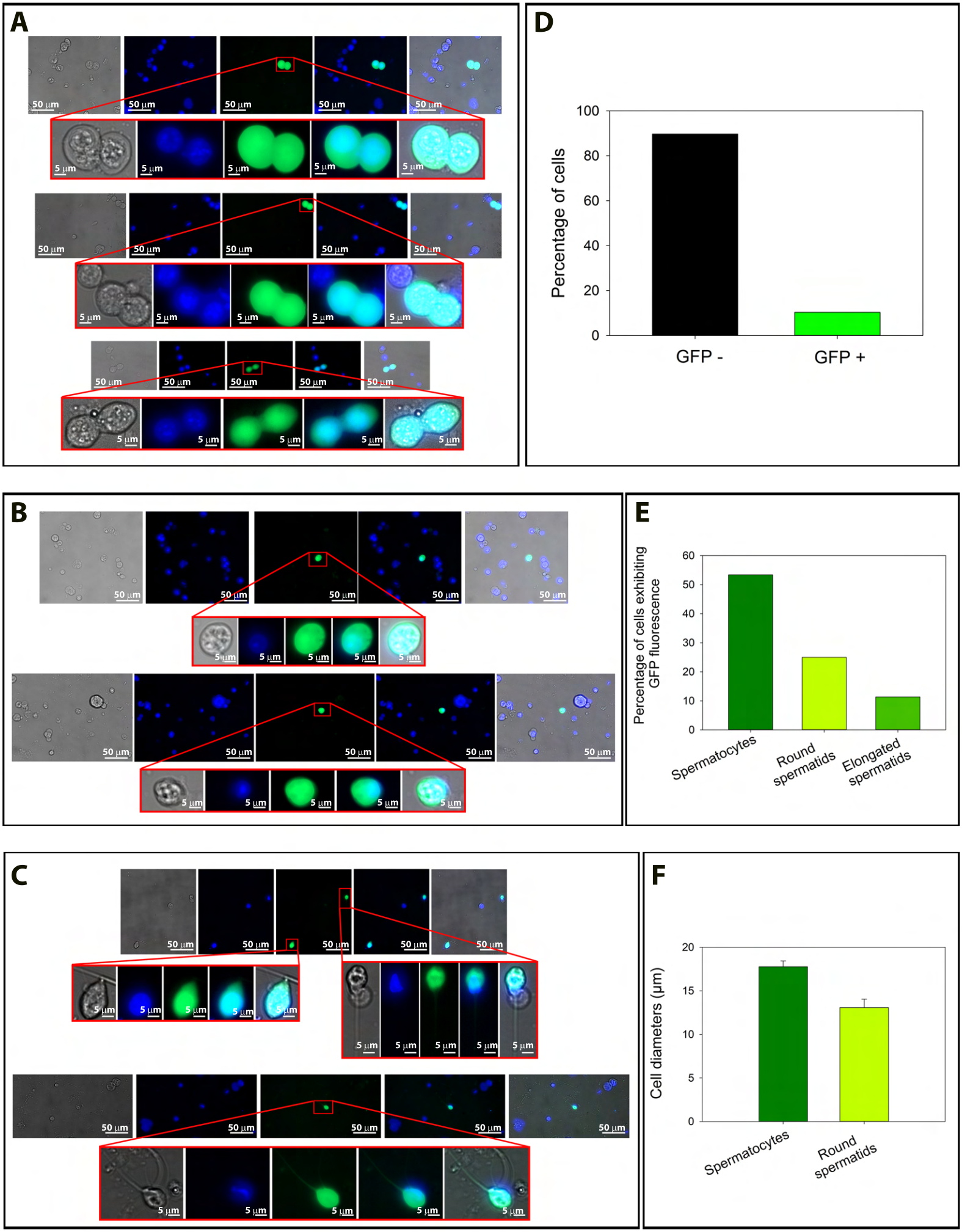

Figure 10, vilpreux et al 2025

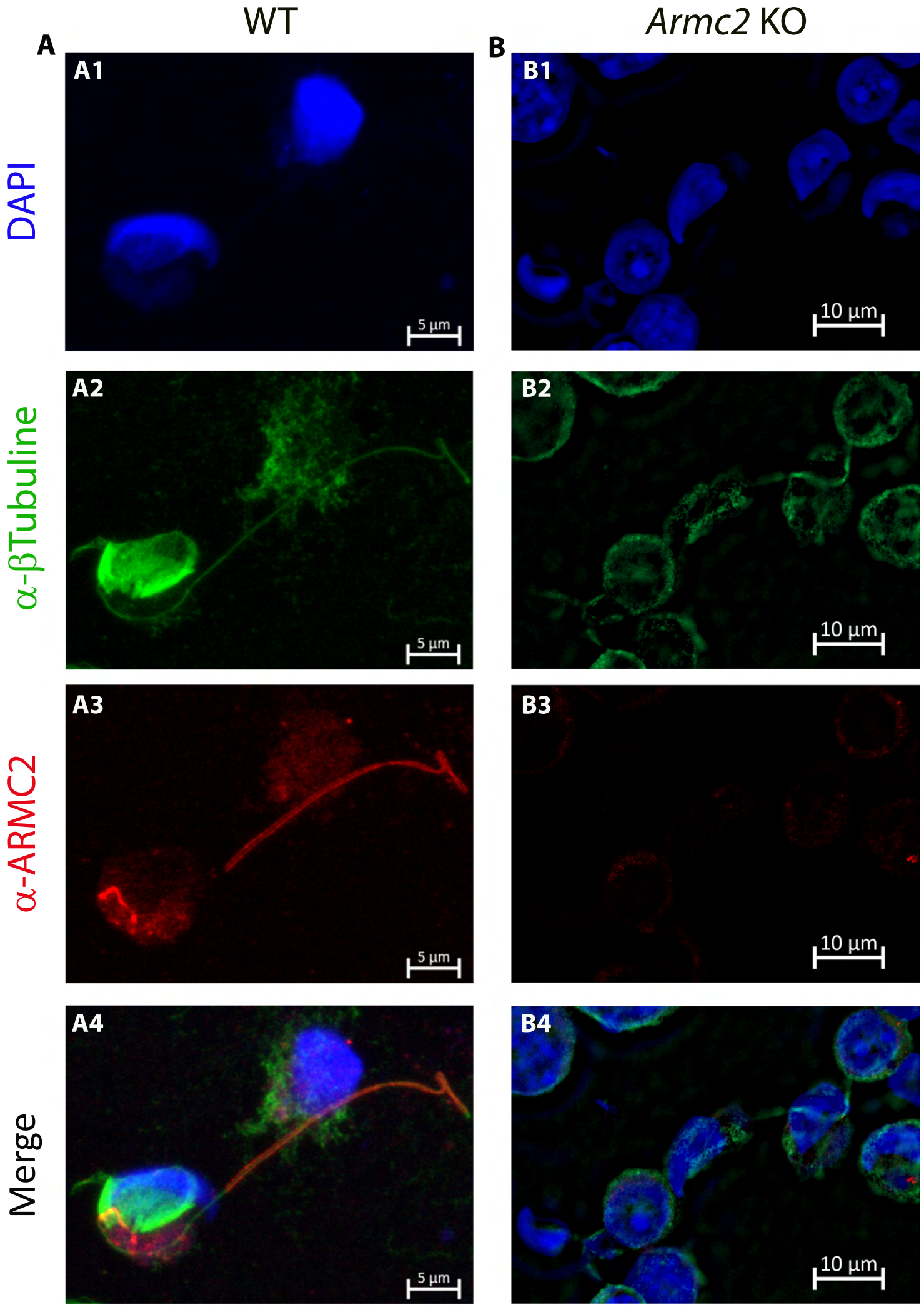

Figure 11, Vilpreux et al 2025

A

Control, 7 days post injection

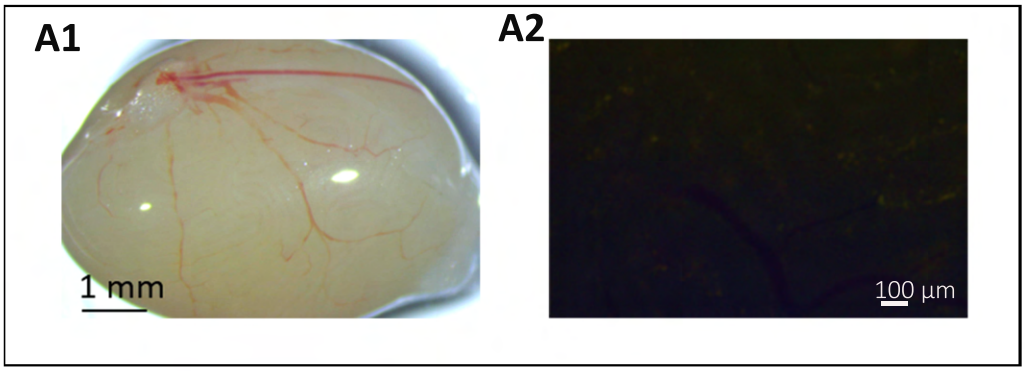

B

Armc2-mRNA + eGFP-mRNA, 7 days post injection

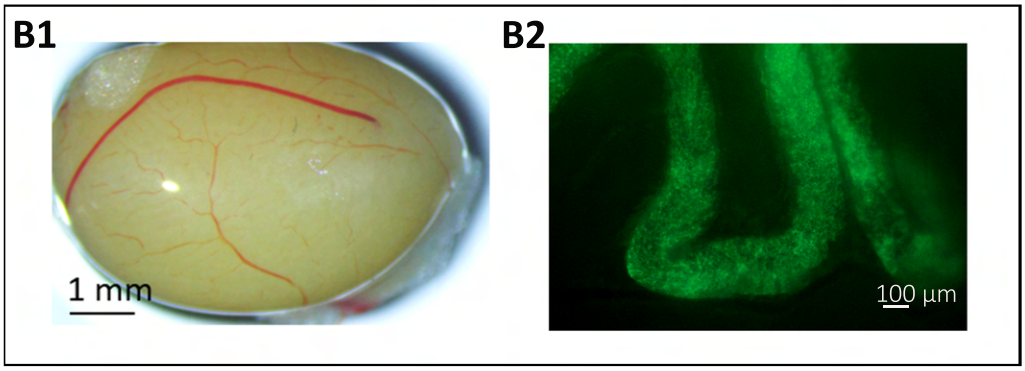

C

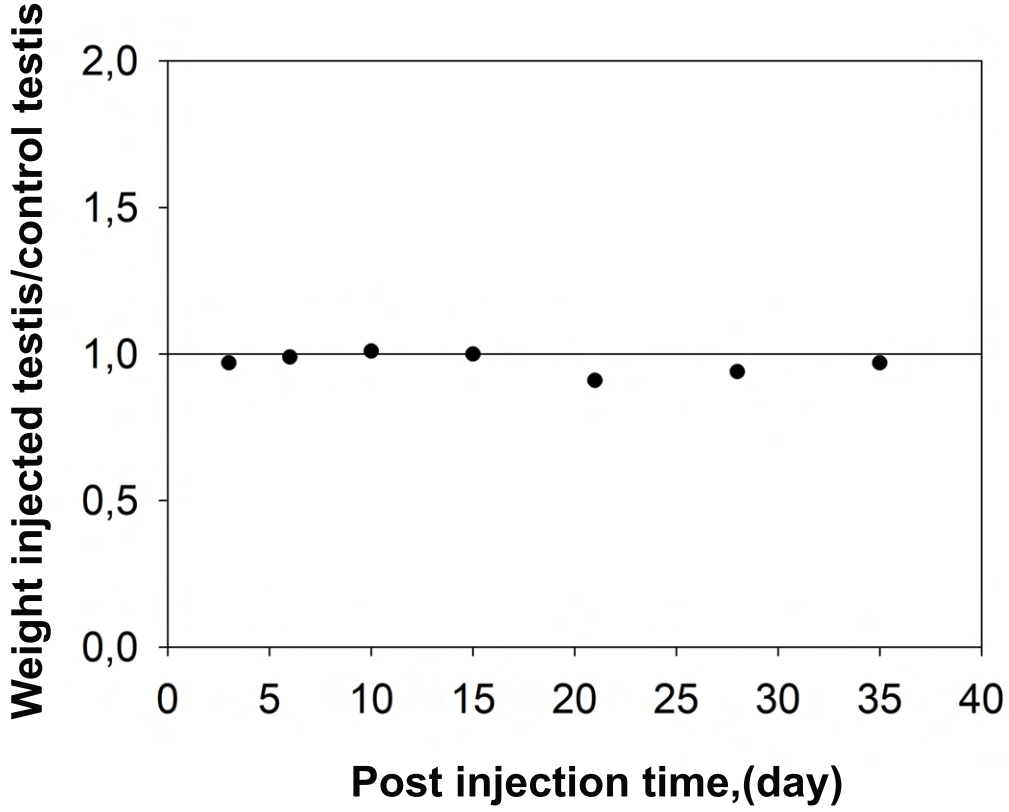

Figure 12, Vilpreux et al 2025

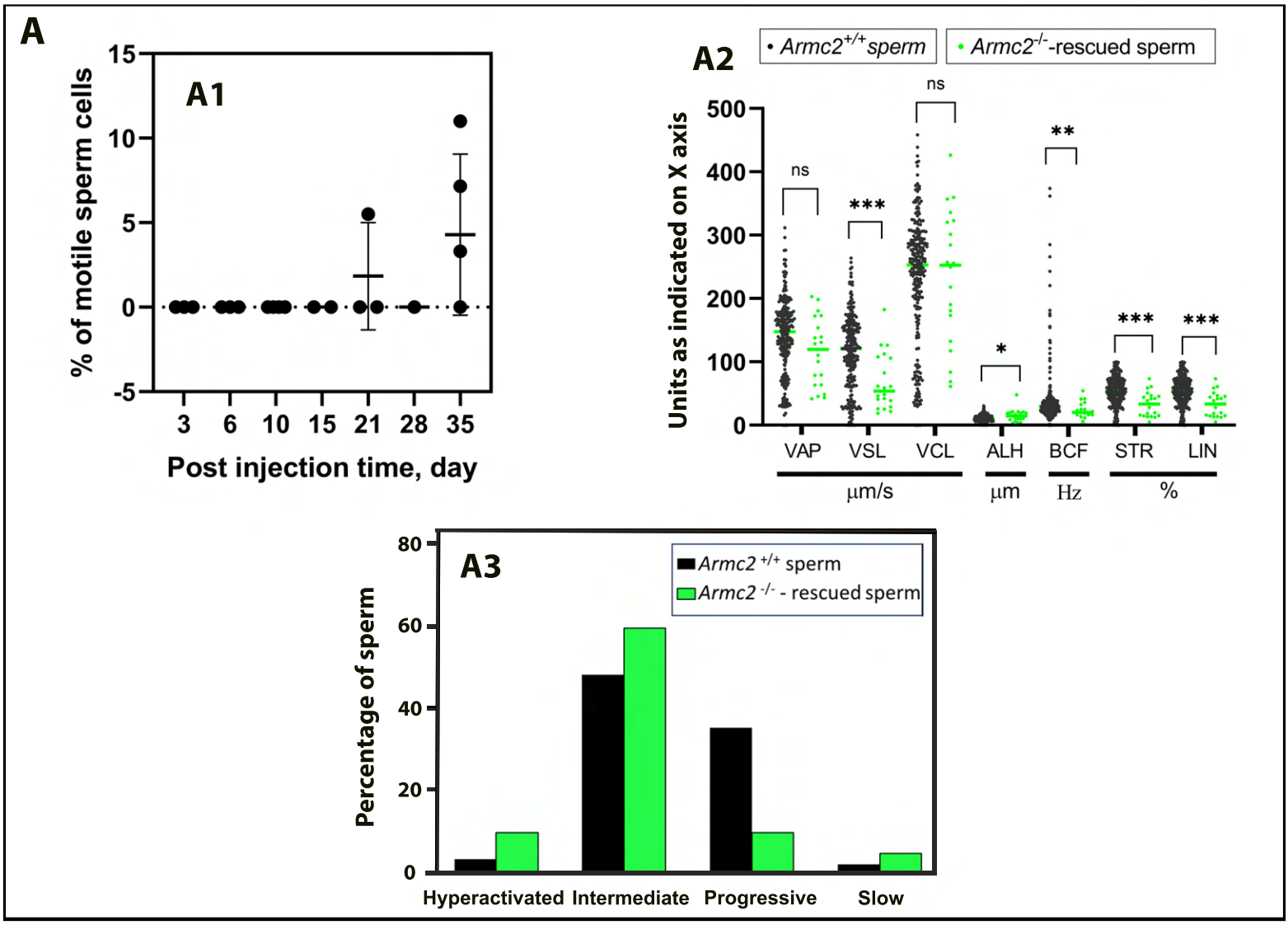

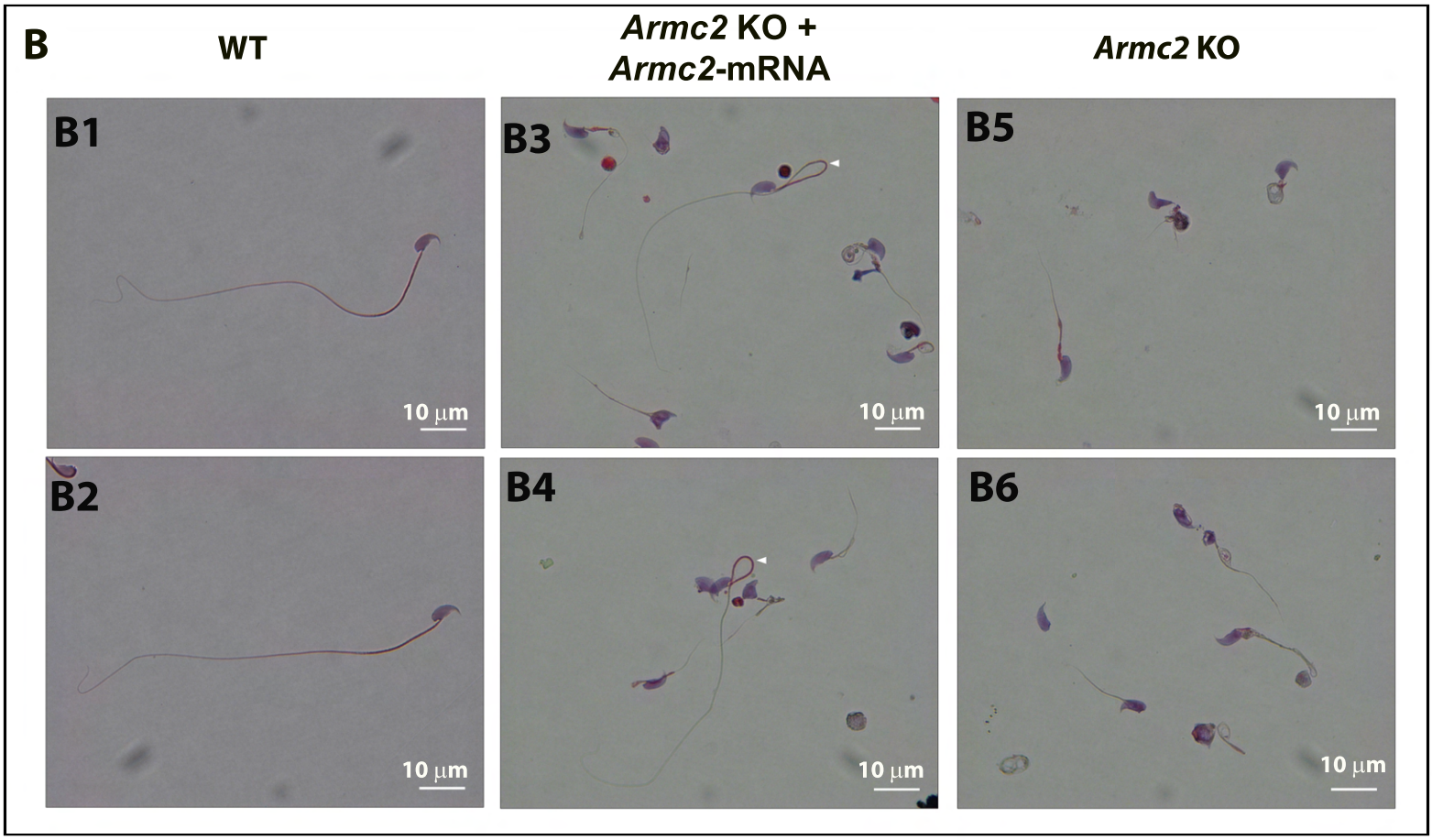

Figure 13,Vilpreux et al 2025

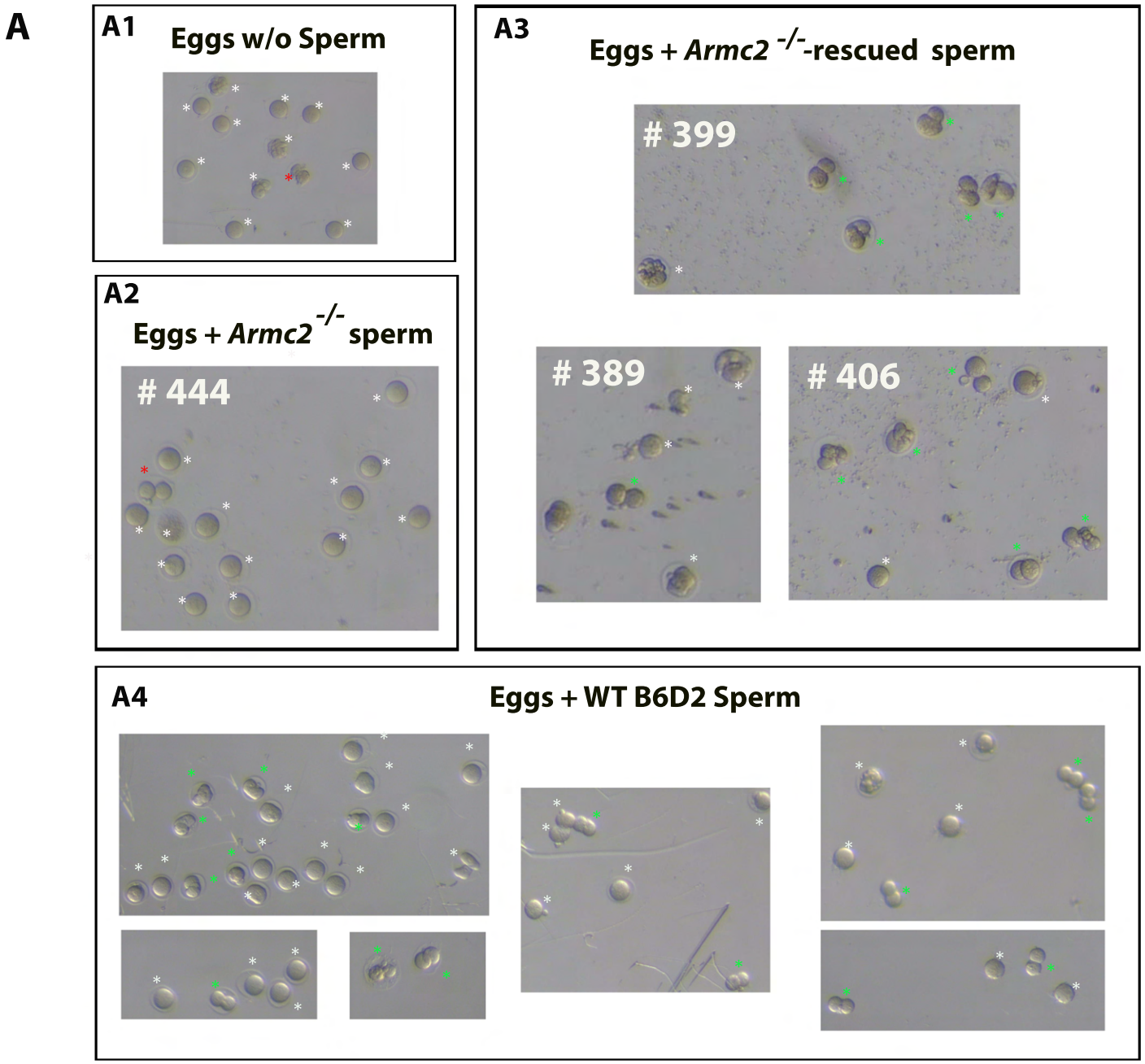

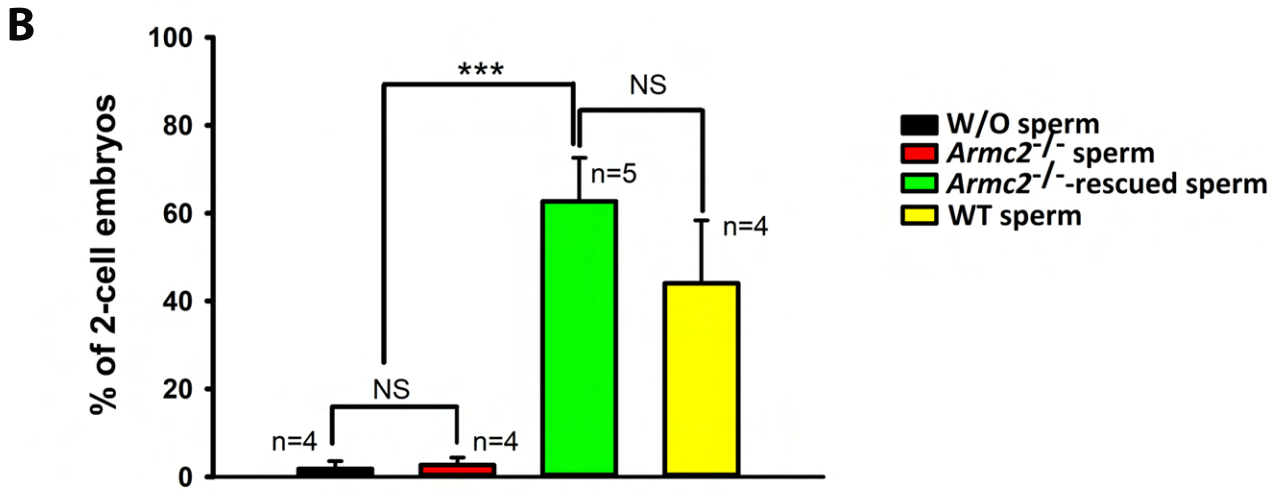

C

# *Armc2* $^{-/-}$ males	Nber collected Eggs	Nber of 2-cell embryos	**% of 2-cell embryos**
399	6	5	**83,33333333**
406	7	5	**71,42857143**
389	6	2	**33,33333333**
388	10	8	**80**
395	11	5	**45,45454545**

Figure 14, Vilpreux et al 2025

A

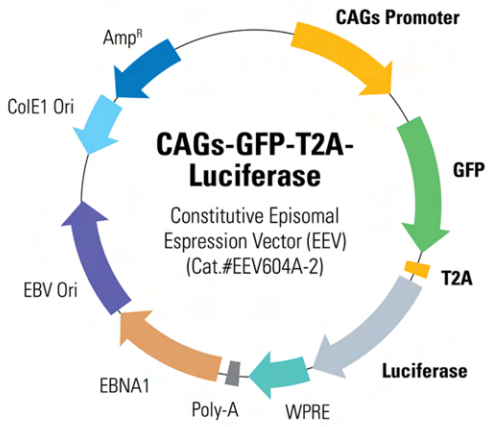

B

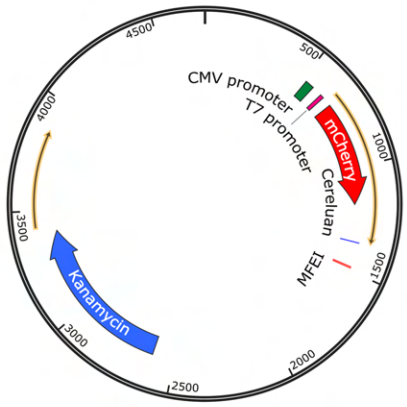

C

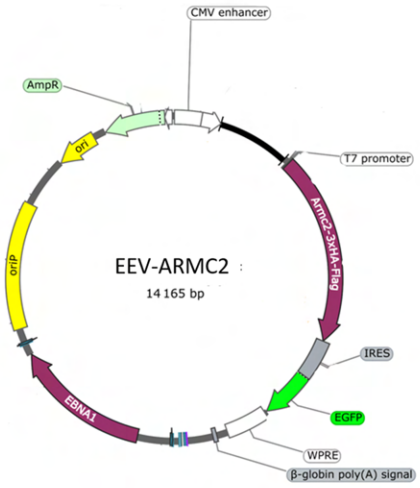

D

	1	2	3
mCherry-mRNA	+	+	+
DNAse	-	+	+
PolyA	-	-	+

DNA Ladder

1 Kb

0.5 Kb

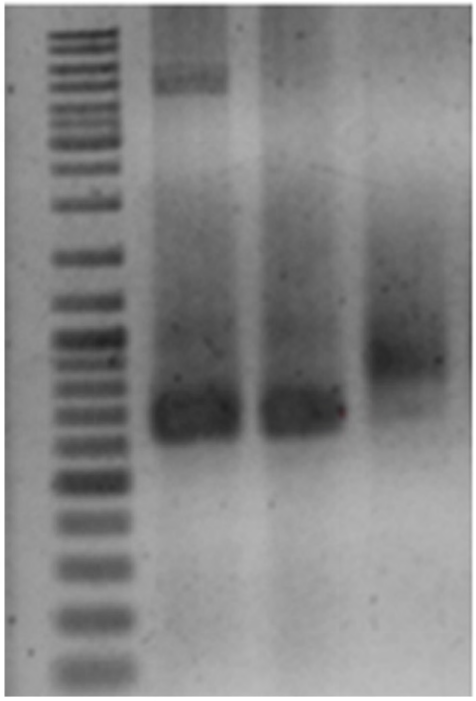

Supp Fig 1 ,Vilpreux et al 2025

A

Control

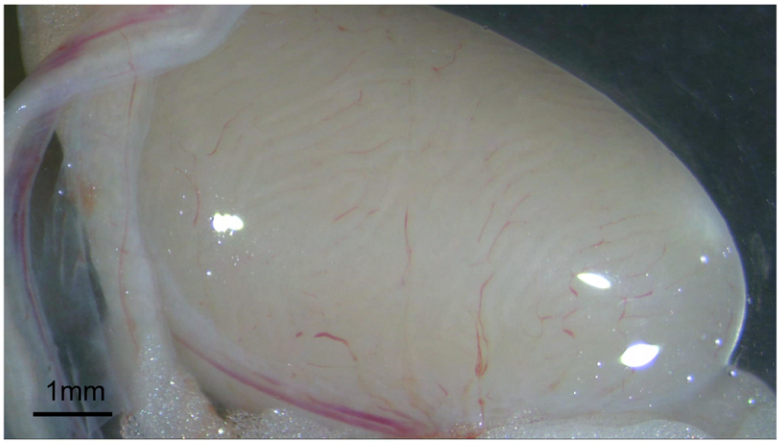

B

Over electroporated

Pearly white lesions

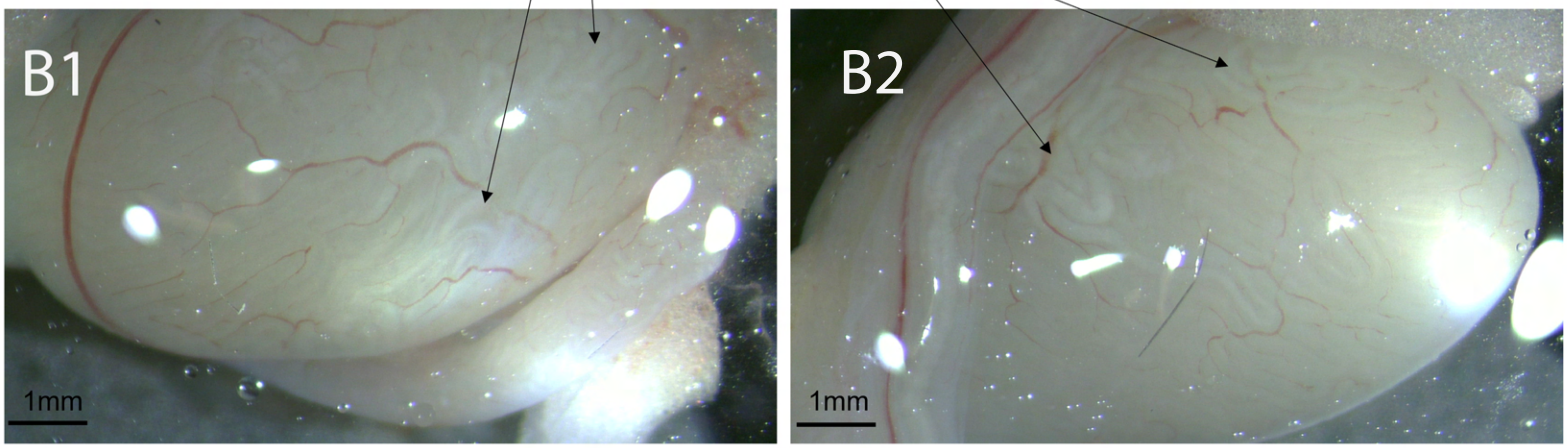

Supp Fig 2 , Vilpreux et al 2025

mCherry-mRNA

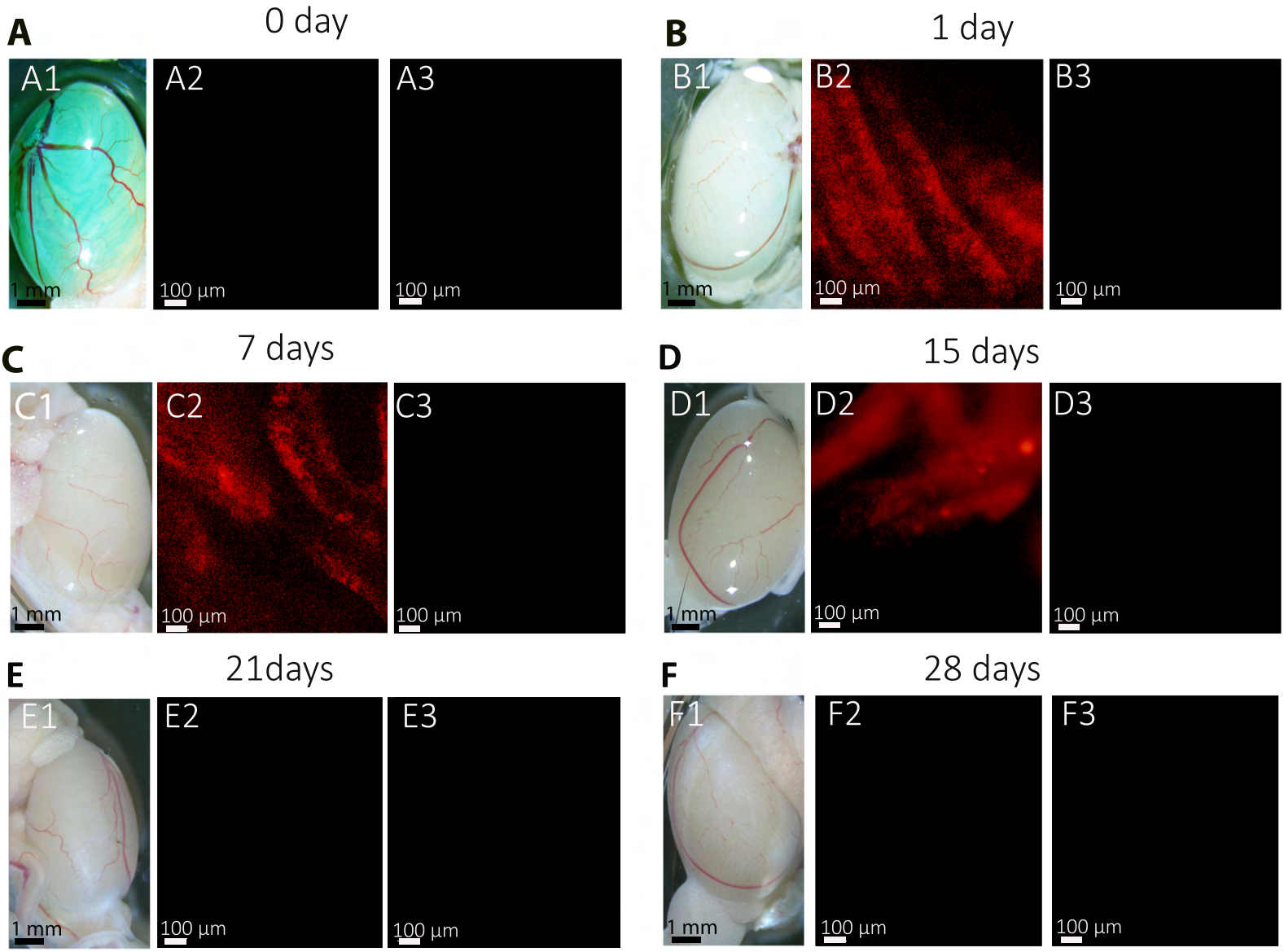

Supp Fig 3, Vilpreux et al 2025

mCherry-mRNA , 1 day post injection

A

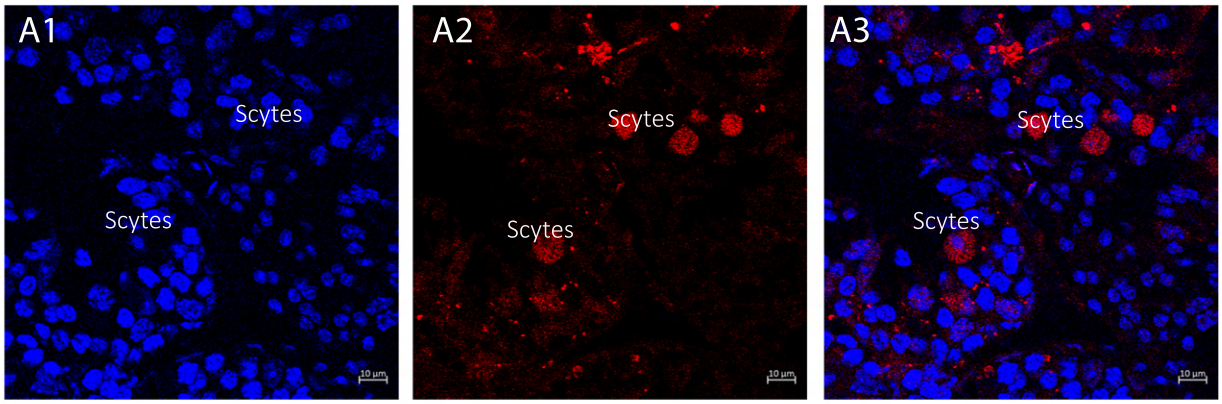

B

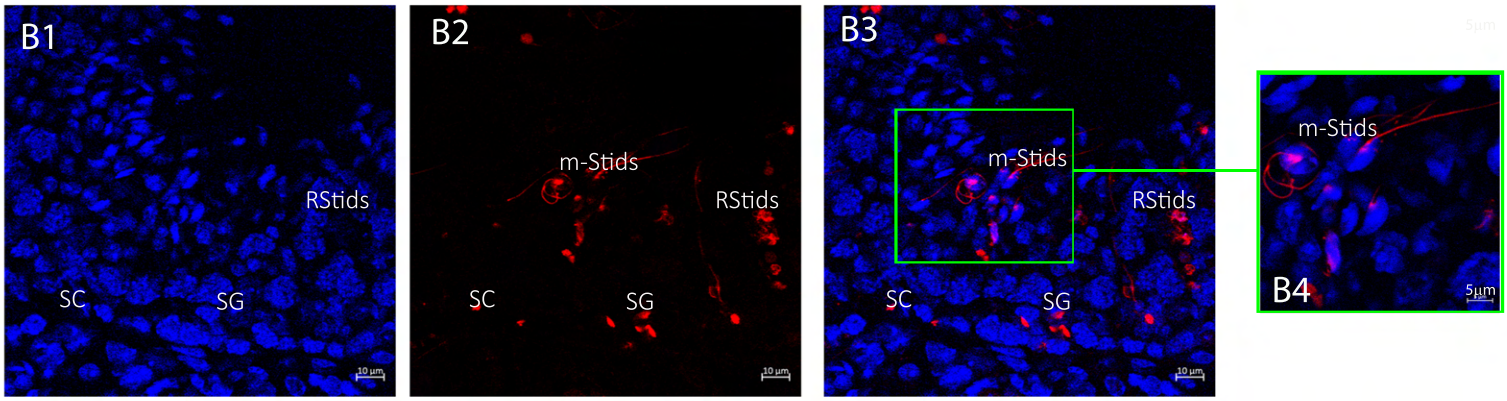

mCherry-mRNA, 7 days post injection

C

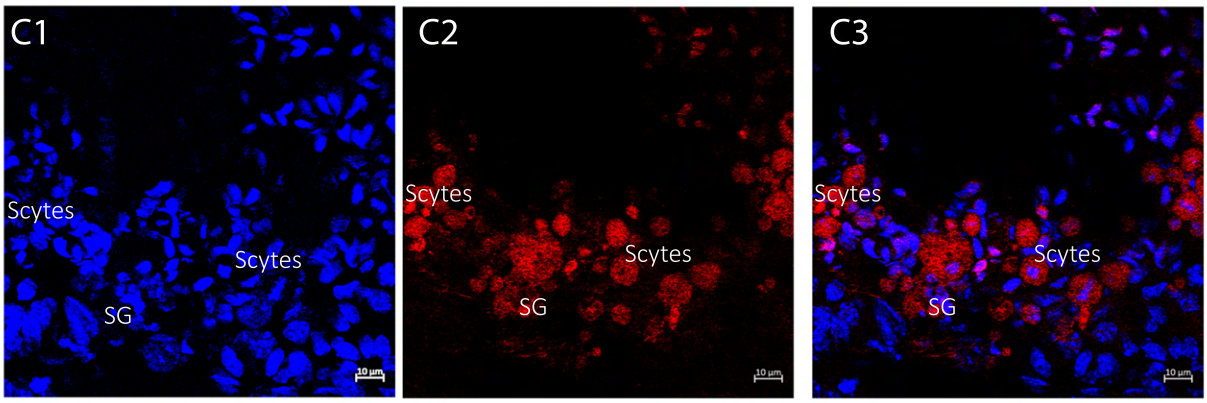

D

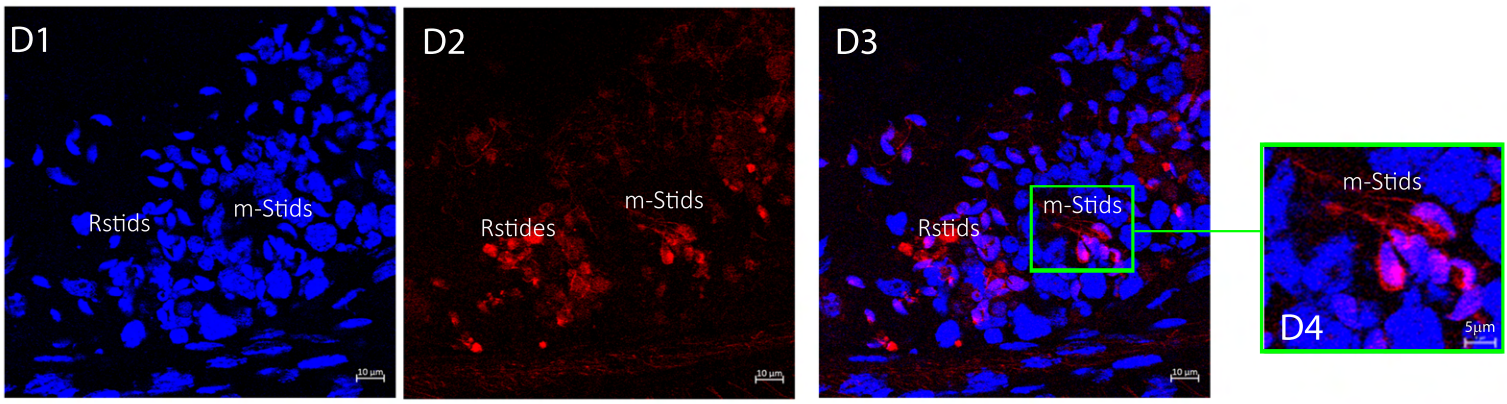

Supp Fig 4, Vilpreux et al 2025

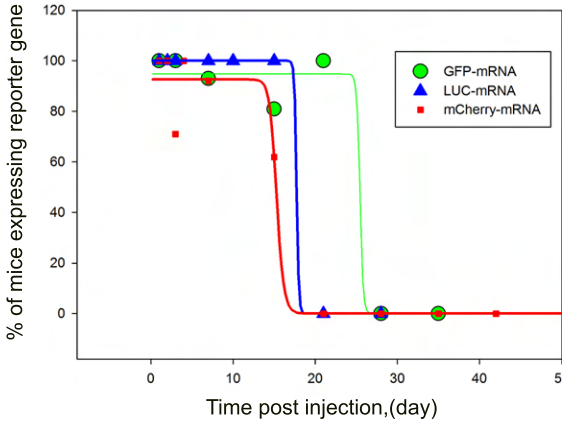

Supp Fig 5, Vilpreux et al 2025

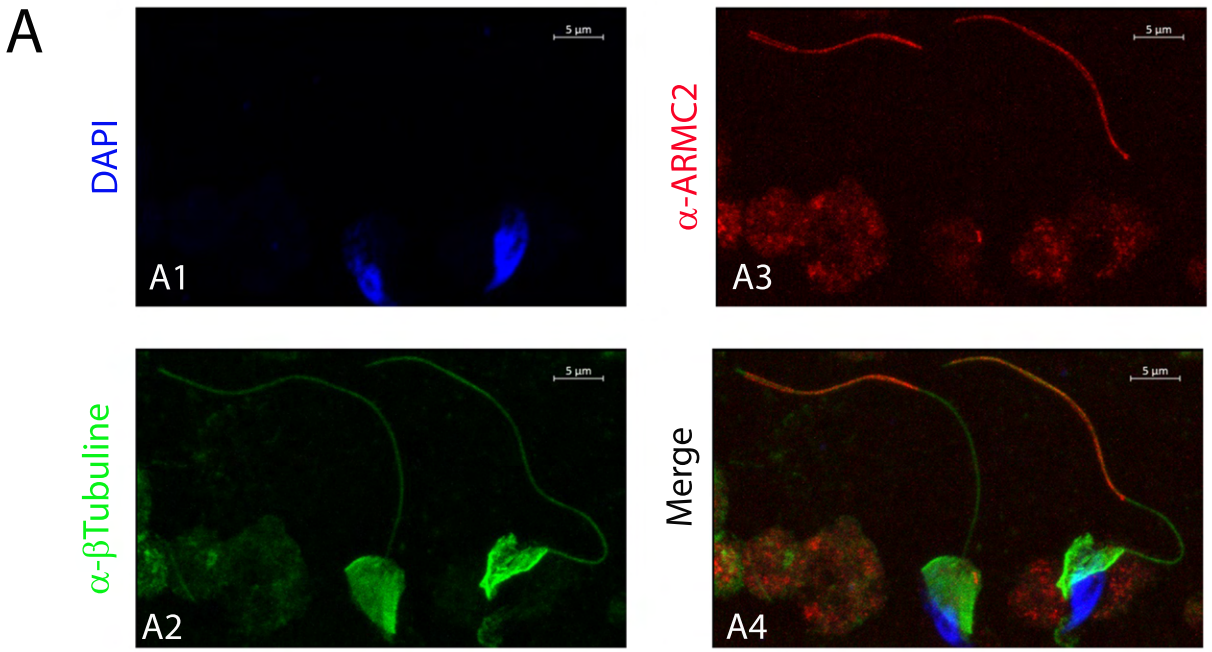

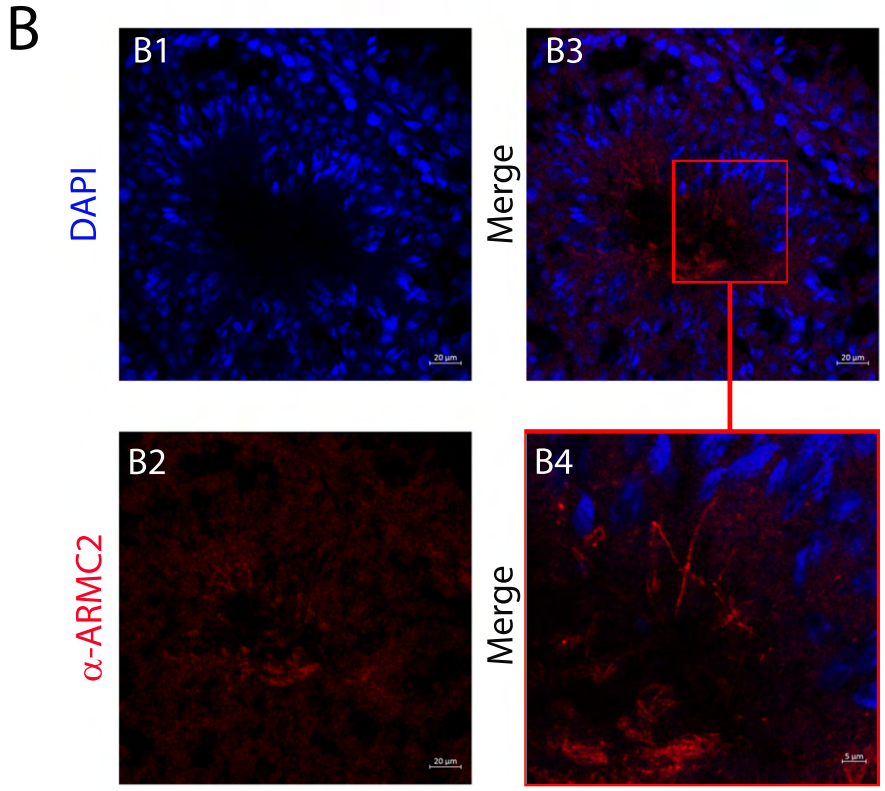

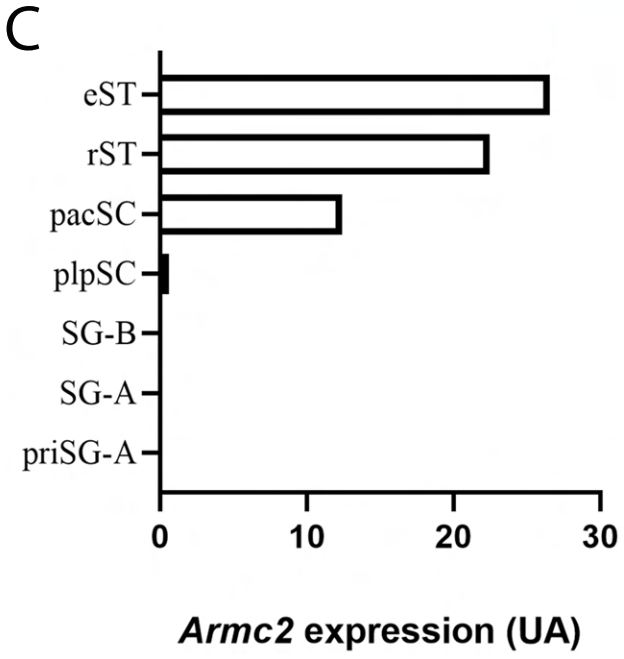

Supp Fig 6, Vilpreux et al 2025

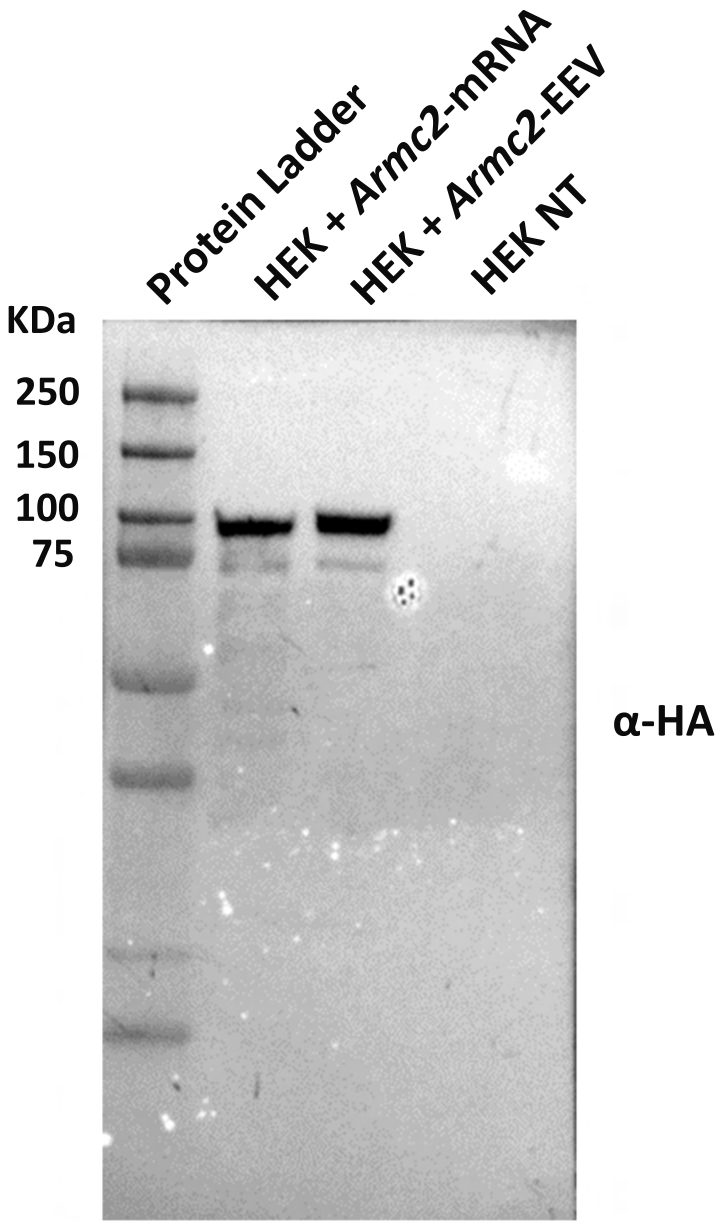

Supp Fig 7, Vilpreux et al 2025

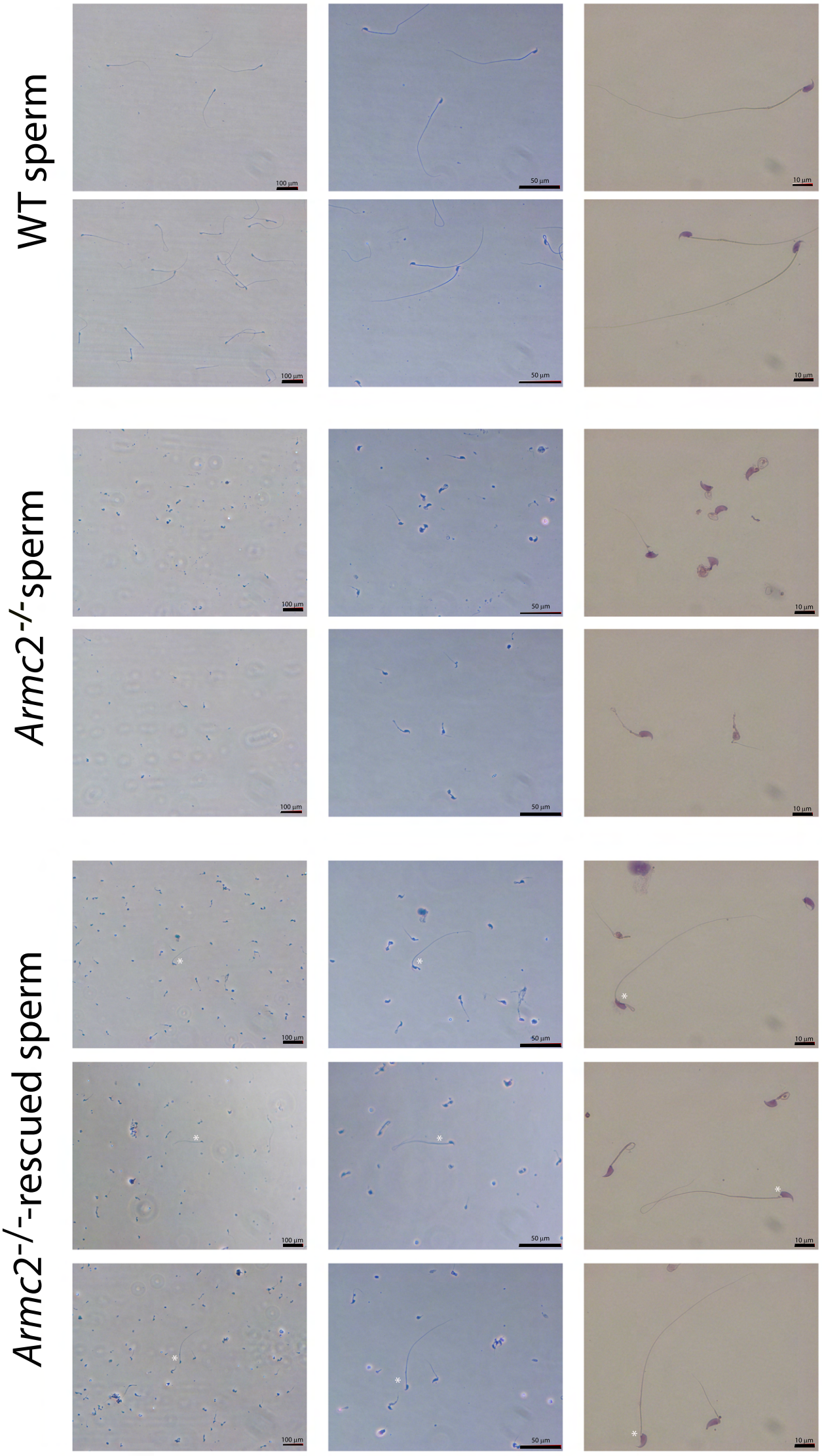

Supp Fig 8,
Vilpreux et al 2025

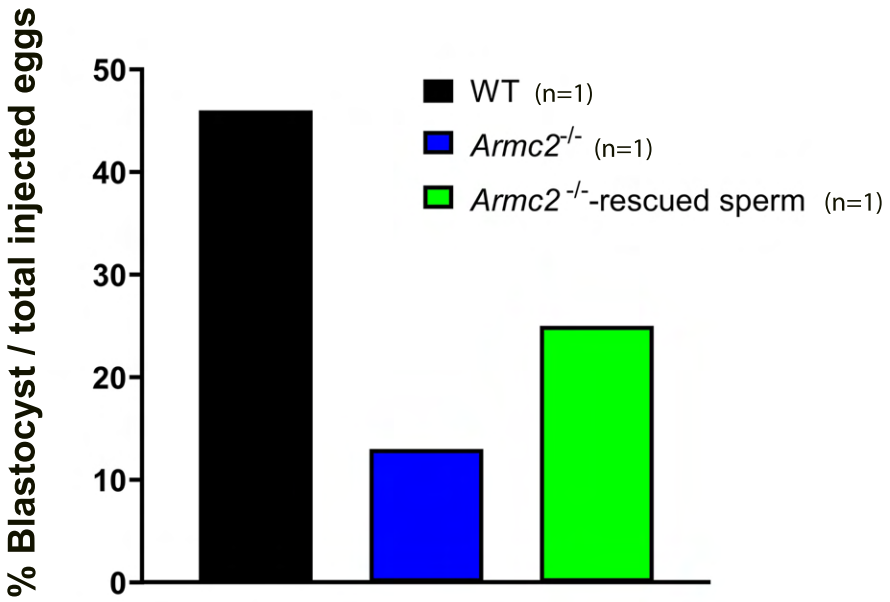

Supp Fig 9, Vilpreux et al 2025

GFP-mRNA , 1 day post injection

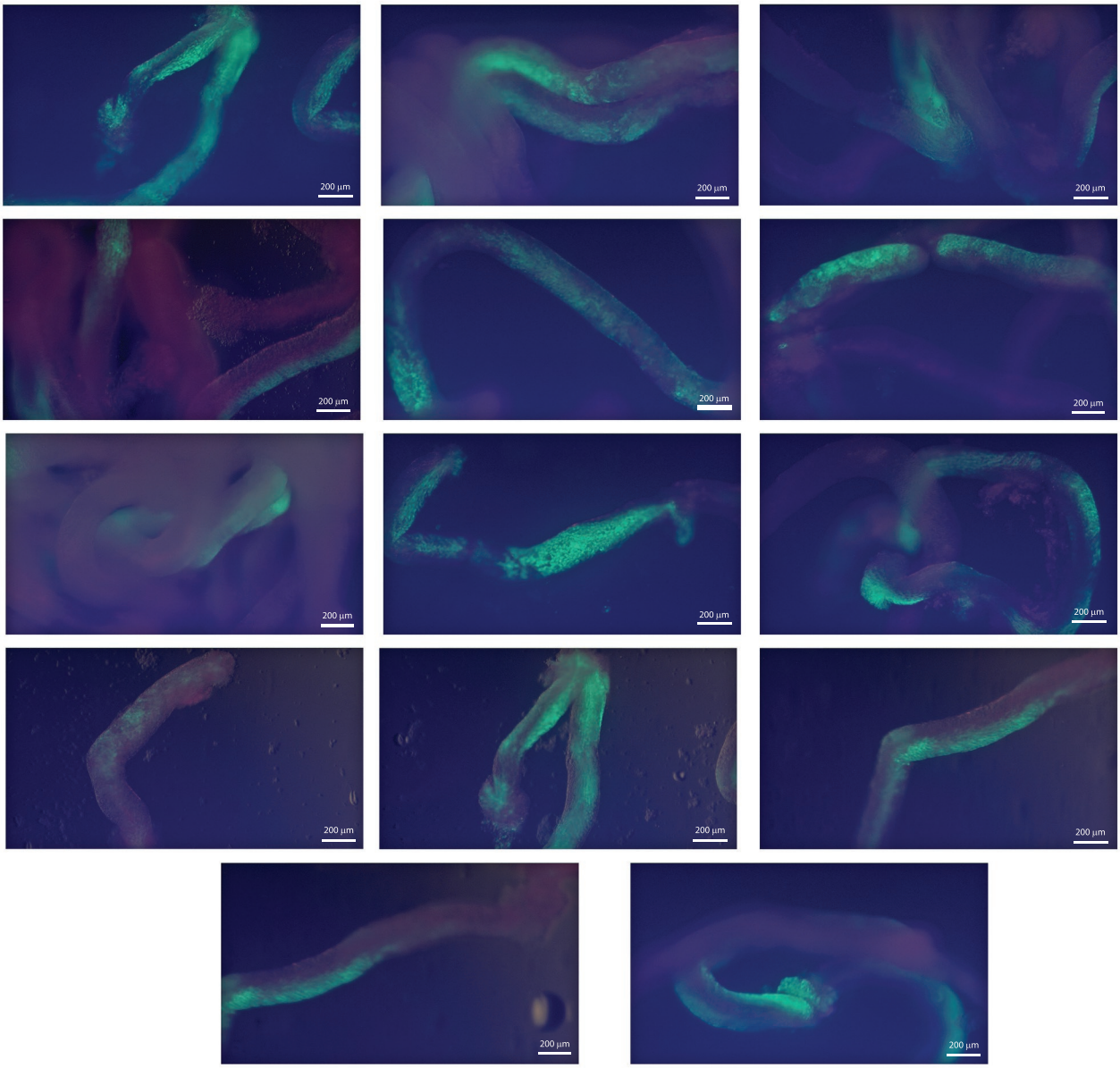

Supp Figure 10, vilpreux et al 2025

A. GAPDH

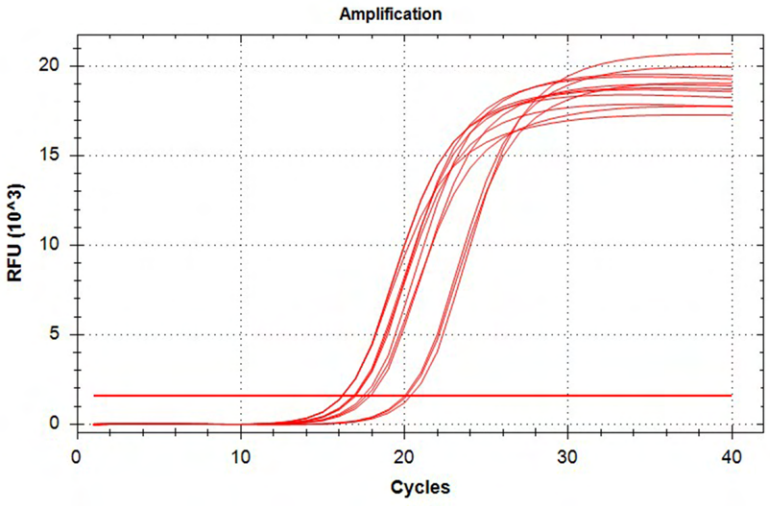

B. ACTB

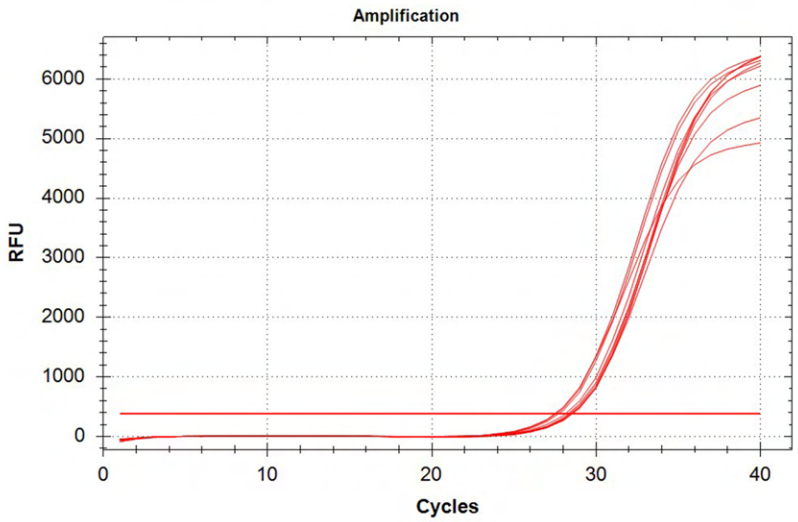

Supp Figure 11, vilpreux et al 2025